For Reference

NOT TO BE TAKEN FROM THIS ROOM

Ex libris
universitatis
albertaensis

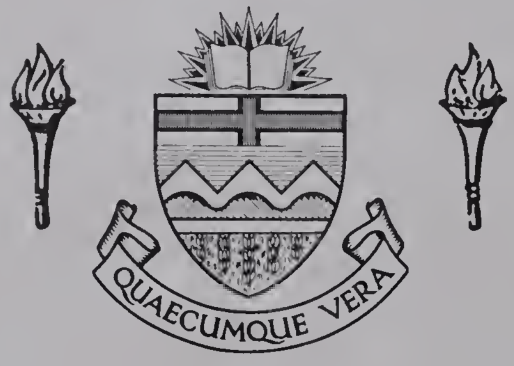

QUAECUMQUE VERA

High Level
BOOK BINDERY LTD.
10372 - 60 Ave., Edmonton
"THE HIGHEST LEVEL OF
CRAFTSMANSHIP"

THE UNIVERSITY OF ALBERTA

NUCLEAR STRUCTURE STUDIES IN ^{53}Mn VIA THE ^{53}Cr(p,nγ)^{53}Mn REACTION

by

© WOON HYUK CHUNG

A THESIS

SUBMITTED TO THE FACULTY OF GRADUATE STUDIES AND RESEARCH
IN PARTIAL FULFILMENT OF THE REQUIREMENTS FOR THE DEGREE
OF DOCTOR OF PHILOSOPHY

DEPARTMENT OF PHYSICS

EDMONTON, ALBERTA
SPRING, 1972

1972
19D

THE UNIVERSITY OF ALBERTA

FACULTY OF GRADUATE STUDIES AND RESEARCH

The undersigned certify that they have read, and recommend to the Faculty of Graduate Studies and Research, for acceptance, a thesis entitled NUCLEAR STRUCTURE STUDIES IN ^{53}Mn VIA THE ^{53}Cr(p,nγ)^{53}Mn REACTION submitted by Woon Hyuk Chung in partial fulfilment of the requirements for the degree of Doctor of Philosophy.

ABSTRACT

The properties of the low-lying excited states in ^{53}Mn were studied by measuring gamma-ray angular distributions and lifetimes using the ^{53}Cr(p,nγ)^{53}Mn reaction. In this reaction, energy levels of ^{53}Mn have been found at 0.378, 1.288, 1.440, 1.619, 2.272, 2.405, 2.572, 2.670, 2.687, 2.705, 2.872, 2.876, 2.914, 2.947, 3.005, 3.095, 3.125, 3.183, 3.193 and 3.250 MeV. The measurement of gamma-ray angular distributions and yield curves together with predictions based on the compound nuclear statistical model have enabled new spin assignments to be made for the following excited states in ^{53}Mn: 2.272 MeV ($\frac{7}{2}$), 2.572 MeV ($\frac{7}{2}$), 2.687 MeV ($\frac{7}{2}$), 2.947 MeV ($\frac{9}{2}$), 3.005 MeV ($\frac{5}{2}$). The spins of the 1.440 and 1.619 MeV levels were confirmed as $J = \frac{11}{2}$ and $J = \frac{9}{2}$, respectively. Multipole mixing ratios and branching ratios were determined for some of the observed transitions.

Lifetimes of nine excited states in ^{53}Mn have been measured using the Doppler-shift attenuation method, i.e., E_x (MeV), τ(ps) = 1.288, > 0.19; 1.440, $0.21^{+0.31}_{-0.10}$; 1.619, $0.29^{+1.0}_{-0.2}$; 2.272, $0.31^{+0.49}_{-0.15}$; 2.405, $0.12^{+0.14}_{-0.05}$; 2.572, $0.042^{+0.058}_{-0.035}$; 2.670, $0.10^{+0.13}_{-0.07}$; 2.687, $0.072^{+0.05}_{-0.03}$; 2.876, $0.065^{+0.090}_{-0.044}$. The reduced transition probabilities, B(M1) and B(E2), derived from the measured lifetimes are compared with intermediate-coupling model predictions. Agreement between theory and

experiment is very good.

The Nilsson model was used to predict energy levels of ^{53}Mn without taking band mixing into consideration. The results were compared with the experimental levels and the predictions with band mixing of Malik and Scholz. In both cases, with band mixing and without band mixing, the theoretical fit to experimental results is fair only for a few low-lying levels.

The properties of the low-lying excited states of ^{51}V and ^{53}Mn have been investigated in the framework of the intermediate-coupling unified nuclear model. Energy levels and electromagnetic properties have been calculated based on the model. In general, the results are found to be in good agreement with the experimentally observed values for the low-lying excited states.

The present experimental results are also compared with the available shell model calculations.

ACKNOWLEDGEMENTS

I would like to thank Drs. W.C. Olsen and D.M. Sheppard for their supervisory help, for suggesting this project, and for encouragement and many useful discussions during the course of this research.

Special thanks are due to Paul Gutowski for his help in the initial stages of the Doppler-shift lifetime experiment.

Appreciation is also extended to Dr. B. Robertson, Peter Green and Ed Wong for their assistance with the experiment and for helpful discussions, and also to Georges Carola, whose computer code I used for the intermediate-coupling calculations.

I wish to thank Tilak Sharma, Sayed El-Bakr, and Jan Soukup for their help in running the experiment, and Ahmed Hussein for his assistance with the modification of the Nilsson model program.

I would also like to thank Bob McCamis, Jim Pasos, and Dave White for proofreading the manuscript.

Special thanks are also due to Miss Audrey Forman for her very careful and efficient typing of this thesis.

I am very grateful to my wife, not only for typing the first draft of this thesis, but also for her patience and understanding during the long years of graduate study and also to my two children, Song Ho and Song Hey.

In particular, I wish to thank my late mother, whose parental encouragement and never-failing efforts stimulated my advancement from elementary school to the threshold of my Ph.D. degree.

I also wish to thank my father and brothers in Korea for their encouragement and for wishing me success in my studies over the last four and a half years.

Finally, I appreciate the financial support provided by the University of Alberta throughout the course of this work.

TABLE OF CONTENTS

Page

CHAPTER I INTRODUCTION 1

CHAPTER II GAMMA-RAY ANGULAR DISTRIBUTIONS 13

2.1 Theory 13
- (a) The angular correlation 13
- (b) The compound nuclear statistical model 20

2.2 Experimental Method 30
- (a) Apparatus 30
- (b) Detector efficiency 30
- (c) Gamma-ray absorption corrections 36
- (d) Yield curves, branching ratios and angular distributions 37

2.3 Method of Analysis 39
- (a) Yield curves 39
- (b) Gamma-ray angular distributions 39

2.4 Experimental results 40
- (a) The levels below 2 MeV 47
- (b) The 2.272 MeV level 51
- (c) The 2.405 MeV level 51
- (d) The 2.572 MeV level 51
- (e) The 2.670 MeV level 54
- (f) The 2.687 MeV level 54
- (g) The 2.705 MeV level 57
- (h) The 2.872 and 2.876 MeV levels 57
- (i) The 2.914 MeV level 57
- (j) The 2.947 MeV level 60
- (k) The 3.005 MeV level 60
- (l) Levels above 3.0 MeV 60

Page

CHAPTER III NUCLEAR LIFETIMES 67

3.1 Doppler-Shift Attenuation Theory 67

(a) Introduction 67

(b) The Doppler-shift attenuation 69

(c) The attenuation factor, F(τ) 71

(d) The lifetimes and transition probabilities 85

3.2 Experimental Method 89

(a) Apparatus 89

(b) n-γ coincidence spectrum 90

3.3 Method of Analysis 94

(a) Kinematic shift 94

(b) Centroid calculations 95

(c) The attenuation factor, F(τ) 96

(d) Nuclear lifetimes and transition probabilities 97

3.4 Experimental Results 100

CHAPTER IV NUCLEAR MODEL CALCULATIONS 108

4.1 Introduction 108

4.2 The Nilsson Model 110

(a) Theory 110

(b) Application to ^{53}Mn 119

4.3 The Shell Model 124

4.4 The Intermediate Coupling in the Unified Model 126

(a) Theory 126

(b) Application to ^{51}V and ^{53}Mn 132

(c) Concluding remarks 152

CHAPTER V CONCLUSIONS 156

LIST OF TABLES

			Page
Table	1	A summary of previously measured low-lying levels of ^{53}Mn (in MeV).	10
Table	2	Legendre coefficients, a_2 and a_4 of the angular distributions of gamma-rays de-exciting levels of ^{53}Mn.	46
Table	3	Summary of angular distribution results. The energy levels, the spin assignments, the branching ratios and multipole mixing ratios, are listed for the excited states of ^{53}Mn.	55-56
Table	4	Methods and estimated ranges for measuring lifetimes of states formed in nuclear reactions.	68
Table	5	Centroid calculations.	102
Table	6	Summary of lifetimes in ^{53}Mn.	106
Table	7	Comparison of theoretical and experimental lifetimes in ^{53}Mn.	107
Table	8	Parameters used in the Nilsson model calculations in ^{53}Mn.	122
Table	9	Parameters used in the intermediate coupling calculations.	135

Page

Table 10 Expansion coefficients corresponding to states $|E\ (\mathrm{MeV});\ I^{\pi}\rangle$ of ^{51}V. 138

Table 11 Expansion coefficients corresponding to states $|E\ (\mathrm{MeV});\ I^{\pi}\rangle$ of ^{53}Mn. 139

Table 12 Reduced transition probabilities B(E2) in ^{51}V. 145

Table 13 Reduced transition probabilities B(M1) in ^{51}V. 146

Table 14 Reduced transition probabilities, B(M1) and B(E2) in ^{53}Mn. 147

Table 15 Nuclear moments of ^{51}V and ^{53}Mn. 148

Table 16 Lifetimes, branching ratios and mixing ratios in ^{51}V. 150

Table 17 Lifetimes, branching ratios and mixing ratios in ^{53}Mn. 151

LIST OF FIGURES

		Page
Fig. 1	A schematic diagram of the (p,nγ) reaction process.	26
Fig. 2	The target chamber.	31
Fig. 3	A typical gamma-ray spectrum of ^{56}Co.	33
Fig. 4	Relative full-energy peak efficiency curve for the Ortec 43.8 cc Ge(Li) detector.	34
Fig. 5	Comparison of the shapes of the relative full-energy peak efficiencies for the three Ge(Li) detectors.	35
Fig. 6	Gamma-ray total absorption coefficients.	38
Fig. 7	A gamma-ray spectrum at 55° for the ^{53}Cr(p,nγ)^{53}Mn reaction, E_p = 5.20 MeV.	41
Fig. 8	A spectrum of gamma-rays in coincidence with neutrons detected at 180° from the beam direction.	42
Fig. 9	A summary of branching ratios, spin assignments and the excited state levels of ^{53}Mn below 3.25 MeV.	43
Fig. 10	Yield curves at 90° for the gamma-ray transitions in ^{53}Mn at the bombarding energies, E_p = 3.0 to 5.0 MeV.	44
Fig. 11	Yield curve analysis based on the compound nuclear statistical model for the 2.687 → 0.0 MeV and 2.272 → 0.378 MeV transitions in ^{53}Mn.	45

Page

Fig. 12 The angular distribution and the χ^2 plot for the 1.440 → 0.0 MeV transition 48

Fig. 13 The angular distribution and the χ^2 plot for the 1.619 → 0.0 MeV transition. 49

Fig. 14 The angular distribution and the χ^2 plot for the 2.272 → 0.0 MeV transition. 50

Fig. 15 The angular distribution and the χ^2 plot for the 2.572 → 0.378 MeV transition. 52

Fig. 16 The angular distribution and the χ^2 plot for the 2.572 → 0.0 MeV transition. 53

Fig. 17 The angular distribution and the χ^2 plot for the 2.687 → 0.378 MeV transition. 58

Fig. 18 The angular distribution and the χ^2 plot for the 2.687 → 0.0 MeV transition. 59

Fig. 19 The angular distribution and the χ^2 plot for the 2.947 → 0.0 MeV transition. 62

Fig. 20 The angular distribution and the χ^2 plot for the 3.005 → 1.288 MeV transition. 63

Fig. 21 Angular distributions for the gamma-ray transitions of the 0.378, 1.288, 1.440, 1.619, 2.272, 2.405 and 2.670 MeV levels. 64

Page

Fig. 22 Angular distributions for the gamma-ray transitions of the 2.876, 2.914, 2.947 and 3.005 MeV levels. 65

Fig. 23 Angular distributions for the gamma-ray transitions of the 2.572, 2.687, 2.705, 3.095 and 3.125 MeV levels. 66

Fig. 24 Universal differential cross section for elastic nuclear collisions derived by LSS. 78

Fig. 25 Nuclear and electronic stopping powers in reduced units, in the low velocity region, $0 < v < \frac{c}{137} \cdot z_1^{\frac{2}{3}}$. 80

Fig. 26 Cascade contribution to $F(\tau)$. 84

Fig. 27 A schematic diagram of the experimental arrangement for the lifetime measurements (cross section in a vertical plane). 91

Fig. 28 The electronics. 92

Fig. 29 A typical n-γ time spectrum. 93

Fig. 30 A typical $F(\tau)$ versus τ curve for the 1.440 MeV level of ^{53}Mn (E_p = 4.9 MeV). 98

Fig. 31 $F(\tau)$ curves corresponding to ^{53}Mn ions recoiling with various initial velocities. 99

Page
Fig. 32 Doppler shifted coincidence spectra of gamma-rays observed at 0° and 120°. 101

Fig. 33 The nuclear coupling scheme on an odd-A nucleus. (a) shows the coupling in the ground state, and (b) shows the coupling in the general case. 118

Fig. 34 The Nilsson model energy diagram. 120

Fig. 35 The calculated energy levels of ^{53}Mn based on the Nilsson model. 123

Fig. 36 Plot of E as a function of the coupling parameter ξ for ^{51}V. 136

Fig. 37 Plot of E as a function of the coupling parameter ξ for ^{53}Mn. 137

Fig. 38 Comparison of energy levels of ^{51}V predicted from the intermediate-coupling calculations with experimental spectra, along with other predictions. 140

Fig. 39 Comparison of energy levels of ^{53}Mn predicted from the intermediate-coupling calculations with experimental spectra, along with other predictions. 141

CHAPTER I

INTRODUCTION

The properties of the low-lying states for the nuclei with atomic mass A in the regions 19-29, 150-190 and 220 upwards have been successfully explained by the rotational model (Bo 52, BO 53, Ni 55). In particular, identification of rotational levels in the nuclei ranging from ^{19}F to ^{29}Si (Pa 56, Sh 56, Ra 57, Li 58) has prompted investigation of the nuclear level structure of light and medium weight nuclei. Outside the rotational regions and excluding the closed-shell nuclei with magic numbers N or Z = 2, 8, 20, 28, 50, 82, 126, there are the vibrational regions (Br 60) $30 < A < 150$ and $190 < A < 220$, where the low levels of many of these nuclei can be described by the surface-vibration model. The point at which rotational excitations begin is astonishingly definite and the structure of spectra beyond the point is purely rotational, while the transition from single-particle excitations to vibrations is not clear-cut and it is quite probable that no level structure is either exclusively the one or the other (El 66).

According to the shell model, ^{53}Mn has five protons in the $1f_{\frac{7}{2}}$ shell and a closed neutron ($N = 28$) shell. From the point of view of the collective model, ^{53}Mn is expected to lie in the vibrational region $30 < A < 150$, where an odd-mass nucleus could be described by coupling one nucleon to an even-even vibrating core. An investigation of the ^{53}Mn level scheme is, therefore,

of interest as a test of the proton configuration in the shell model and as an application of the collective model to the nucleus.

Experimental knowledge of decay modes, spins and parities, energies, and the electromagnetic properties of the excited states is basic to any theoretical investigation and these are quantities which must be known before comparisons with theoretical models can be made. The properties of the electromagnetic transitions connecting the nuclear levels provide the most important and direct test of a particular nuclear model since the electromagnetic matrix elements obtained from the above properties could provide a direct and accurate test of the nuclear wave functions without referring to relatively unknown factors related to nuclear forces or nuclear reaction mechanisms.

The $^{53}Cr(p,n\gamma)^{53}Mn$ reaction is one of the most useful reactions for investigating the electromagnetic properties of the excited states in ^{53}Mn, since, firstly, it yields most of the low-lying excited levels in ^{53}Mn at the corresponding bombarding energy, secondly, the 6 MV Van de Graaff is especially suited for the investigations of the excited states up to 3 MeV, and thirdly, because of the negative Q-value (-1.3804 MeV for the ground state) the proton bombarding energies could be chosen just above threshold for the angular distributions so that analysis in terms of the statistical compound nucleus is appropriate.

This thesis is concerned with experimental investigation of the electromagnetic properties, including the lifetimes of the excited states in ^{53}Mn through the $^{53}Cr(p,n\gamma)^{53}Mn$ reaction, and

with some theoretical approaches to the ^{53}Mn level structure, including the intermediate coupling in the unified model.

Experimental information on the excited states in ^{53}Mn above 2 MeV is scarce. In the last decade a number of experiments have been carried out to obtain the level positions, angular momentum transfers, spectroscopic factors and electromagnetic properties of lower excited states in ^{53}Mn through the β^+ decay, the (p,γ) reaction, the (p,n) and $(p,n\gamma)$ reactions and stripping and pick-up reactions.

From the β^+ decay studies (Ju 59, De 68) and the microwave paramagnetic resonance hyperfine structure (Do 56), spins of the ground state and the first excited state were found to be $\frac{7}{2}^-$ and $\frac{5}{2}^-$, respectively, and the magnetic moment was determined to be $|\mu(^{53}\mathrm{Mn})| = 5.050 \pm 0.07$ n.m. Juliano _et al_. (Ju 59) observed the emission of a gamma ray of energy 380 KeV and positron groups corresponding to the ground state, the first excited state and the second excited state from the disintegration of ^{53}Fe.

The (p,γ) reactions: Arnell _et al_. (Ar 64, St 65) and Vuister (Vu 66, Vu 67) extensively investigated the level properties of ^{53}Mn by means of the $^{52}\mathrm{Cr}(p,\gamma)^{53}\mathrm{Mn}$ reaction. In these investigations (Vu 66, Vu 67), the spins of the 0.38 MeV and 1.29 MeV levels were assigned as $\frac{5}{2}^-$ and $\frac{3}{2}^-$, respectively. The multipole mixing ratio of the 0.38 MeV gamma transition obtained was $\delta = -0.61 \pm 0.08$. Abzeid _et al_. (Ab 70) also reported the multipole mixing ratios for gamma transitions with energies of 910 keV ($\delta_1 = -0.09 \pm 0.06$) and 380 keV ($\delta_2 = -0.47 \pm 0.1$) from the triple γ-γ correlation measurements for

the cascade 1290 → 380 → 0 in ^{53}Mn through the ^{52}Cr(p,γ)^{53}Mn reaction. More recently, some properties of the excited levels in ^{53}Mn, i.e., excitation energies, gamma-ray branching ratios, amplitude mixing ratios, spins, parities, and lifetimes were reported from the (p,γ) reaction by Maripuu (Ma 70). In this experiment, the spins and parities of the excited levels in ^{53}Mn were assigned as follows: 0.38 ($\frac{5}{2}^-$), 2.28 ($\frac{5}{2}^-$), 2.41 ($\frac{3}{2}^-$), 2.67 ($\frac{1}{2}^-$), 2.69, ($\frac{5}{2}^-$), 2.88 ($\frac{3}{2}^-$), 2.91 ($\frac{3}{2}^-$), 3.10 ($\frac{3}{2}^-$), 3.18 ($\frac{3}{2}^-$) and 3.48 ($\frac{1}{2}^-$). Lifetimes for some of the excited levels in ^{53}Mn were also measured by the Doppler-shift attenuation method using thick ^{52}Cr targets such that the slowing-down of the ^{53}Mn ions takes place in the ^{52}Cr target material. Sparks (Sp 71) also reported a decay scheme and branching ratios for ^{53}Mn from the (p,γ) reaction.

The stripping reactions: Okorokov et al. (Ok 67) investigated the neutron spectra and angular distributions in the (d,n) reactions on ^{52}Cr at E_d = 11.7 MeV using the plane wave analysis to examine the assumption that the low-lying levels of the odd nuclei in this region could be described as a result of an interaction between an odd nucleon and the excited states of an even-even core, and could be regarded as collective (Be 61). In the ^{52}Cr(d,n)^{53}Mn reaction, an analysis of the angular distribution for the first group of neutrons, corresponding to capture of a proton in the ground and first excited levels of ^{53}Mn, which were not resolved, yielded $\ell_p = 3$ ($J = \frac{7}{2}^-, \frac{5}{2}^-$). The second group of neutrons ($\ell_p = 1$) was observed corresponding to the second excited level (1.29 MeV) in

^{53}Mn. The strong neutron groups with energy at 2.42 MeV were found to correspond to a p-state. No states with high spins ($\frac{11}{2}^-$, $\frac{9}{2}^-$) which were observed in other reactions for ^{53}Mn appeared here, suggesting a decrease in the probability of capture of a proton by these states owing to the large transferred ℓ_p and to the collective nature of these levels.

O'brien et al. (Ob 67) investigated the proton single-particle levels of the N = 28 nuclei, ^{51}V, ^{53}Mn and ^{55}Co by (τ,d) reactions at E_τ = 10, 11 and 12 MeV. In this experiment, it was found that the first excited state at 385 keV was only weakly excited. Armstrong (Ar 65) et al. used the (τ,d) reaction on the N = 28 nuclei, ^{48}Ca, ^{51}V, ^{52}Cr and ^{54}Fe at E_τ = 22 MeV to study the single proton states in the corresponding residual nuclei. The 2.275 MeV level in ^{53}Mn was not observed and the 0.383 MeV level was very weakly excited in this ^{52}Cr(τ,d)^{53}Mn reaction. Cujec et al. (Cu 69) reported energy levels in ^{53}Mn from the (τ,d) reaction at E_τ = 10 and 9.5 MeV. By a systematic study of level positions, the $d_{\frac{3}{2}}$ and $s_{\frac{1}{2}}$ proton hole states and the $p_{\frac{3}{2}}$ spectroscopic strength, it was concluded that the shell model (Mc 64, Au 67) adequately describes these nuclei, whereas the coriolis strong-coupling in the rotational model (Ma 66) fails to explain the observed splitting of the $p_{\frac{3}{2}}$ spectroscopic strength.

The (α,t) reaction on medium-weight nuclei was reported by Armstrong et al. (Ar 67). It was suggested that the spins and parities of the 2.40 and 2.69 MeV states are $\frac{3}{2}^-$ and $\frac{1}{2}^-$,

respectively. Cujec et al. (Cu 68, Sz 70) carried out the $^{50}Cr(\alpha,p\gamma)^{53}Mn$ reaction at E_α = 10 MeV and assigned the following spins: 1.296 MeV ($\frac{3}{2}^-$), 1.439 MeV ($\frac{7}{2}^-$ or $\frac{11}{2}^-$), 1.606 MeV ($\frac{9}{2}^-$ or $\frac{7}{2}^-$), 2.269 MeV ($\frac{3}{2}^-$) and 2.410 MeV ($\frac{3}{2}^-$).

The pick-up reactions: Newman et al. (Ne 68) investigated the (d,τ) reaction on the N = 28 nuclei at E_d = 34.4 MeV to obtain information concerning the target ground state wave functions, the single-particle and single-hole states of the final nuclei. The results were, in general, consistent with the simple shell model considering $f_{\frac{7}{2}}$ protons outside an inert ^{48}Ca core, while for ^{54}Fe evidence for both $f_{\frac{5}{2}}$ and $p_{\frac{3}{2}}$ admixtures were noted in the ground state. They also found that the centroid of the $2s_{\frac{1}{2}}$ subshell is at lower excitation than the $1d_{\frac{3}{2}}$ shell for the N = 28 nuclei. Proton separation energies were studied from the (d,τ) reaction on f-p shell nuclei at 52 MeV by Mairle et al. (Ma 69). They found the systematic behaviour of the binding energies, i.e., in the lower f-p shell for nuclei with $A \leq 48$, the $2s_{\frac{1}{2}}$ protons are on the average more tightly bound than the $1d_{\frac{3}{2}}$ protons, and the reverse is true for $A > 48$.

Bassani et al. (Ba 62, Ba 64, Co 61) investigated the (n,d) and (p,t) reactions on medium-weight nuclei. In the $^{54}Fe(n,d)^{53}Mn$ reaction, Bassani et al. (Ba 62) observed only one high energy deuteron group corresponding to two levels of ^{53}Mn, that is, the ground state and the first excited state at 0.39 MeV, which could not be separated. The result of the DWBA analysis showed that the

first excited level of ^{53}Mn must have spin $\frac{3}{2}$, but it has now been established to be $\frac{5}{2}$.

Glover and Jones (Gl 66) investigated proton hole states in the 1$f_{\frac{7}{2}}$ shell of ^{51}V and ^{53}Mn by means of the ^{52}Cr(t,α)^{51}V and ^{54}Fe(t,α)^{53}Mn reactions. Here angular distributions of the emitted α particles were obtained up to an excitation of 5.6 MeV in ^{51}V and up to 3.0 MeV in ^{53}Mn. Strong $\ell = 0$ and $\ell = 2$ transitions were observed at a low (2 ~ 3 MeV) excitation. There was also good agreement between the low-lying states of ^{53}Mn and ^{51}V. The similarity between ^{51}V (3 proton particles in the $f_{\frac{7}{2}}$ shell) and ^{53}Mn (3 proton holes in the $f_{\frac{7}{2}}$ shell) spectra shows that to a first approximation, ^{53}Mn can be treated in a $(f_{\frac{7}{2}})^{-3}$ representation.

Veje _et al_. (Ve 64) investigated (p,α) reactions leading to the N = 28 nuclei in ^{51}V, ^{53}Mn, ^{55}Co and ^{52}Cr at E_p = 11 to 12.5 MeV. It was concluded that compound nucleus formation plays a major role in the observed (p,α) reactions. Brown _et al_. (Br 66) reported new data on the positions of the energy levels of ^{53}Mn with the ^{56}Fe(p,α)^{53}Mn reaction.

The charge-exchange reactions : From the ^{53}Cr(p,n)^{53}Mn reaction, low-lying excited levels in ^{53}Mn and the ground state Q-value were measured by many authors (St 52, Jo 64, Mc 52). Gorodetzky _et al_. (Go 66, Be 66) studied the electromagnetic properties of ^{53}Mn from the ^{53}Cr(p,nγ)^{53}Mn reaction. They measured the half-life of the 0.377 MeV level in ^{53}Mn by the delayed-coincidence technique and

found $\tau_{\frac{1}{2}} = (1.17 \pm 0.06) \times 10^{-10}$ sec. From angular distribution measurements, plane polarization, and gamma-gamma angular correlations, the following spin and parity assignments were made: $J_1^{\pi} = \frac{5}{2}^-$ for the first excited state at 0.380 MeV and $J_2^{\pi} = \frac{3}{2}^-$ for the second excited state at 1.290 MeV.

The mechanism of (p,n) reactions on some medium mass nuclei at $E_p = 6.8$ MeV were investigated, within the framework of the statistical theory, by Dryapachenko _et al_. (Dr 68). In this study it was shown that the compound nucleus mechanism is predominant for the (p,n) reaction in this region.

The ^{53}Cr(p,nγ)^{53}Mn reaction has been extensively studied by many authors (Mc 52, Ch 70, Sa 67). Saad _et al_. (Sa 67) performed the n - γ angular correlation measurements for the ^{53}Cr(p,nγ)^{53}Mn reaction at $E_p = 2.3$, 2.4 and 2.5 MeV. The experimental results were found to be in good agreement with predictions of the statistical compound nucleus theory (Sh 66) using the known values of the spins and parities of the ground state ($J^{\pi} = \frac{7}{2}^-$) and first excited state ($J^{\pi} = \frac{5}{2}^-$) of ^{53}Mn and the multipolarity mixing parameter for 0.38 MeV gamma transitions ($\delta = 1.2^{+0.6}_{-0.4}$).

More recently, studies on the ^{53}Cr(p,n)^{53}Mn reaction by Tanaka _et al_. (Ta 70) and the ^{53}Cr(p,nγ)^{53}Mn reaction by McEllistrem _et al_. (Mc 70) have been reported. Tanaka _et al_. used the time-of-flight method to measure neutron spectra with ^{53}Cr(p,n)^{53}Mn and found the excited levels in ^{53}Mn up to an excitation energy of 4 MeV. In the study of the ^{53}Cr(p,nγ)^{53}Mn

reaction by McEllistrem et al. (Mc 70), levels and spins of ^{53}Mn have been found to be 377.5 ($\frac{5}{2}$), 1288.4 ($\frac{3}{2}$), 1440.1 ($\frac{11}{2}$) and 1619.1 ($\frac{9}{2}$) keV. Mixing ratios for the 377.5 and 1619.1 keV transitions were measured and found to be -0.6 ± 0.3 and -3.2 ± 0.8, respectively. Wiest et al. (Wi 71) also reported differential cross sections of the (p,n) reactions and angular distributions of the (p,nγ) transitions.

A summary of the previously measured low-lying levels of ^{53}Mn is shown in table 1.

Theoretically, there have been relatively few nuclear model calculations for ^{53}Mn (Ki 60, Sh 63, Mc 64, Ma 66, Au 67, Ra 69, Li 70). The calculations have been limited to the shell model and the strong coupling rotational model.

According to the shell model, in all nuclei with 28 neutrons and with $20 \leq Z \leq 28$, the 28 neutrons form an "inert" closed shell and the protons all fill the $f_{\frac{7}{2}}$ shell, one of these protons being considered as the test particle which probes the structure of the wave function.

De-Shalit (Sh 63) calculated energy levels and spins of nuclei with 28 neutrons and with $20 \leq Z \leq 28$ in terms of the proton configuration $(f_{\frac{7}{2}})^n$, and in the case of ^{53}Mn, the levels and spins have been predicted: 0.32 ($\frac{5}{2}^-$), 1.30 ($\frac{3}{2}^-$), 1.69 ($\frac{11}{2}^-$), 1.97 ($\frac{9}{2}^-$) and 2.92 MeV ($\frac{15}{2}^-$).

Similar calculations under the pure configuration assumption were carried out by McCullen et al. (Mc 64). Spins and energy

Table 1

A summary of previously measured low-lying levels of ^{53}Mn (in MeV).

(p,γ)			Stripping		Pick-up			(p,n)	
St 65	Vu 67	Ma 70	(τ,d) Ob 67	$(\alpha,p\gamma)$ Sz 70	(t,α) Gl 66	(p,α) Ve 64	(p,α) Br 66	$(p,n\gamma)$ Mc 70	(p,n) Ta 70
0.376	0.378	0.378	0.385	0.378		0.378	0.383	0.378	0.379
1.293	1.290	1.289		1.290		1.28	1.286	1.288	1.290
				1.438		1.43	1.438	1.440	1.440
				1.617		1.60	1.606	1.619	1.622
	(1.94)		(1.96)						
2.26	2.28	2.275	2.370	2.271		2.26	2.269		2.277
2.413	2.41	2.405	2.413	2.404	2.410	2.39	2.404		2.410
	2.58	2.573				2.55	2.572		2.575
2.673		2.672	2.678			2.67			2.672
	2.68	2.689					2.689		2.690
	2.70	2.708	2.720		2.707				2.707
		(2.839)							
	2.86	2.876				2.86			2.873
2.882			2.882				2.882		2.880
2.917	2.91	2.913							2.914
						2.92	2.944		2.947
	(3.00)		3.010		3.010	2.98	3.010		3.008
			3.061						
3.100	3.10	3.098	3.104			3.10	3.109		3.100
									3.127
3.187		3.182				3.18			3.183
	3.19						3.193		3.201
							3.251		3.249

levels were predicted at 0.28 ($\frac{5}{2}^-$), 1.3 ($\frac{3}{2}^-$), 1.75 ($\frac{11}{2}^-$), 2.05 ($\frac{9}{2}^-$) and 3.1 MeV ($\frac{15}{2}^-$), which show disagreement with the observed values of energy level positions.

Auerbach (Au 67) tried the mixed proton configuration for the shell model calculations, assuming the ${}^{48}_{20}Ca_{28}$ nucleus to be an inert core and the extra n-protons outside of this core forming $f_{\frac{7}{2}}{}^{n}$ and $f_{\frac{7}{2}}{}^{n-1}p_{\frac{3}{2}}$ configurations. Since M1 transitions are forbidden between $(1f_{\frac{7}{2}})^n$ configuration states (Sh 63), the presence of such transitions experimentally is an indication of configuration mixing.

More recently, calculations with relatively simple configuration mixing, allowing states with proton configurations of $(1f_{\frac{7}{2}}{}^{n-1}\ 2p_{\frac{3}{2}})$ and $(1f_{\frac{7}{2}}{}^{n-1}\ 1f_{\frac{5}{2}})$ as well as the pure $(1f_{\frac{7}{2}})^n$ configurations, were performed by Lips and McEllistrem (Li 70), showing considerable improvement over the pure configuration model. The strengths calculated with the real M1 operator successfully reproduced the measured value for the ground state magnetic moment of ${}^{53}Mn$. However, the 1.440 MeV level in the low-lying states in ${}^{53}Mn$ could not be reproduced at the proper position, and the E2/M1 mixing ratios and branching ratios were not successful.

The strong coupling rotational model has been applied to ${}^{53}Mn$ by Malik and Scholz (Ma 66), but was not successful in most cases in reproducing the experimental data.

In the present work, the excited states of ${}^{53}Mn$ up to 3 MeV

excitation energy have been investigated by the $^{53}Cr(p,n\gamma)^{53}Mn$ reaction. Angular distributions, yield curves, branching ratios of the gamma decay of each level, and lifetimes of the ^{53}Mn levels were measured. The Doppler-shift attenuation method was used for the lifetime measurements. The angular distributions and yield curves were then compared with the predictions of the compound nuclear statistical model (Sh 66). The comparison yielded the level spins and multipole mixing ratios of the several transitions. The measured levels and electromagnetic properties of ^{53}Mn were compared with available theoretical calculations. The intermediate coupling unified model has been applied to ^{51}V and ^{53}Mn to investigate the nuclear structure, the properties of the low-lying excited states of those nuclei, and the similarity in the level structures of two nuclei.

CHAPTER II

GAMMA - RAY ANGULAR DISTRIBUTIONS

2.1 Theory

(a) The angular correlation

The first theoretical study of the angular correlations of a cascade of gamma rays was made by Hamilton (Ha 40). Since then, the theory of the angular correlations has been further developed and established in its present form by many authors (Bl 52, Bi 53).

The procedures for the measurement and analysis of angular correlations of gamma radiations from nuclear reactions were generalized by Litherland and Ferguson (Li 61) and have since been applied to numerous determinations of nuclear spins and mixing ratios of nuclear gamma-ray transitions. A form of the general gamma-ray distribution formula particularly suitable for use with the Litherland-Ferguson method was presented by Poletti and Warburton (Po 65). Recently, Rose and Brink (Ro 67) have given the angular distribution formulae expressed in terms of phase-defined reduced matrix elements. Therefore, no attempt will be made in this thesis to derive the detailed expressions involved in the theory. Instead, the principles and ideas involved in the general angular distribution formula will be stressed including the limitations encountered.

General case

The probability for a transition from a state $|J_1M_1\rangle$ to a state $|J_2M_2\rangle$ with emission of a circularly polarized photon (circular polarization quantum q) along the direction of $\vec{k}$ is given by (Ro 67)

$$W(J_1 \rightarrow J_2;\ \vec{k}\ q) \ = \ (k/2\pi\hbar) \sum_{KLL'\pi\pi'} B_K(J_1)\ P_K(\cos\theta)\ (-)^{q+J_1-J_2+L'-L-K}$$

$$\times\ (2J_1+1)^{\frac{1}{2}}\ (LL'q{-}q\,|\,K0)\ W\,(J_1J_1LL';KJ_2)$$

$$\times\ q^{\pi+\pi'} \langle J_1 \| T_L^{<\pi>} \| J_2\rangle \langle J_1 \| T_{L'}^{<\pi'>} \| J_2\rangle^{*}, \qquad \text{(II.1)}$$

with

$$B_K(J_1) \ = \sum_{M_1=-J_1}^{J_1} \omega\,(M_1)\ (-)^{J_1-M_1}\ (2J_1+1)^{\frac{1}{2}}\ (J_1J_1M_1{-}M_1\,|\,K0),$$

$$B_0\ (J_1) \ = 1, \qquad \sum_{M_1} \omega\ (M_1) \ = 1, \qquad \text{(II.2)}$$

where $(LL'q{-}q\,|\,K0)$ is a Clebsch-Gordan coefficient, $W\,(J_1J_1LL';KJ_2)$ is a Racah coefficient, $\langle J_1 \| T_L^{<\pi>} \| J_2\rangle$ is a reduced matrix element for a multipole operator, $\omega(M_1)$ is the population parameter of the substate M_1. There are restrictions in the formula, namely (i) the initial state has definite J_1 and does not necessarily have to have definite parity, (ii) the sum runs independently over all possible L, L', π, π' and K, where K can be odd as well as even, and (iii) the allowed (integer) values of L, L' are $|J_1-J_2| \leq L, L' \leq J_1+J_2$ and $L, L' \neq 0$.

Alignment case

The nuclear reaction is usually of the form $A(a,b)B^*$, where A is the target nucleus, a and b are the incoming and outgoing particles respectively, and B^* is the residual nucleus left in an excited state. The particles, b, leading to a state of spin J_1 in the residual nucleus are usually detected in a counter located on the beam axis. The angular distribution of the gamma rays from the de-excitation of the state $|J_1>$ is measured in coincidence with these particles. In these measurements, the beam and target nucleus are both unpolarized and the excited states of B^* are assumed to have definite parity. Under these conditions and the condition of cylindrical symmetry about the beam axis, the state $|J_1>$ will be aligned. An aligned state is one where the probability of population of the magnetic substate with projection M_1 on the beam axis is the same as for $-M_1$, i.e., $\omega(M_1) = \omega(-M_1)$.

When circular polarization is not observed, the angular distribution of gamma rays is expressed by (Ro 67)

$$W(\theta) = \sum_{\substack{(L\pi)(L'\pi') \\ K \text{ even}}} \frac{\{B_K(J_1)R_K(LL'J_1J_2)\delta_L^{<\pi>}\delta_{L'}^{<\pi'>}P_K(\cos\theta)\}}{\sum_L |\delta_L^{<\pi>}|^2}$$

$$\equiv \sum_{K \text{ even}} B_K(J_1)\ R_K\ (J_1J_2)\ P_K\ (\cos\theta) \qquad (11.3)$$

with

$$\delta_L^{<\pi>} = \frac{<J_1 \| T_L^{<\pi>} \| J_2>/(2L+1)^{\frac{1}{2}}}{<J_1 \| T_{\bar{L}}^{<\bar{\pi}>} \| J_2>/(2\bar{L}+1)^{\frac{1}{2}}},$$

$$R_K(J_1J_2) = \sum_{(L\pi)(L'\pi')} \frac{\{R_K(LL'J_1J_2)\delta_L^{<\pi>}\delta_{L'}^{<\pi'>}\}}{\sum\limits_L |\delta_L^{<\pi>}|^2} ,$$

$$R_K(LL'J_1J_2) = (-)^{1+J_1-J_2+L'-L-K} \{(2J_1+1)\ (2L+1)\ (2L'+1)\}^{\frac{1}{2}}$$

$$\times \ (LL'\ 1-1\,|\,K0)\ W\ (J_1J_1LL';KJ_2) \ , \qquad (II.4)$$

$$B_K(J_1) = \sum_{M_1=-J_1}^{J_1} \omega(M_1)\ (-)^{J_1-M_1}\ (2J_1+1)^{\frac{1}{2}}\ (J_1J_1M_1-M_1|K0) \ ,$$

$$B_0(J_1) = 1 \ , \qquad \sum_{M_1} \omega(M_1) = 1 \ ,$$

where $\delta_L^{<\pi>}$ is the mixing ratio and $\bar{L}$, $\bar{\pi}$ stand for the lowest-order multipolarity occurring in the transition $J_1 \rightarrow J_2$. The formula is restricted to the cases (i) J_1 and J_2 have definite parities, (ii) the sum over $(L\pi)$ is over all multipoles consistent with conservation of angular momentum and parity. The allowed values of L, L' are $|J_1 - J_2| \leq L, L' \leq (J_1 + J_2)$, $L, L' \neq 0$, and (iii) the sum is taken over even values of K only.

$B_K(J_1)$ depends on the nuclear alignment only and $R_K(J_1J_2)$ depends only on quantities which characterize the nuclear transition.

In a cascade decay, if the primary transition is not observed and the second transition is observed instead, the nuclear

alignment parameters $B_K(J_1)$ must be replaced by $B_K(J_1)\ U_K(J_1J_2)$. The distribution formula is then given by (Ro 67)

$$W(\theta) = \sum_K B_K(J_1)\ U_K\ (J_1J_2)\ R_K\ (J_2J_3)\ P_K\ (\cos\theta)\ , \qquad (II.5)$$

with

$$U_K(J_1J_2) = \sum_{L_{12}} (\delta_{L_{12}})^2\ U_K\ (L_{12}J_1J_2) / \sum_{L_{12}} (\delta_{L_{12}})^2,$$

$$U_K(L_{12}J_1J_2) = (-)^K\ \frac{W(J_1J_1J_2J_2;KL_{12})}{W(J_1J_1J_2J_2;0L_{12})}\ , \qquad (II.6)$$

$$(\delta_{L_{12}})^2 = \left| \frac{\langle J_1 \| T_{L_{12}}^{\langle \pi_{12} \rangle} \| J_2 \rangle / (2L_{12}+1)^{\frac{1}{2}}}{\langle J_1 \| T_{\bar{L}_{12}}^{\langle \bar{\pi}_{12} \rangle} \| J_2 \rangle / (2\bar{L}_{12}+1)^{\frac{1}{2}}} \right|^2$$

where $J_1 \rightarrow J_2$ is the primary transition (with L_{12}, L'_{12}) unobserved and $J_2 \rightarrow J_3$ is the second transition (with L, L') observed.

The expression of the angular distribution is simplified with a specialization to the most common in practice when only two multipoles ($\bar{L}$ and L being the lowest order multipoles in ascending order, respectively) contribute to the transition (Ro 67) :

$$W(\theta) = \sum_K B_K(J_1)\ P_K(\cos\theta) \frac{\{R_K(\bar{L}\bar{L}J_1J_2) + 2\delta R_K(\bar{L}LJ_1J_2) + \delta^2 R_K(LLJ_1J_2)\}}{(1+\delta^2)}\ , \qquad (II.7)$$

with

$$\delta = \frac{<J_1 \| T_L^{<\pi>} \| J_2>/(2L+1)^{\frac{1}{2}}}{<J_1 \| T_{\bar{L}}^{<\bar{\pi}>} \| J_2>/(2\bar{L}+1)^{\frac{1}{2}}} ,$$

$$R_K(L\bar{L}J_1J_2) = (-)^{1+J_1-J_2+\bar{L}-L-K}\{(2J_1+1)\ (2L+1)\ (2\bar{L}+1)\}^{\frac{1}{2}}$$

$$\times\ (L\bar{L}\ 1-1 \mid K0)\ W\ (J_1J_1L\bar{L};KJ_2) ,$$

$$B_K(J_1) = \sum_{M=-J_1}^{J_1} \omega(M_1)\ (-)^{J_1-M_1}(2J_1+1)^{\frac{1}{2}}\ (J_1J_1M_1-M_1 \mid K0) .$$

In a cascade decay, similarly $U_K(J_1J_2)$ is given by

$$U_K(J_1J_2) = \frac{\{U_K(\bar{L}_{12}J_1J_2) + (\delta_{L_{12}})^2 U_K(L_{12}J_1J_2)\}}{[1+(\delta_{L_{12}})^2]} . \qquad (II.8)$$

A finite sized gamma-ray detector has an effect on the distribution, i.e., it simply reduces the variation of counting rate with angle. This effect can be accounted for by inserting an attenuation coefficient Q_K in the distribution formula. The Q_K coefficients are tabulated by Rutledge (Ru 59).

In general, all magnetic substates with $|M_1| \leq J_1$ can be populated by the reaction and the $\omega(M_1)$ depend critically on the reaction mechanism and must be treated as unknowns. When

the particles are detected on axis at 180° (or 0°), however, the number of these parameters is limited because the orbital angular momentum has zero projection along the direction of motion of the particle. The maximum magnetic substate is given by

$$M_1\ (\mathrm{MAX}) = |S_A| + |S_a| + |S_b|, \tag{II.9}$$

where S_A, S_a, and S_b are the spins of the target nucleus, incoming and outgoing particle, respectively.

Both the experimental and theoretical angular distributions of a gamma ray de-excitation of a residual state formed in a nuclear reaction can be expressed in terms of a Legendre polynomial series of θ, the angle made with the beam direction:

$$W(\theta)_{\mathrm{exp}},\ W(\theta)_{\mathrm{th}} = \sum_{K\ \mathrm{even}} a_K P_K\ (\cos\theta) \tag{II.10}$$

Therefore, the experimental a_K can be compared with the theoretical one,

$$a_K = B_K\ (J_1)\ \frac{\{R_K(LLJ_1J_2) + 2\delta R_K(L\bar{L}J_1J_2) + \delta^2 R_K(\bar{L}\bar{L}J_1J_2)\}}{1+\delta^2}, \tag{II.11}$$

to determine the quantities associated with the properties of levels and gamma-ray transitions.

In the χ^2 analysis, gamma-ray intensities measured at a series of angles $Y(\theta_i)$ are to be compared with the $W(\theta_i)$

calculated assuming certain spin J_1, mixing ratio δ and population parameters, $\omega(M_1)$. The goodness of fit is measured by the value of χ^2, defined by

$$\chi^2 = \frac{1}{n} \sum_i \frac{[Y(\theta_i) - W(\theta_i)]^2}{E^2(\theta_i)} , \tag{II.12}$$

where $E(\theta_i)$ is the uncertainty assigned to the gamma-ray yield $Y(\theta_i)$ at angle θ_i, and n is the number of degrees of freedom. The value of n is given by

n = (no. of angles taken for data) - (no. of substates populated).

A plot of χ^2 versus δ will then show dips corresponding to possible solutions for at least one set of the allowed spins.

(b) The compound nuclear statistical model

The compound nucleus

The compound nucleus picture was first proposed by Bohr (Bo 36) and developed into the evaporation model by Bohr and Kalcker (Bo 37), Bethe (Be 37) and Weisskopf (We 37). The early compound nucleus theory has been described in detail in a review article of Bethe (Be 37). The compound nucleus process can be briefly described:

In the nuclear reaction, the incident particle passing between two nucleons in the target nucleus must interact strongly with them, since the average distance between the

nucleons is of the same order as the range of the nuclear forces and the nuclear forces are very strong inside their range of action. The incident particle will therefore lose part of its energy as soon as it strikes the surface of the nucleus, by transferring it to the nucleons. Thus the initial energy of the incident particle will be distributed among all the particles of the system, "compound nucleus", consisting of the original nucleus and the incident particle. After a comparatively long time, the energy may again be concentrated by accident on one particle, so that this particle can escape.

Therefore, the nuclear reaction can primarily be described by the scheme:

$$\begin{pmatrix}\text{Incident}\\ \text{nucleus}\end{pmatrix} + \begin{pmatrix}\text{Incident}\\ \text{particle}\end{pmatrix} \rightarrow \begin{pmatrix}\text{Compound}\\ \text{nucleus}\end{pmatrix} \rightarrow \begin{pmatrix}\text{Final}\\ \text{nucleus}\end{pmatrix} + \begin{pmatrix}\text{Outgoing}\\ \text{particle}\end{pmatrix}$$

The early evaporation model

The evaporation model first proposed by Bethe (Be 37) and Weisskopf (We 37) was fully developed into a rough workable model as described by Blatt and Weisskopf (Bl 52a).

As mentioned before, the compound nucleus model divides the nuclear reaction into two events. The first is the formation of a compound nucleus in a well-defined state in which the incident energy is shared among all the constituents; the second is the disintegration of that compound system, which can be treated as independent of the first stage of the process.

The compound nucleus has some analogy with the thermodynamical processes. The energy stored in the compound nucleus can be compared with the heat energy of a solid body or a liquid, and the subsequent expulsion of particles is analogous to an evaporation process.

The compound nucleus process, $c \to c^* \to c'$, is assumed to have an average cross section,

$$\bar{\sigma}_{cc'} = [\sigma_{comp}(c)] \left[\frac{G_{c'}}{G}\right] , \qquad (11.13)$$

where c stands for the initial pair of particles, c^* the compound nucleus, and c' the final reaction products. $\sigma_{comp}(c)$ depends only on c and is called a cross section for the formation of the compound nucleus. $G_{c'}/G$ depends only on c' and is called a branching ratio. G is a sum of the factor $G_{c'}$ over all the pairs of reaction products available to the compound nucleus, i.e., $G \equiv \sum_{c''} G_{c''}$. This is an expression of the independence of formation and decay of the compound nucleus, which is frequently referred to as the Bohr assumption.

By the reciprocity theorem, $k_c^2 \bar{\sigma}_{cc'} = k_{c'}^2 \bar{\sigma}_{c'c}$, the average cross section is given by (Vo 68)

$$\bar{\sigma}_{cc'} = \sigma_{comp}(c) \frac{k_{c'}^2 \sigma_{comp}(c')}{\sum\limits_{c''} k_{c''}^2 \sigma_{comp}(c'')} , \qquad (11.14)$$

where k_c is the wave number for the relative motion of the pair c.

There are two major defects in the early evaporation theory: (i) the cross section formula lacks conservation of total angular momentum and parity, and (ii) it does not exhibit the giant resonances which are one of the dominant features of the interaction between a nucleon and a nucleus.

The Hauser - Feshbach model

The early evaporation model can be defined on the basis of conservation of total angular momentum (and parity) and of consideration of absorption cross section with the optical model.

Hauser and Feshbach (Ha 52), following suggestions by Wolfenstein (Wo 51), first added conservation of total angular momentum and parity to the neutron cross section of the old theory and established the compound nuclear statistical theory in the present form, which is often referred to as the Hauser-Feshbach model, after the authors. The Hauser - Feshbach model has been described in detail in a review article by Vogt (Vo 68).

Hauser and Feshbach assumed that the probability of decay of the compound nucleus yielding a neutron of given orbital angular momentum ℓ is a function of the transmission coefficient T_ℓ (α).

In the Hauser - Feshbach model, the average cross section may be written (Vo 68)

$$\bar{\sigma}_{\alpha\alpha'} = \frac{\pi}{k_\alpha^2} \sum_{J,\Pi} \frac{2J+1}{(2I+1)(2i+1)} \left\{ \sum_{s\ell} T_\ell(\alpha) \right\} \left\{ \frac{\sum_{s'\ell'} T_{\ell'}(\alpha')}{\sum_{\alpha''s''\ell''} T_{\ell''}(\alpha'')} \right\}, \quad (11.15)$$

where the unprimed quantities refer to the incoming channels of the reaction, the primed quantities refer to the outgoing channels, and the double-primed quantities in the denominator are summed over all channels into which the compound nucleus can decay. α labels the pair of particles and their state of excitation, I and i are the intrinsic spins of the pair of particles α, s is the channel spin ($\vec{s} = \vec{I} + \vec{i}$), ℓ is the orbital angular momentum of the pair, J is the total angular momentum ($\vec{J} = \vec{\ell} + \vec{s}$). $T_\ell(\alpha)$ are called transmission functions and are given by the optical-model phase shifts $\delta_{\alpha\ell}$ of the pair α

$$T_\ell(\alpha) \equiv 1 - |e^{2i\delta_{\alpha\ell}}|^2 . \qquad \text{(II.16)}$$

Π is the total parity: the product of $(-)^\ell$ with the intrinsic parities of the pair α.

The differential cross section is given by (Vo 68)

$$\frac{d\bar{\sigma}_{\alpha\alpha'}}{d\Omega} = \sum_L \frac{1}{4k\alpha^2} \sum_{J\Pi} \frac{1}{(2I+1)(2i+1)} \left\{\sum_{s\ell} T_\ell(\alpha)\right\} \qquad \text{(II.17)}$$

$$\times \sum_{s'\ell'} \left\{\frac{T_{\ell'}(\alpha')}{\sum_{s''\ell''\alpha''} T_{\ell''}(\alpha'')}\right\} Z(\ell J \ell J; sL) Z(\ell' J \ell' J; s'L) (-)^{s-s'}$$

$$\times P_L(\cos\theta) ,$$

where the Z's are the Z coefficients of Blatt and Biedenharn (Bl 52). In eq. (II.17) all interference of incoming partial waves with each other and of outgoing partial waves with each other are ignored; the lack of

interference has a direct consequence on the shape of the average angular distributions which are symmetric about 90°. This property is manifested through the coefficients $Z(\ell J \ell J; sL)$, which vanish unless L is even. The sums of eqs. (II.15) and (II.17) run over the following values: $J = 0, 1, 2 \ldots$ if the compound nucleus has even mass number and $J = \frac{1}{2}, \frac{3}{2}, \frac{5}{2} \ldots$ otherwise; $I - i \leq s$ (integer) $\leq I + i$; $|J - s| \leq \ell$ (even) $\leq |J + s|$ if the pair α has the same parity as Π and $|J - s| \leq \ell$ (odd) $\leq |J + s|$ otherwise.

The gamma-ray angular distributions

The angular distribution of gamma rays following a nuclear reaction based on the Hauser-Feshbach theory was first derived by Satchler (Sa 54, Sa 56) and emended, with inclusion of the effect of spin-orbit interactions, by Sheldon (Sh 63a, Sh 66).

Sheldon replaced the standard transmission coefficient T_ℓ by the generalized penetrability $T_{\ell j}$ under consideration of the spin-orbit interaction in the optical potential (Sh 67, Sh 69):

$$T_\ell = \frac{[(\ell+1)\, T_\ell^{(+)} + \ell\, T_\ell^{(-)}]}{2\ell + 1} \qquad \text{(II.18)}$$

where the superscript (±) labels the value of j according as $J = \ell \pm \frac{1}{2}$. The theory of the gamma-ray angular distributions based on the compound nuclear statistical model has been described in detail in a review article of Sheldon and van Patter (Sh 66).

Assume the reaction $A(a,b)B^*$ proceeds in two steps: first formation of the compound nucleus C^*, a state $|J_1\rangle$ with definite angular momentum and parity, then decay by emission of a nucleon b, leading to a state $|J_2\rangle$ in the residual nucleus B^* (see Fig. 1).

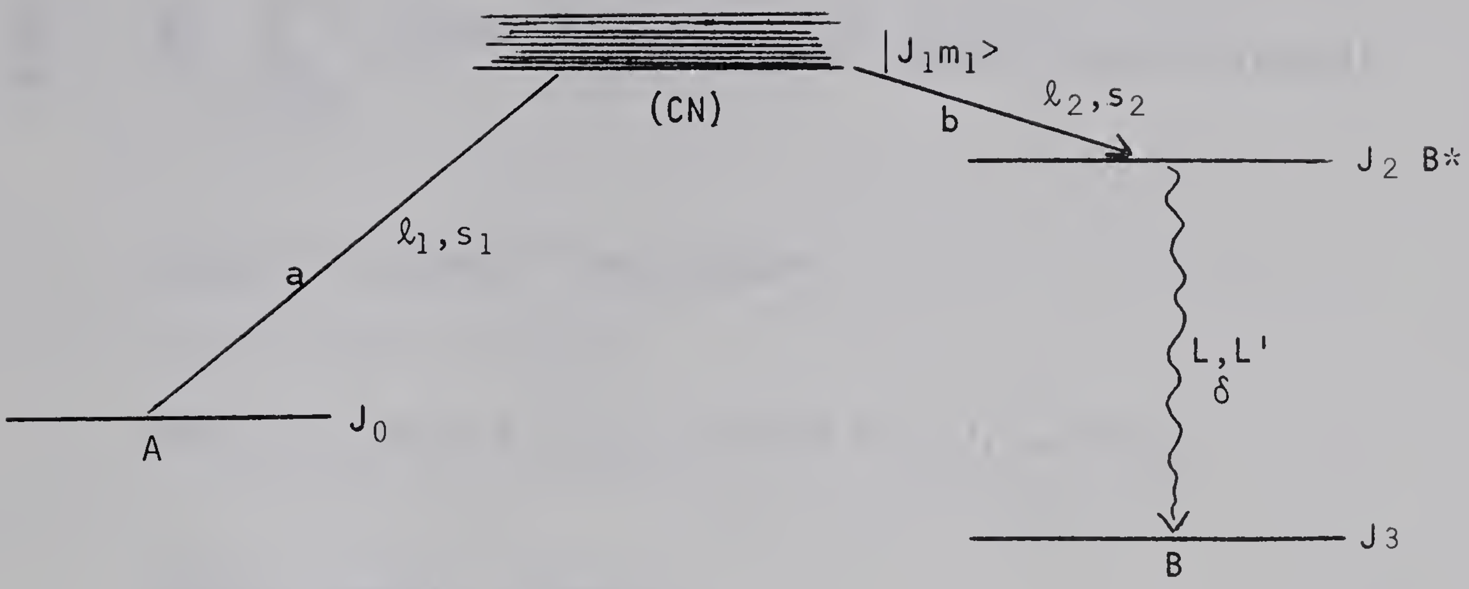

Fig. 1

A schematic diagram of the (p,nγ) reaction process.

Under the alignment conditions that (i) neither the beam of incident particles nor the target nuclei are polarized, (ii) the beam direction is chosen as the quantization axis (z-axis), and (iii) the outgoing particles are assumed to have s-waves ($\ell = 0$), the substates in C* are populated up to $|m_1|_{max} = J_0 + s_1$ and for the residual nuclear state B*, $|m_2|_{max} = (J_0 + s_1) + s_2$.

The general expression for a differential cross section is given as a Legendre polynomial expansion of even order:

$$\frac{d\sigma}{d\Omega} = \sum_K a_K P_K (\cos\theta) \ . \qquad (II.19)$$

For the (a,bγ) process, the predicted angular distribution for a gamma-ray transition of mixed multipolarity L, L' with a mixing ratio δ is given by (Sh 69)

[illegible]

[illegible]

[illegible]

[illegible]

[illegible]

$$\frac{d\sigma}{d\Omega} = \frac{\lambda\!\!\!^{-2}}{4} \sum_{j_1 j_2 K} (-)^{J_0+J_3-s_1-j_2-1} (2J_1+1)^2 \; (2\ell_1+1) \; (2j_1+1) \; (2J_2+1)$$

$$\times \; (2J_0+1)^{-1} \; (2s_1+1)^{-1} \; \langle K0 | \ell_1 \ell_1 00 \rangle$$

$$\times \; W(\ell_1 \ell_1 j_1 j_1 ; K s_1) \; W\,(j_1 j_1 J_1 J_1 ; K J_0) \; W\,(J_1 J_1 J_2 J_2 ; K j_2)$$

$$\times \; \frac{M(\bar{L}\bar{L}) + 2\delta M(\bar{L}L) + \delta^2 M(LL)}{1 + \delta^2}$$

$$\times \; \frac{T_{\ell_1}(E_1) \cdot T_{\ell_2}(E_2)}{\sum\limits_{\ell j E} T_\ell (E)} \cdot P_K \; (\cos\theta) \qquad \text{(II.20)}$$

with

$$M(\bar{L}L) = \sqrt{(2\bar{L}+1)(2L+1)} \; \langle K0 \,|\, \bar{L}L \; 1-1 \rangle \; W(J_2 J_2 \bar{L}_2 L_2 ; K J_3)$$

$$T_\ell (E) = \frac{(\ell+1) \; T_\ell^{(+)}(E) + \ell T_\ell^{(-)}(E)}{2\ell + 1} \qquad \text{(II.21)}$$

$$\delta = \frac{\langle J_3 || L || J_2 \rangle}{\langle J_3 || \bar{L} || J_2 \rangle}$$

where K is restricted to $0 \leq K \leq 2j_1, 2J_1, 2J_2, 2L$, $\langle J_3 || L || J_2 \rangle$ is a reduced matrix element proportional to multipole amplitude, $\lambda\!\!\!^{-}$ is a rationalized de Broglie incident

wavelength, $\lambda\!\!\!^{-} = \frac{\hbar}{\sqrt{2M_1E_1}}$, and $\bar{L}$, L are the lowest order multipoles in ascending order, respectively.

The angular distribution formula can be expressed in terms of the notation of Rose and Brink (Ro 67). The $R_k(\bar{L}LJ_2J_3)$ coefficient is given by (Ro 67)

$$R_K(\bar{L}LJ_2J_3) = (-)^{1+J_2-J_3+L-\bar{L}-K}\{(2J_2+1)(2\bar{L}+1)(2L+1)\}^{\frac{1}{2}}$$

$$\times <K0|\bar{L}L\,1-1>W(J_2J_2\bar{L}L;KJ_3),$$

since $L = \bar{L}+1$ and K = even ,

$$= (-)^{J_2-J_3}\{(2J_2+1)(2\bar{L}+1)(2L+1)\}^{\frac{1}{2}}$$

$$\times <K0|\bar{L}L\,1-1>W(J_2J_2\bar{L}L;KJ_3) \tag{II.22}$$

Therefore, $M(\bar{L}L)$ is expressed in terms of $R_K(\bar{L}LJ_2J_3)$ by

$$M(\bar{L}L) = \{(2\bar{L}+1)(2L+1)\}^{\frac{1}{2}}<K0|\bar{L}L\,1-1>W(J_2J_2\bar{L}L;KJ_3)$$

$$= (-)^{J_3-J_2}(2J_2+1)^{-\frac{1}{2}}R_K(\bar{L}LJ_2J_3). \tag{II.23}$$

Substituting $M(\bar{L}L)$ in the angular distribution formula,

$$\frac{d\sigma}{d\Omega} = \frac{\lambda\!\!\!^{-2}}{4}\sum_{j_1j_2K}(-)^{J_0-J_2-s_1-j_2-1}(2J_1+1)^2(2\ell_1+1)(2J_1+1)(2J_2+1)^{\frac{1}{2}}$$

$$\times \; (2J_0 + 1)^{-1} \; (2s_1 + 1)^{-1} \langle K0 | \ell_1 \ell_1 00 \rangle \; W \, (\ell_1 \ell_1 j_1 j_1 ; K s_1)$$

$$\times \; W \, (j_1 j_1 J_1 J_1 ; K J_0) \; W \, (J_1 J_1 J_2 J_2 ; \; K j_2)$$

$$\times \; \frac{R_K(\bar{L}\bar{L}J_2J_3) \; + 2\delta \, R_K(\bar{L}LJ_2J_3) \; + \; \delta^2 R_K(LLJ_2J_3)}{1 + \delta^2}$$

$$\times \; \frac{T_{\ell_1}(E_1) \cdot T_{\ell_2}(E_2)}{\sum\limits_{\ell j E} T_\ell(E)} \cdot P_K \, (\cos\theta) \; . \qquad \text{(II.24)}$$

Although the compound nucleus picture is an old one, it has been adapted surprisingly well to modern ideas about the nucleus and has developed into one of the most reliable quantitative tools we have in nuclear physics.

The CN statistical model of Sheldon and van Patter can be used to analyze angular distributions following reactions of the forms (p,nγ), (α,nγ), (p,p'γ) and (n,n'γ). To fulfill the condition $\ell_2 = 0$, the energy of the outgoing particle must be near zero; this can be arranged by suitably selecting the bombarding energy to produce the reaction near threshold. Since this approach requires only an angular distribution measurement rather than angular correlation and coincidence data, it has the advantage of experimental simplicity.

2.2 Experimental Method

(a) Apparatus

The experiments were performed with protons from the University of Alberta 5.5 MV Van de Graaff accelerator.

Thick targets were prepared by mixing an enriched ($<0.05\%$ ^{50}Cr, 3.44% ^{52}Cr, 96.4% ^{53}Cr and 0.18% ^{54}Cr) Cr_2O_3 powder into a glue formed by dissolving polyurethane in benzene and applying the viscous mixture to a tantalum backing.

The target chamber was a 5 cm diam. cylindrical piece of lucite faced at 60° to the beam direction; the beam entered the target chamber through a 1.35 cm diam. aperture. A thin aluminum plate at the back of the target served as a charge collector. The target chamber is described in Fig. 2.

Gamma rays were detected in a 43.8 cc Ge(Li) crystal for the angular distribution measurements and in a 15 cc Ge(Li) crystal for the yield curve measurements.

The gamma-ray pulses from a Ge(Li) detector-pre-amplifier assembly were amplified in a main-amplifier and then sent into an analog-to-digital converter (ADC), and thence to the on-line SDS 920 computer equipped with display.

(b) Detection efficiency

The Ge(Li) detector must be calibrated for detection efficiency before analysis of the experimental data, in particular, the branching ratio analysis.

Fig. 2 The target chamber.

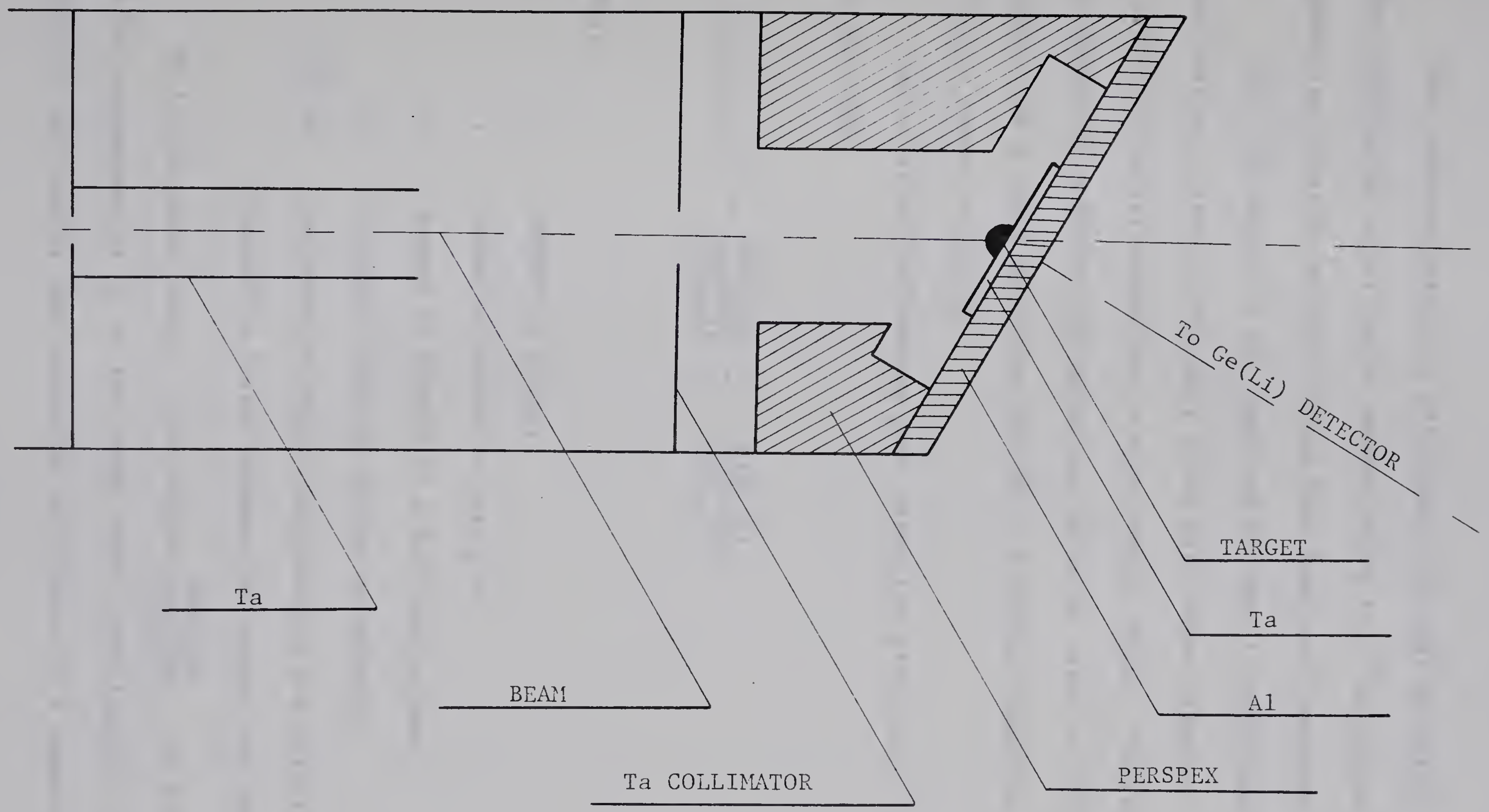
To Ge(Li) DETECTOR
TARGET
Ta
Al
PERSPEX
Ta COLLIMATOR
BEAM
Ta

The relative detection efficiency (Ch 70a) of Ge(Li) detectors was obtained by a pair-point method using the ^{56}Co source whose gamma-ray relative emission rates have been well measured (Ma 68).

The ^{56}Co source is of great usefulness in efficiency calibration, since it has many lines with known relative intensities distributed over a wide energy range. The values of gamma-ray energies and gamma-ray emission rates of ^{56}Co were taken from a table by Marion (Ma 68). A typical spectrum of ^{56}Co is shown in Fig. 3.

The relative full-energy peak detection efficiency is given by (Ch 70a)

$$\varepsilon\,(E_1,\, E_2,\, d) \;=\; \frac{A(E_1,d)}{A(E_2,d)} \cdot \frac{I_2}{I_1} \cdot \frac{\alpha(E_2,d)}{\alpha(E_1,d)}\,, \qquad \text{(II.25)}$$

where

E : Gamma-ray energy

I : Gamma-ray emission rate /sr

A : Number of counts in a full-energy peak

d : Distance from the source to detector

$\alpha(E,d)$: Attenuation factor representing the effects of absorbing layers between the source and detector.

As in the usual case, if the ratios, $\frac{A(E_1,d)}{A(E_2,d)}$, are assumed to be independent of d in the range under investigation, the relative full-energy peak detection efficiency of a gamma-ray

Fig. 3 A typical gamma-ray spectrum of ^{56}Co

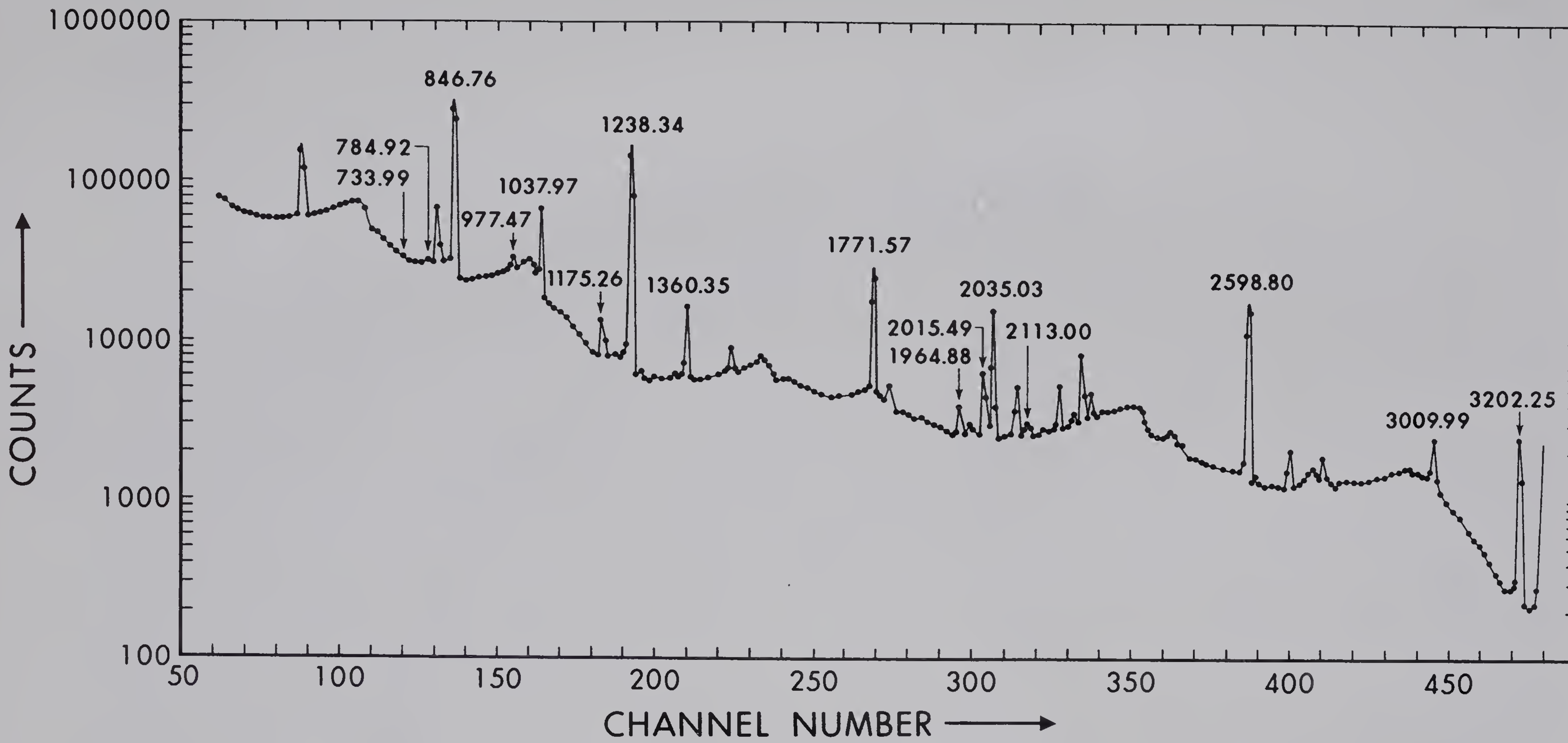
846.76
784.92
733.99
1238.34
1037.97
977.47
1175.26
1360.35
1771.57
2035.03
2015.49
1964.88
2113.00
2598.80
3009.99
3202.25
1000000
100000
10000
1000
100
COUNTS
50
100
150
200
250
300
350
400
450
CHANNEL NUMBER

Fig. 4 Relative full-energy peak efficiency curve for the Ortec 43.8 cc Ge(Li) detector.

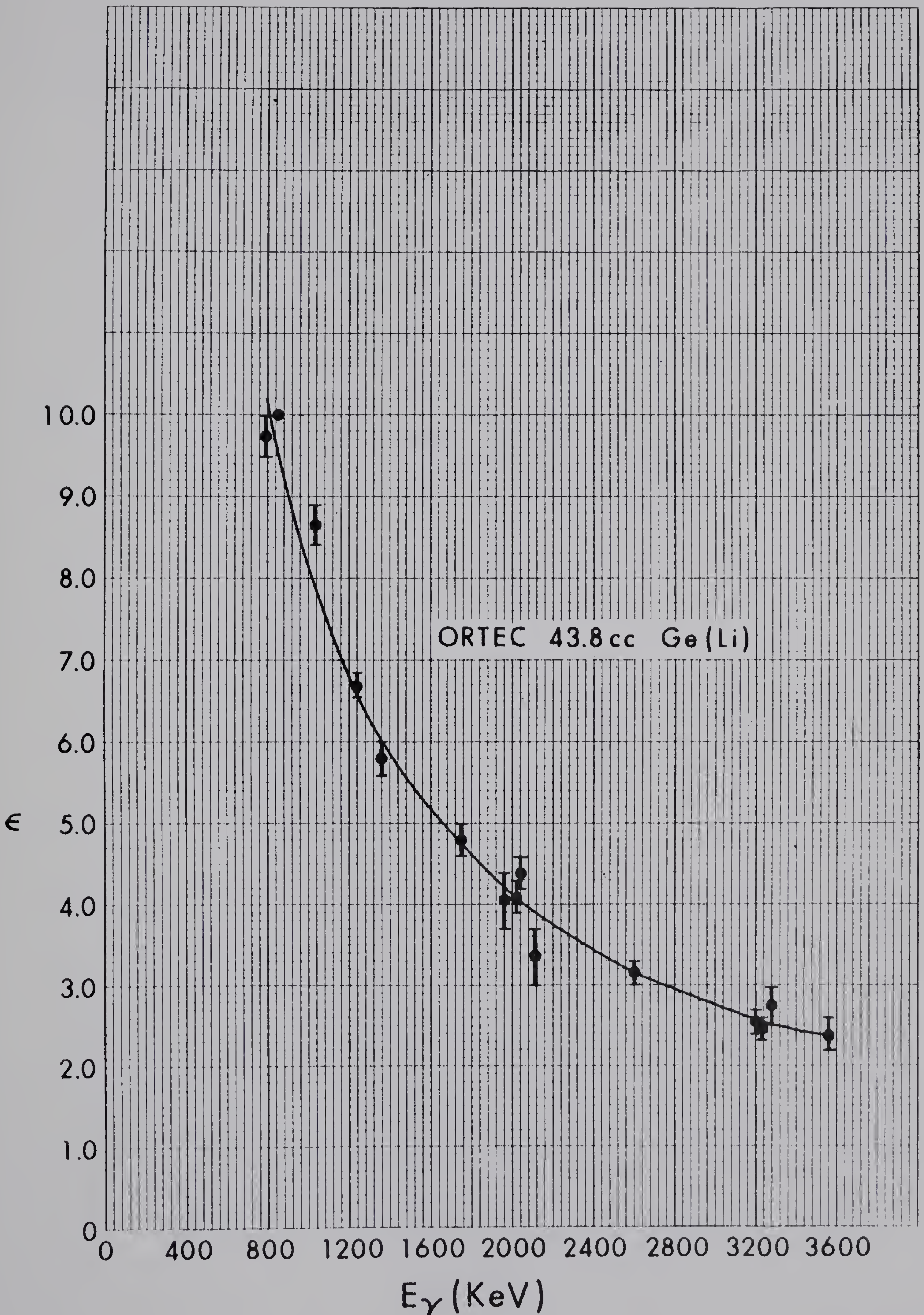
ORTEC 43.8cc Ge(Li)
ε
10.0
9.0
8.0
7.0
6.0
5.0
4.0
3.0
2.0
1.0
0
0
400
800
1200
1600
2000
2400
2800
3200
3600
Eγ (KeV)

Fig. 5 Comparison of the shapes of the relative full-energy peak efficiencies for the three Ge(Li) detectors.

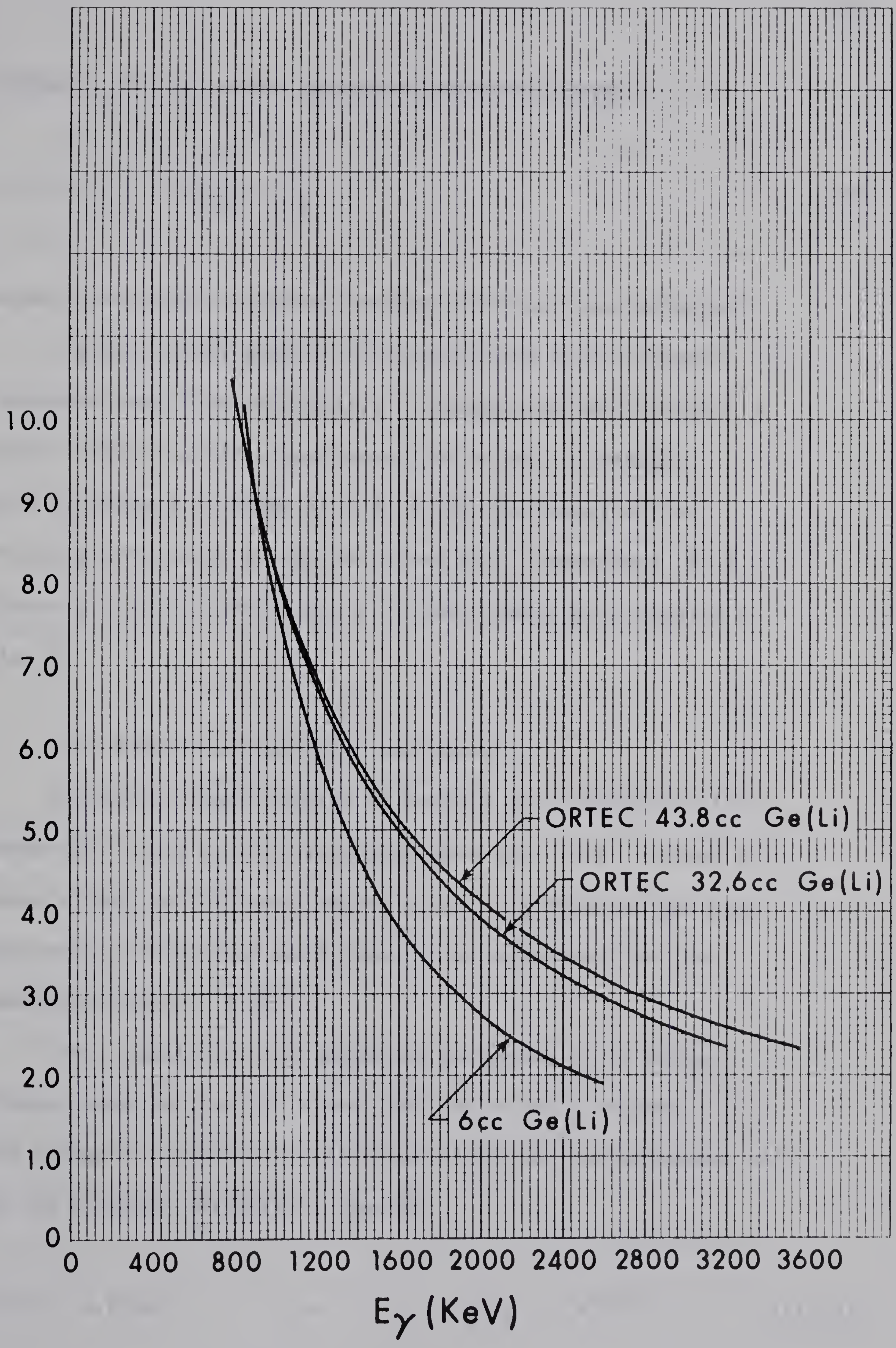
10.0
9.0
8.0
7.0
6.0
5.0
4.0
3.0
2.0
1.0
0
0
400
800
1200
1600
2000
2400
2800
3200
3600
E_γ (KeV)
ORTEC 43.8cc Ge(Li)
ORTEC 32.6cc Ge(Li)
6cc Ge(Li)

energy E_i to the common reference gamma-ray energy E_o is

$$\varepsilon\ (E_i,\ E_o) \;=\; \frac{A(E_i)}{A(E_o)} \cdot \frac{I_o}{I_i}\ , \tag{II.26}$$

without any absorbing layer between the source and detector.

The 846.76 keV peak of ^{56}Co was chosen as the common reference peak with which pairs of gamma-rays were formed. A typical relative efficiency curve for a Ge(Li) detector, 43.8 cc (Ortec) is shown in Fig. 4 and the shapes of the relative efficiency curves for three Ge(Li) detectors, 43.8 cc (Ortec), 32.6 cc (Ortec) and 6 cc (home made) are compared in Fig. 5.

(c) Gamma-ray absorption corrections

Corrections were applied to account for absorption of the gamma-ray in the target background materials (i.e., Ta and Al) whose effective thickness varies with the γ-detector position. Absorption corrections were found to be necessary for the gamma-rays below 1.5 MeV.

The intensity of the gamma-ray decreases as it passes through material in such a way that for a small thickness Δx, the change in intensity ΔI is proportional to the thickness and to the incident intensity I (Da 52):

$$\Delta I \;=\; -\mu I \Delta x \qquad \text{or} \qquad I/I_o \;=\; e^{-\mu x}\ , \tag{II.27}$$

where μ is known as the absorption coefficient.

The total absorption coefficient, μ, is composed of three partial cross-sections of gamma-ray interaction with matter, Compton σ, photoelectric τ, and pair production κ, where $\mu = \sigma + \tau + \kappa$. Fig. 6 shows the curves for the total absorption coefficients plotted against gamma-ray energies using available data (Da 52, Al 70, Da 66) for Ta, Al, Pt and Pb in unit of cm^{-1}.

(d) Yield curves, branching ratios and angular distributions

The energy calibration was made with ^{56}Co, ^{22}Na and ^{60}Co sources, and also the known lines in the ^{53}Mn spectrum below 2 MeV excitation energy. Levels were identified by the appearance of a new gamma-ray in the spectra as the bombarding energy was increased above threshold for that level. The contaminants were mainly due to the ^{72,74}Ge(n,n'γ), ^{52,53}Cr(p,p'γ) reactions. A ^{28}Si contaminant was also present.

The branching ratios were measured at 55°. Gamma-ray yield curves were measured in the proton energy range from 3 MeV to 5 MeV in 200 keV steps. The proton bombarding energies for the angular distributions were chosen close to threshold for the states under investigation. The angular distributions were measured at angles of 0°, 30°, 45°, 60° and 90° with respect to the beam direction at several proton bombarding energies between 3.78 and 5.00 MeV. The measurement at each

Fig. 6 Gamma-ray total absorption coefficients.

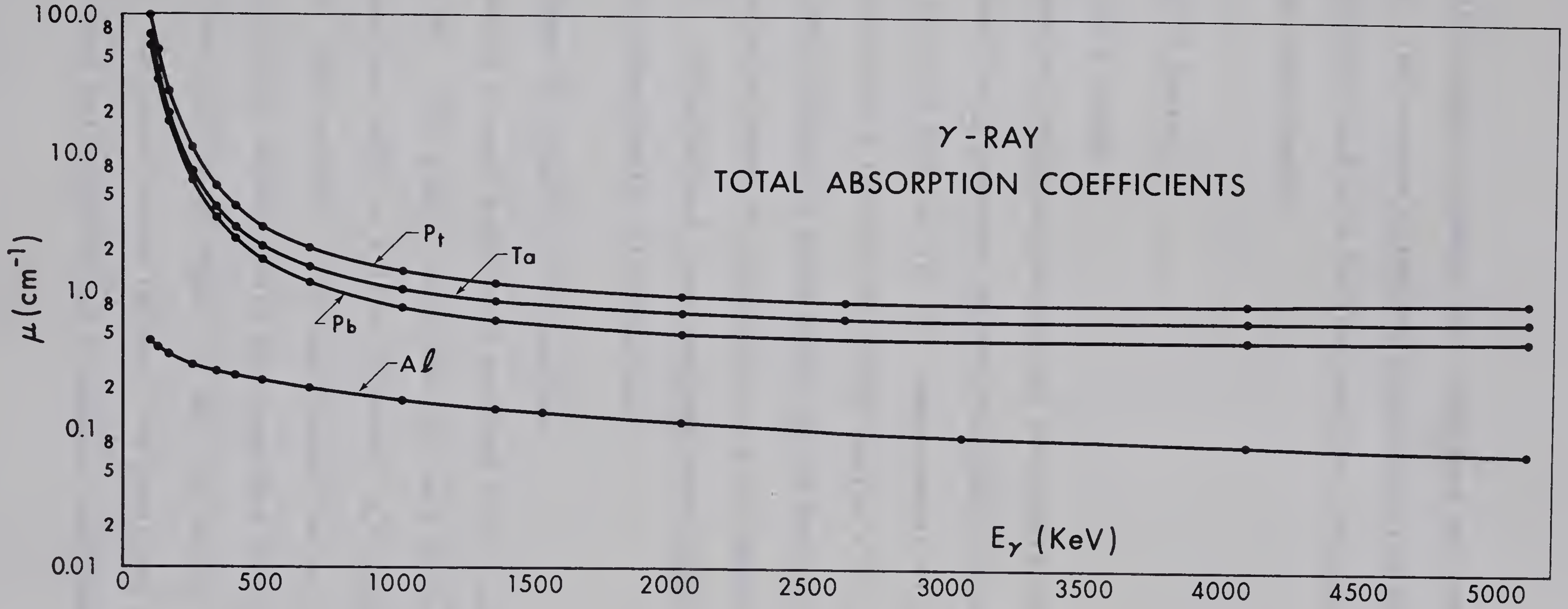
γ-RAY
TOTAL ABSORPTION COEFFICIENTS
Pt
Ta
Pb
Al
μ (cm⁻¹)
100.0
8
5
2
10.0
8
5
2
1.0
8
5
2
0.1
8
5
2
0.01
0
500
1000
1500
2000
2500
3000
3500
4000
4500
5000
Eγ (KeV)

angle required typically about four hours and was repeated at least once. The intense 0.378 MeV transition from the first excited state was used as a monitor peak for the angular distribution measurements.

2.3 Method of Analysis

(a) Yield curves

The absolute cross section (Ha 52) for population of the decaying level via a compound nuclear reaction is directly related to its spin (and parity) J^{π}. Measurements of the change in cross section as a function of proton energy will yield, in practice, some information about spins of the levels in ^{53}Mn, since the detailed shape of the yield curve can depend on the value of J^{π}. The predicted cross sections were calculated and compared with experimental distributions.

(b) Gamma-ray angular distributions

The spectra at each angle were analyzed with a peak-fitting program (Te 66). The angular distributions were fitted to a Legendre expansion, $W(\theta) = A_0(1 + a_2P_2(\cos\theta) + a_4P_4(\cos\theta))$ using the method of least squares. The experimental values of a_2 and a_4 coefficients were compared with the predicted values of the compound nuclear statistical model (Sh 66) for various spin sequences and multipole mixing ratios. The predicted a_2 and a_4 coefficients were calculated using a computer code MANDY (Sh 66).

The proton and neutron transmission coefficients required in the statistical model analysis were obtained from a Hauser-Feshbach (Ha 52) calculation using the Perey (Pe 62) proton optical model parameters and the Rosen (Au 62) neutron parameters. A quantitative comparison between the predictions and the experimental data was made using a χ^2 analysis (Gr 70). Combinations of spin and mixing ratio were rejected if χ^2 exceeded the 0.1% confidence limit. The Rose and Brink (Ro 67) sign convention for the mixing ratio δ was adopted.

2.4 Experimental Results

Typical gamma-ray spectra, singles and coincidence, are shown in Figs. 7 and 8. The spectrum in Fig. 7 shows the relative intensities of the excited states of ^{53}Mn and other peaks from (p,p'γ) and (n,n'γ) reactions on ^{52,53}Cr, ^{28}Si and ^{72,74}Ge, respectively. All excited levels in ^{53}Mn up to 3.250 MeV which were found in the (p,n) experiment (Ta 70) appear in this spectrum. The Legendre polynomial coefficients obtained for the present gamma-ray angular distributions are given in table 2. Summaries of all the angular distribution results and a decay scheme are given in Fig. 9. The yield curves measured at 90° and their comparison with theoretical curves are shown in Figs. 10 and 11. Angular distributions of all the gamma-ray transitions observed are shown in Figs. 21 to 23.

Fig. 7 A gamma-ray spectrum at 55° for the $^{53}Cr(p,n\gamma)^{53}Mn$ reaction, E_p = 5.20 MeV. Single primes and double primes denote single escape peaks and double escape peaks of the corresponding gamma-rays, respectively.

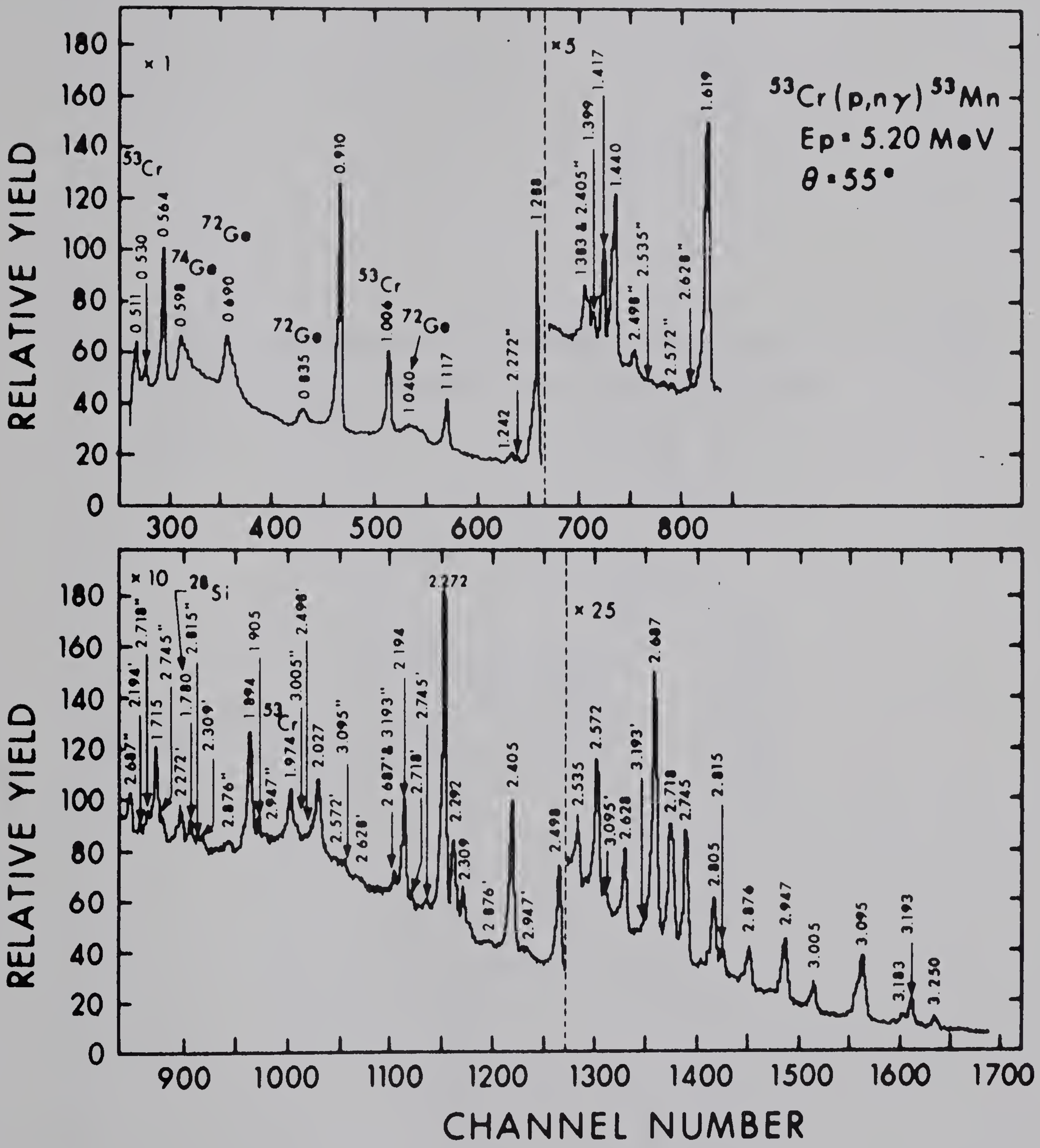

$^{53}Cr(p,n\gamma)^{53}Mn$
Ep = 5.20 MeV
θ = 55°
× 1
× 5
× 10
× 25
^{53}Cr
^{72}Ge
^{74}Ge
^{28}Si
0.511
0.530
0.564
0.598
0.690
0.835
0.910
1.006
1.040
1.117
1.242
2.272"
1.288
1.383 & 2.405"
1.399
1.417
1.440
2.498"
2.535"
2.572"
2.628"
1.619
2.687"
2.194'
2.718"
1.715
2.745"
2.272'
1.780
2.815"
2.309'
2.876"
1.894
1.905
2.947"
1.974
3.005"
2.498'
2.027
3.095"
2.572'
2.628'
2.687'& 3.193"
2.194
2.718'
2.745'
2.272
2.292
2.309
2.876'
2.405
2.947'
2.498
2.535
2.572
3.095'
2.628
3.193'
2.687
2.718
2.745
2.805
2.815
2.876
2.947
3.005
3.095
3.183
3.193
3.250
RELATIVE YIELD
CHANNEL NUMBER
0
20
40
60
80
100
120
140
160
180
300
400
500
600
700
800
900
1000
1100
1200
1300
1400
1500
1600
1700

Fig. 8 A spectrum of gamma-rays in coincidence with neutrons detected at 180° from the beam direction.

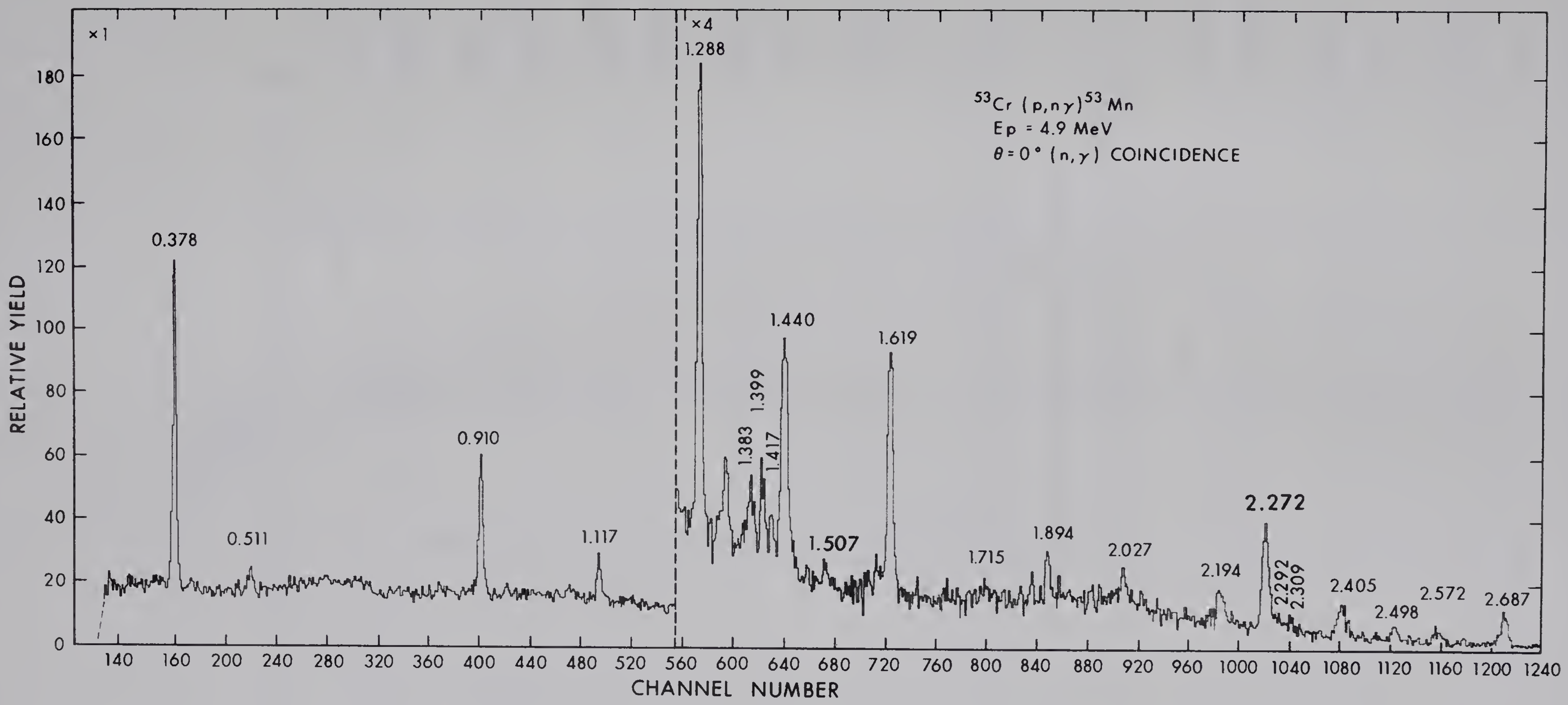
×1
×4
^{53}Cr (p,nγ)^{53}Mn
Ep = 4.9 MeV
θ = 0° (n,γ) COINCIDENCE
0.378
0.511
0.910
1.117
1.288
1.383
1.399
1.417
1.440
1.507
1.619
1.715
1.894
2.027
2.194
2.272
2.292
2.309
2.405
2.498
2.572
2.687
RELATIVE YIELD
0
20
40
60
80
100
120
140
160
180
CHANNEL NUMBER
140
160
200
240
280
320
360
400
440
480
520
560
600
640
680
720
760
800
840
880
920
960
1000
1040
1080
1120
1160
1200
1240

Fig. 9 A summary of branching ratios, spin assignments and the excited state levels of ^{53}Mn below 3.25 MeV. The spin assignments include our measurements as well as all previously available information.

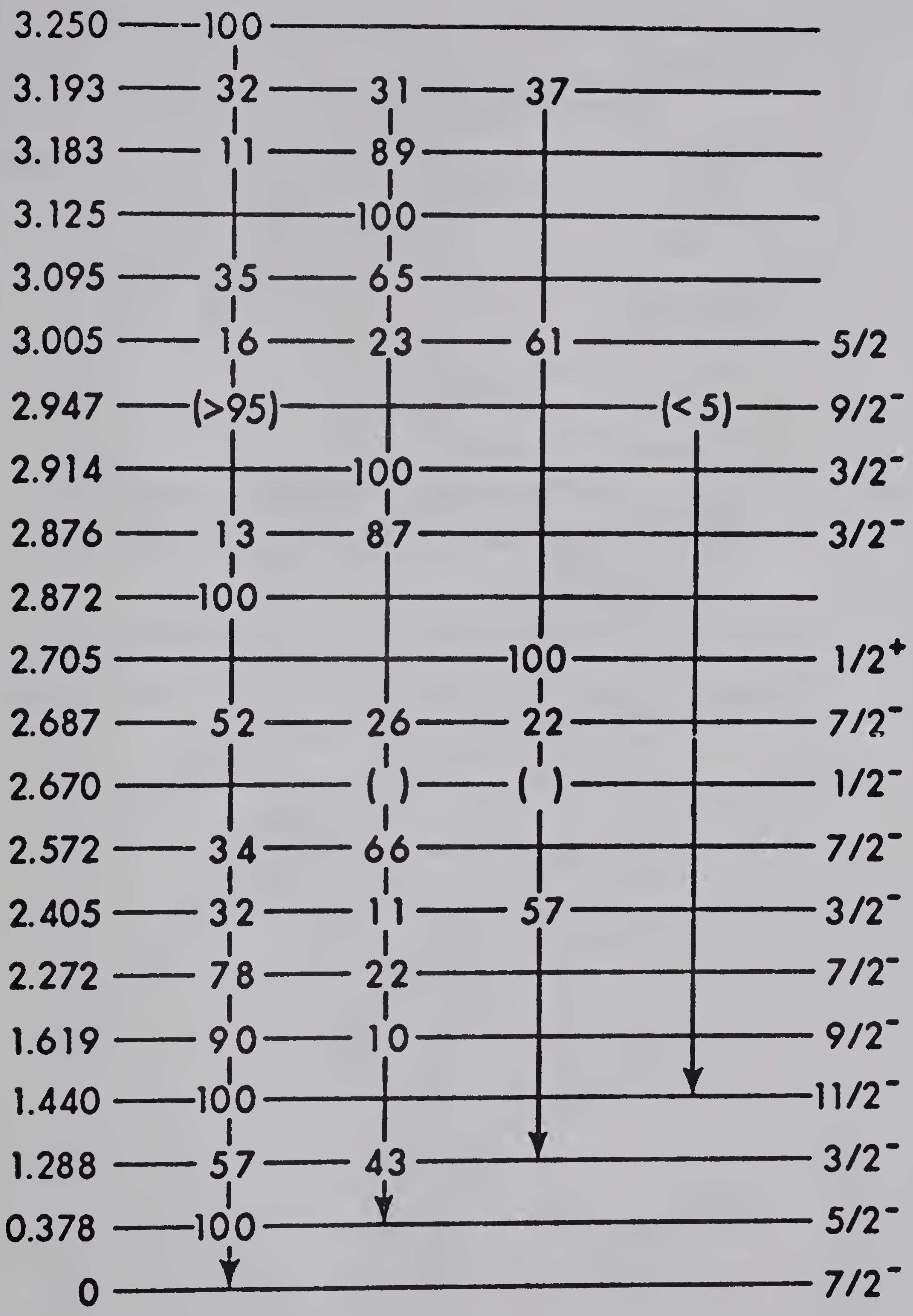
3.250 100
3.193 32 31 37
3.183 11 89
3.125 100
3.095 35 65
3.005 16 23 61 5/2
2.947 (>95) (< 5) 9/2⁻
2.914 100 3/2⁻
2.876 13 87 3/2⁻
2.872 100
2.705 100 1/2⁺
2.687 52 26 22 7/2⁻
2.670 ( ) ( ) 1/2⁻
2.572 34 66 7/2⁻
2.405 32 11 57 3/2⁻
2.272 78 22 7/2⁻
1.619 90 10 9/2⁻
1.440 100 11/2⁻
1.288 57 43 3/2⁻
0.378 100 5/2⁻
0 7/2⁻

^{53}Mn

Fig. 10 Yield curves at 90° for the gamma-ray transitions in ^{53}Mn at the bombarding energies, E_p = 3.0 MeV to 5.0 MeV.

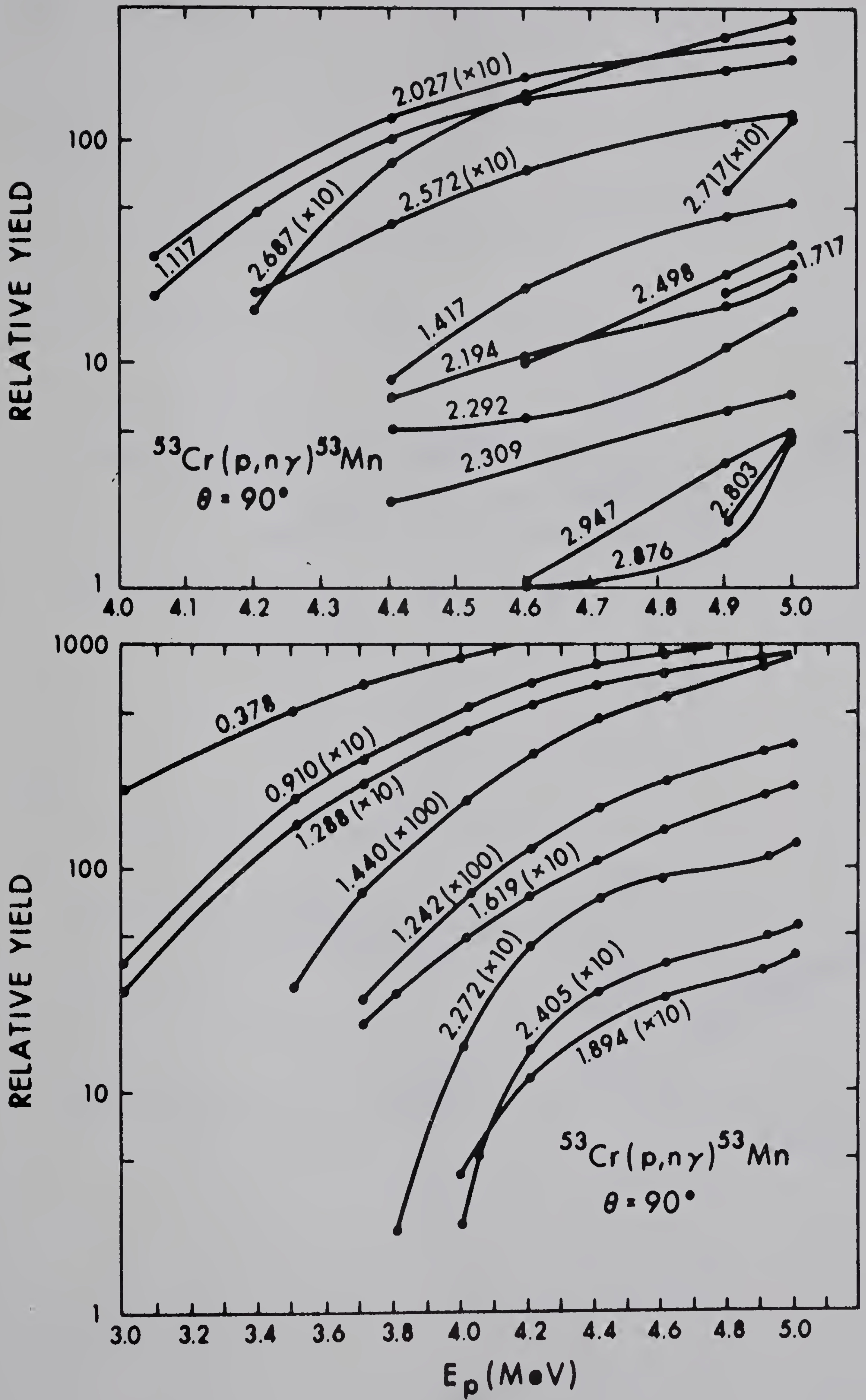
RELATIVE YIELD
100
10
1
1.117
2.027 (×10)
2.687 (×10)
2.572 (×10)
2.717 (×10)
1.417
2.194
2.498
1.717
2.292
2.309
2.947
2.803
2.876
^{53}Cr(p,nγ)^{53}Mn
θ = 90°
4.0
4.1
4.2
4.3
4.4
4.5
4.6
4.7
4.8
4.9
5.0
RELATIVE YIELD
1000
100
10
1
0.378
0.910 (×10)
1.288 (×10)
1.440 (×100)
1.242 (×100)
1.619 (×10)
2.272 (×10)
2.405 (×10)
1.894 (×10)
^{53}Cr(p,nγ)^{53}Mn
θ = 90°
3.0
3.2
3.4
3.6
3.8
4.0
4.2
4.4
4.6
4.8
5.0
E$_p$ (MeV)

Fig. 11 Yield curve analysis based on the compound nuclear statistical model for the 2.687 → 0.0 MeV and 2.272 → 0.378 MeV transitions in ^{53}Mn.

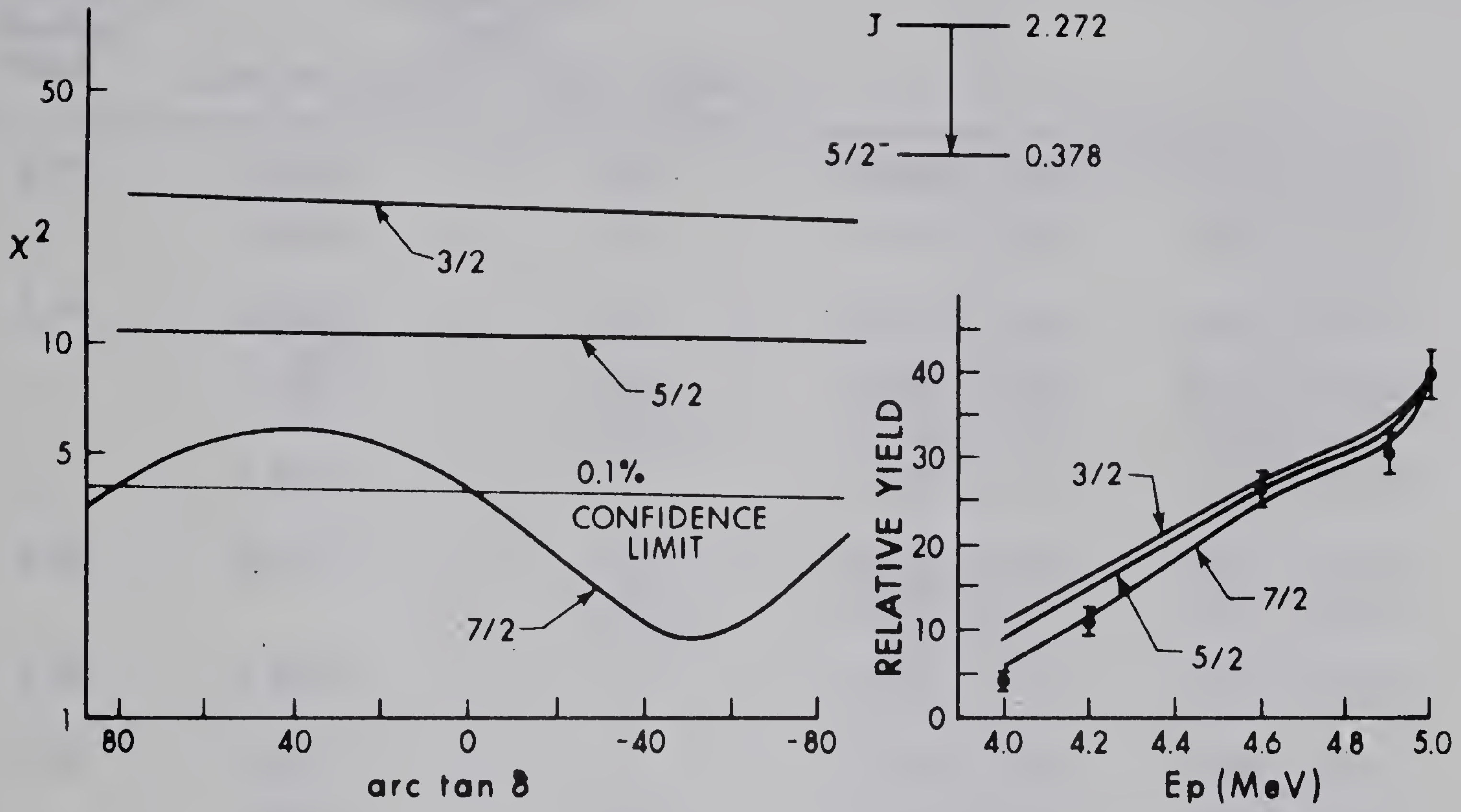
J
2.272
5/2⁻
0.378
50
χ²
10
5
1
3/2
5/2
0.1%
CONFIDENCE
LIMIT
7/2
80
40
0
-40
-80
arc tan δ
40
30
20
10
0
RELATIVE YIELD
3/2
7/2
5/2
4.0
4.2
4.4
4.6
4.8
5.0
Ep (MeV)

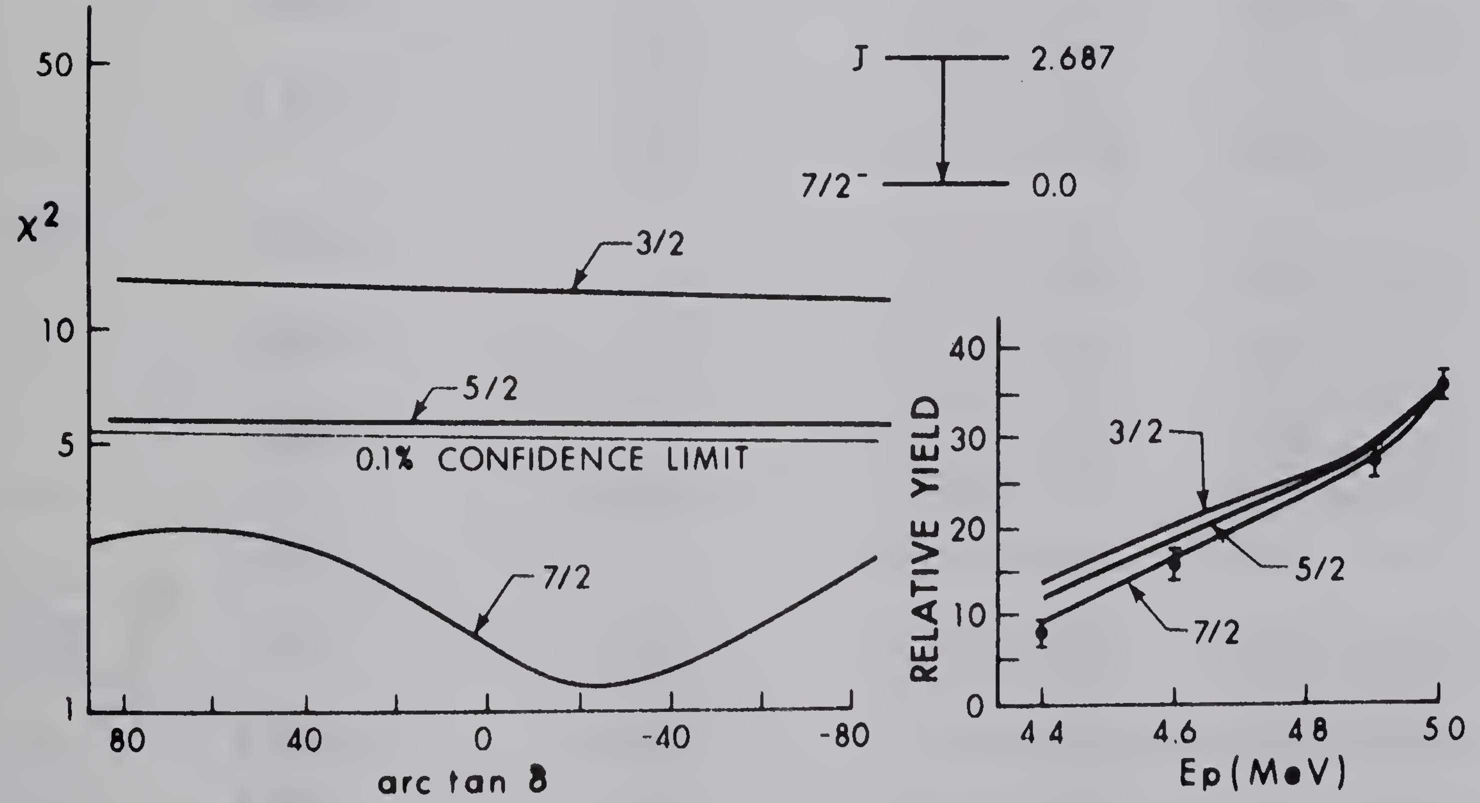
J
2.687
7/2⁻
0.0
50
χ²
10
5
1
3/2
5/2
0.1% CONFIDENCE LIMIT
7/2
80
40
0
-40
-80
arc tan δ
40
30
20
10
0
RELATIVE YIELD
3/2
5/2
7/2
4.4
4.6
4.8
5.0
Ep (MeV)

Table 2

Legendre coefficients, a_2 and a_4 of the angular distributions of gamma-rays de-exciting levels of ^{53}Mn.

Bombarding Energy (MeV)	Transition (MeV)		a_2	a_4
	Initial state	Final state		
3.78	1.440	0	0.26 ± 0.01	-0.02 ± 0.02
	1.619	0	0.31 ± 0.02	0.07 ± 0.02
3.88	0.378	0	-0.13 ± 0.01	0.02 ± 0.01
	1.288	0	-0.04 ± 0.01	0.02 ± 0.01
		0.378	-0.06 ± 0.01	0.03 ± 0.01
	1.619	0	0.27 ± 0.02	0.09 ± 0.02
3.90	2.272	0	-0.10 ± 0.02	0.01 ± 0.02
		0.378	-0.28 ± 0.07	0.01 ± 0.07
3.96	2.405	0	0.01 ± 0.04	0.01 ± 0.04
4.26	2.272	0	-0.08 ± 0.01	0.02 ± 0.01
	2.572	0	0.22 ± 0.04	0.02 ± 0.04
		0.378	0.49 ± 0.03	0.01 ± 0.03
	2.670	0.378	-0.03 ± 0.06	-0.08 ± 0.07
		1.288	-0.01 ± 0.03	0.03 ± 0.03
4.50	2.572	0	0.25 ± 0.01	0.01 ± 0.02
		0.378	0.47 ± 0.03	-0.08 ± 0.03
	2.687	0	0.17 ± 0.01	-0.02 ± 0.01
		0.378	-0.47 ± 0.07	0.06 ± 0.07
	2.876	0	-0.05 ± 0.07	-0.08 ± 0.07
		0.378	-0.02 ± 0.02	0.01 ± 0.02
	2.947	0	0.85 ± 0.11	0.07 ± 0.12
4.55	2.572	0	0.25 ± 0.01	0.01 ± 0.01
		0.378	0.49 ± 0.02	-0.03 ± 0.02
	2.670	1.288	0.07 ± 0.02	0.01 ± 0.02
	2.687	0	0.22 ± 0.01	0.01 ± 0.01
		0.378	-0.17 ± 0.03	-0.05 ± 0.03
	2.914	0.378	-0.05 ± 0.07	-0.07 ± 0.07
	2.947	0	0.73 ± 0.05	0.01 ± 0.06
4.65	2.947	0	0.68 ± 0.04	0.05 ± 0.04
5.0	2.947	0	0.59 ± 0.08	-0.02 ± 0.08
	3.005	1.288	-0.31 ± 0.04	-0.03 ± 0.04

(a) The levels below 2 MeV

From previous experiments including β^+-decay (Ju 59) of ^{53}Fe, the spin and parity of the 0.378 MeV level has been established as $\frac{5}{2}^-$.

The 1.288 MeV state decays to the ground state (57 %) and to the first excited state (43%). The spin and parity of this level have been assigned as $\frac{3}{2}^-$ in the previous work (Vu 66, Vu 67), where the mixing ratio for the 0.910 MeV transition has been assigned as -0.18 ± 0.03 or 30^{+270}_{-15}. The angular distributions of both transitions were nearly isotropic in the present work.

The 1.440 MeV state decays only to the ground state. A comparison of the angular distribution of the decay at E_p = 3.78 MeV with predictions for the 1.440 MeV transition is shown in Fig. 12. The spin of this level can be uniquely assigned as $\frac{11}{2}$; this confirms the previous assignment (Mc 70).

The branching ratio of the 1.619 MeV level is in agreement with the values of McEllistrem et al. (Mc 70), but in disagreement with the measurements of Cujec et al. (Cu 69, Sz 70). The χ^2 analysis of the angular distribution of the decay to the ground state, shown in Fig. 13, leads to a unique spin assignment of $\frac{9}{2}$ for this level, thus confirming the previous measurement (Mc 70). The E2/M1 mixing ratios of $-3.2^{+1.5}_{-0.5}$ or $-0.6^{+0.1}_{-0.2}$ is in agreement with the values of Szöghy et al. (Sz 70) and McEllistrem et al. (Mc 70).

Fig. 12 The angular distribution and the χ^2 plot for the 1.440 → 0.0 MeV transition.

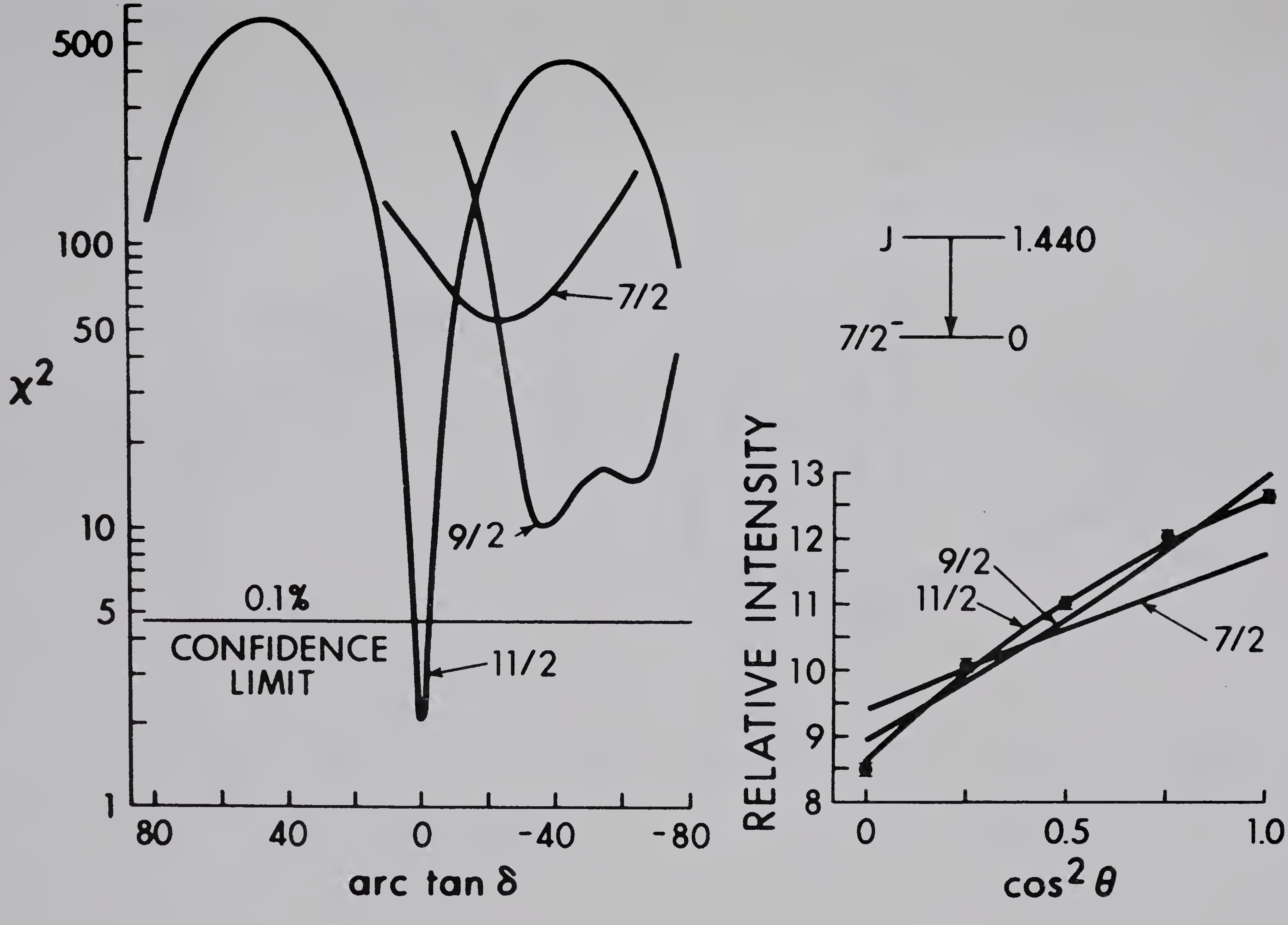
500
100
50
10
5
1
χ^2
80
40
0
-40
-80
arc tan δ
7/2
9/2
11/2
0.1%
CONFIDENCE
LIMIT
J
1.440
7/2⁻
0
RELATIVE INTENSITY
13
12
11
10
9
8
0
0.5
1.0
$\cos^2\theta$
9/2
11/2
7/2

Fig. 13 The angular distribution and the χ^2 plot for the 1.619 → 0.0 MeV transition.

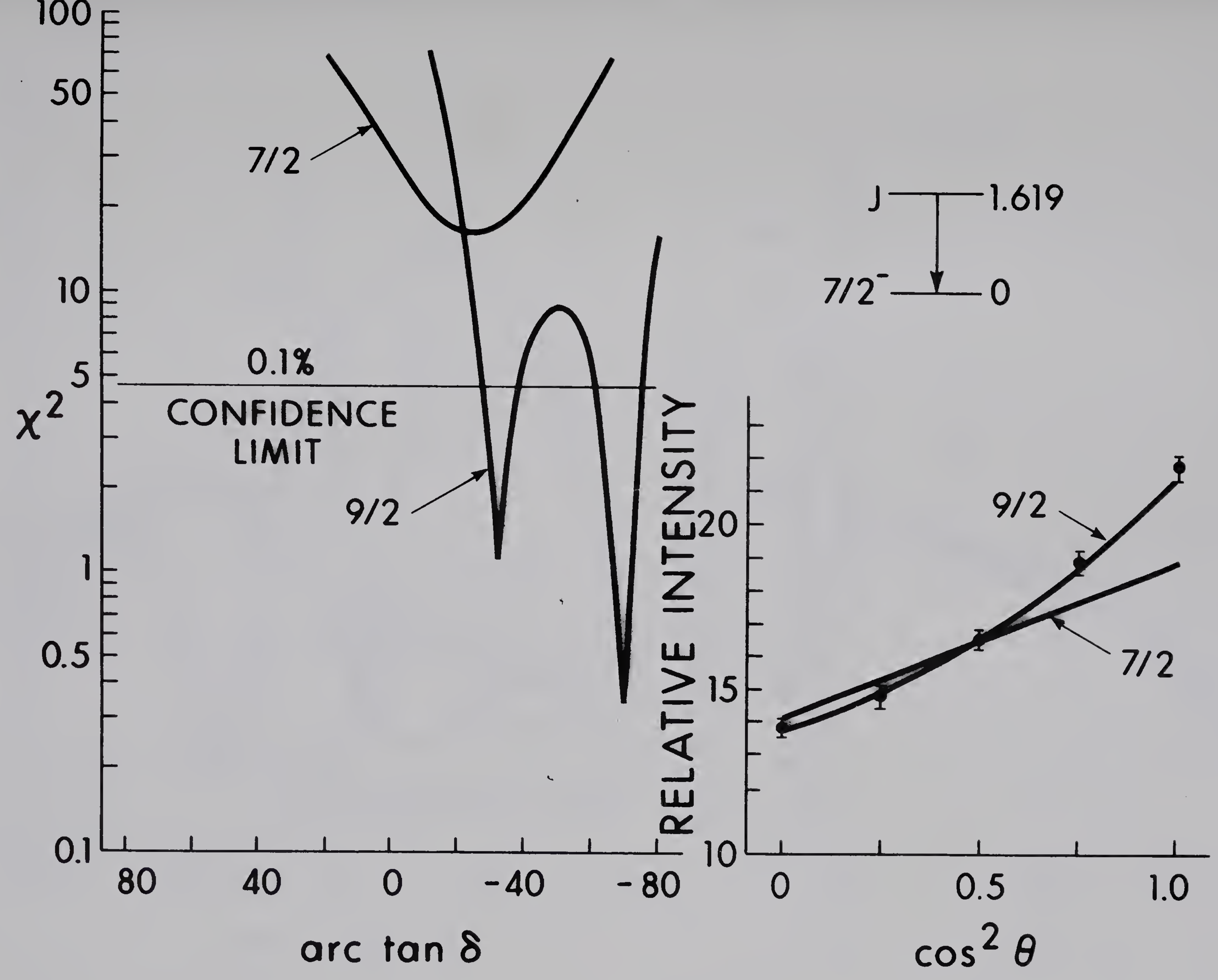
100
50
10
5
1
0.5
0.1
χ^2
7/2
0.1%
CONFIDENCE
LIMIT
9/2
80
40
0
-40
-80
arc tan δ
J
1.619
7/2⁻
0
RELATIVE INTENSITY
20
15
10
9/2
7/2
0
0.5
1.0
$\cos^2 \theta$

Fig. 14 The angular distribution and the χ^2 plot for the 2.272 → 0.0 MeV transition.

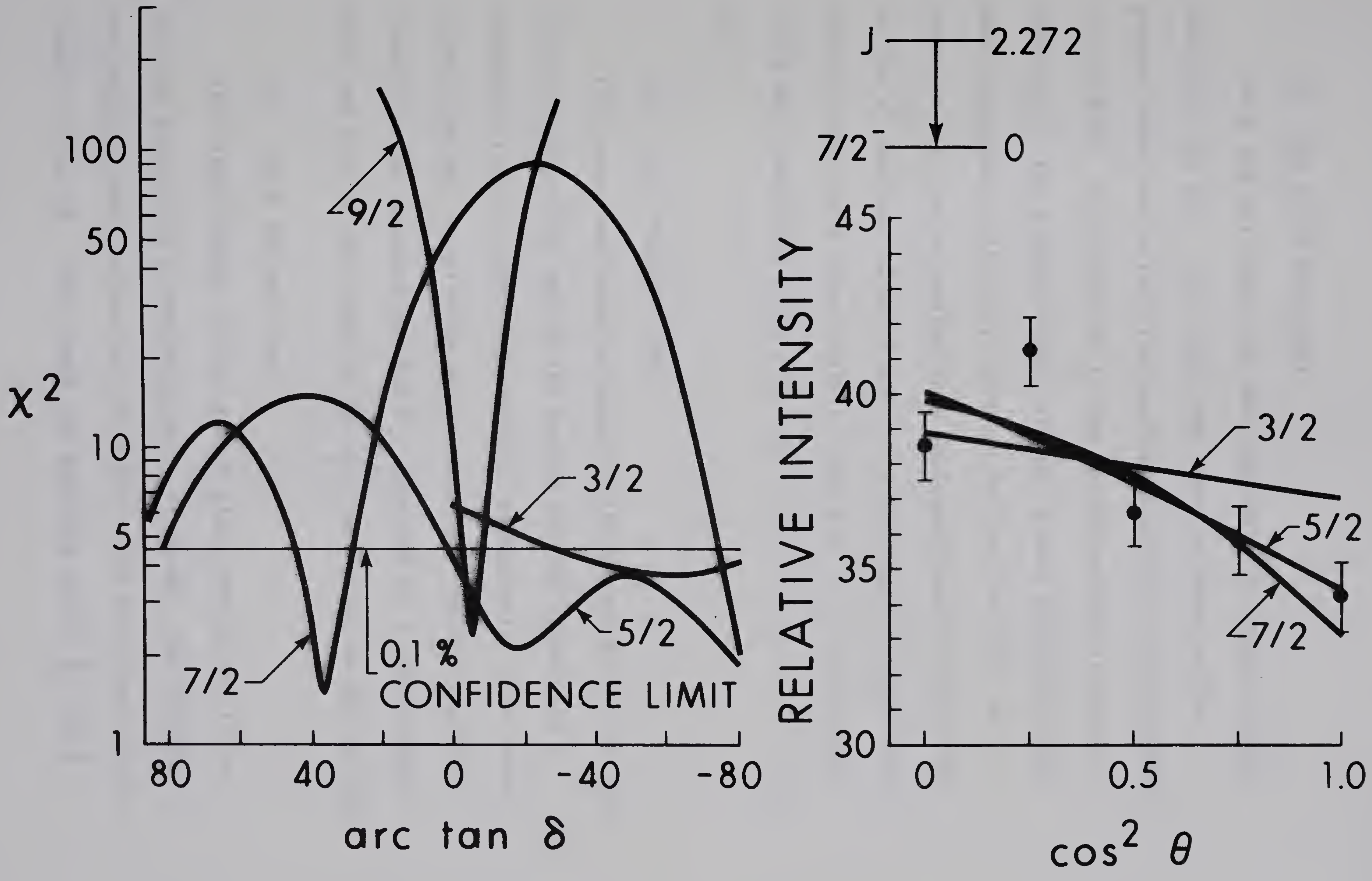
J
2.272
7/2⁻
0
χ^2
100
50
10
5
1
80
40
0
-40
-80
arc tan δ
9/2
3/2
5/2
7/2
0.1 %
CONFIDENCE LIMIT
RELATIVE INTENSITY
45
40
35
30
0
0.5
1.0
cos² θ
3/2
5/2
7/2

(b) The 2.272 MeV level

The 2.272 MeV level has been seen only in proton induced reactions (Nu 70). This level was found to decay to the ground state and to the first excited state with the branching ratio 78:22. No transition to the second excited state was observed in the present work, although a weak transition has been suggested in the (p,γ) work of Maripuu (Ma 70). As shown in Fig. 14, no unique spin assignment would be obtained in the χ^2 analysis of the 2.272 → 0.0 MeV angular distribution. However, the yield curve analysis (see Fig. 11) for the 2.272 → 0.378 MeV transition shows the best fit for $J = \frac{7}{2}$, $\delta = -1.2 \pm 0.2$.

(c) The 2.405 MeV level

This level was found to decay to the ground state, to the first excited state and to the second excited state with a branching ratio of 32%, 11% and 57%, respectively. The transitions from this level were nearly isotropic, which in conjunction with the measured (Ob 67) ℓ_p- transfer of 1 could determine the spin of the state to be $\frac{3}{2}^-$ (see Ar 67, Cu 69, Ne 68).

(d) The 2.572 MeV level

This level decays to the ground state and to the first excited state with a branching ratio of 34:66. The χ^2-plot and angular distribution for the 2.572 → 0.0 MeV transition is shown in Fig. 16. This shows two possible spins, $\frac{9}{2}$ and $\frac{7}{2}$

Fig. 15 The angular distribution and the χ^2 plot for the 2.572 → 0.378 MeV transition.

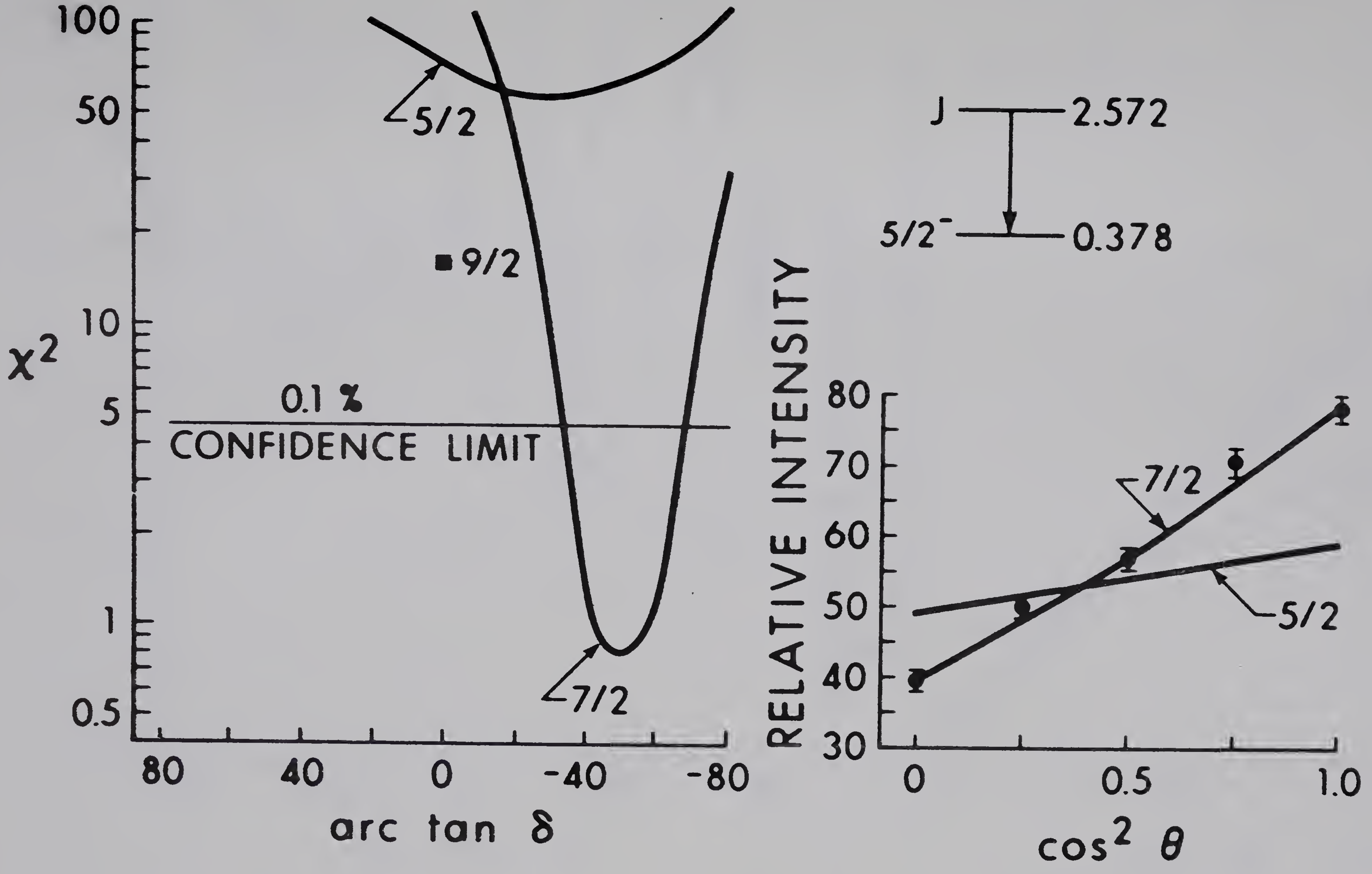
100
50
10
5
1
0.5
χ²
5/2
9/2
0.1 %
CONFIDENCE LIMIT
7/2
80
40
0
-40
-80
arc tan δ
J
2.572
5/2⁻
0.378
RELATIVE INTENSITY
80
70
60
50
40
30
7/2
5/2
0
0.5
1.0
cos² θ

Fig. 16 The angular distribution and the χ^2 plot for the 2.572 → 0.0 MeV transition.

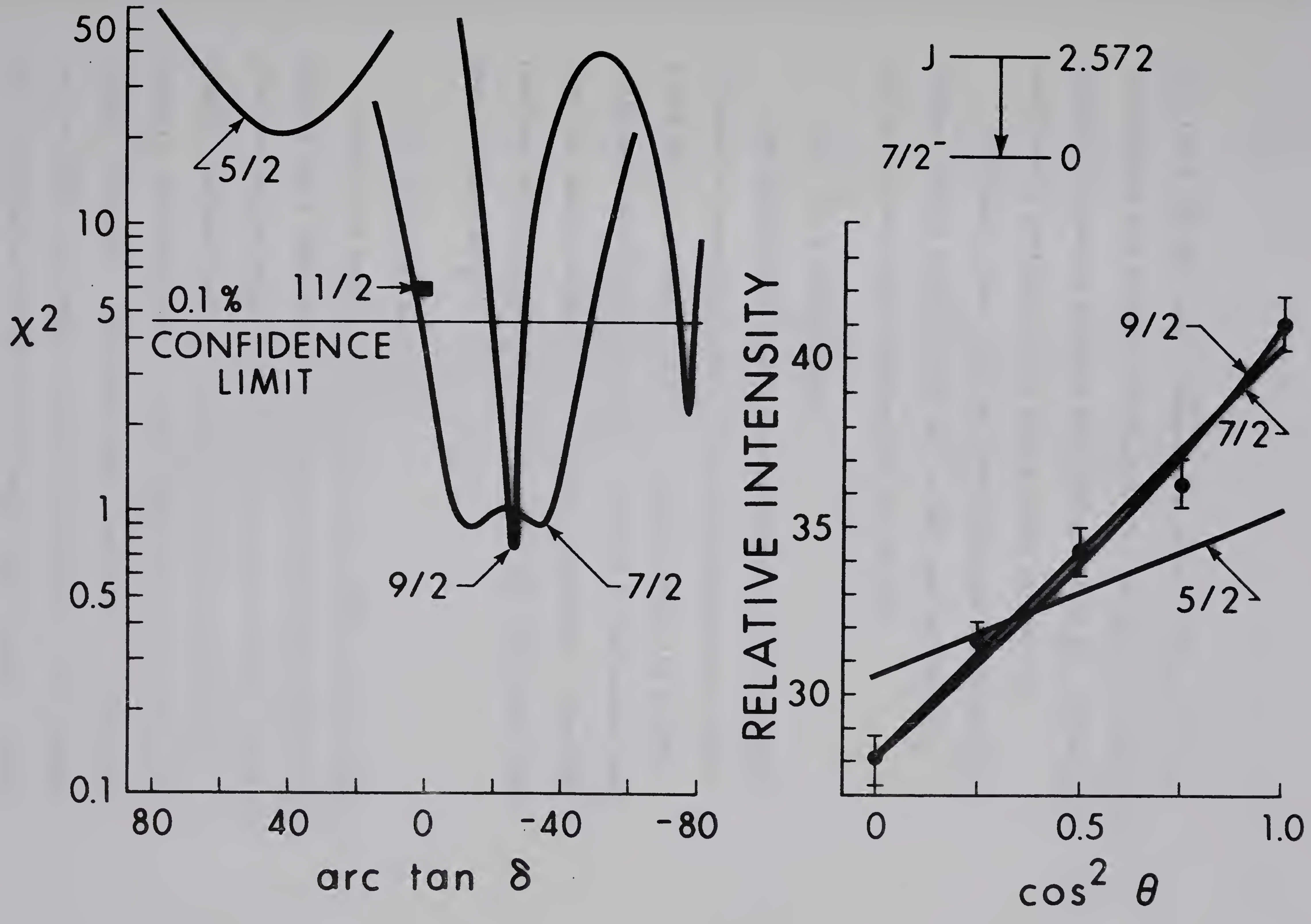
50
10
5
1
0.5
0.1
χ²
5/2
11/2
0.1 %
CONFIDENCE
LIMIT
9/2
7/2
80
40
0
-40
-80
arc tan δ
J
2.572
7/2⁻
0
RELATIVE INTENSITY
40
35
30
9/2
7/2
5/2
0
0.5
1.0
cos² θ

for the 2.572 MeV level. However, as shown in Fig. 15, the χ^2-analysis and angular distribution for the 2.572 → 0.378 MeV transition lead to a unique spin assignment of $\frac{7}{2}$, the mixing ratio being confined to the limits shown in table 3.

Previously, the 2.572 MeV level has been found only in proton induced reactions (Br 66, Ve 64), and not found in stripping and pickup reactions (Ob 67, Ne 68).

(e) The 2.670 MeV level

The angular distribution measurements do not provide any information about the spin of this level because the 2.670 → 0.378 MeV transition is nearly isotropic, while the 2.670 → 1.288 MeV transition could not be resolved in the present work from the double escape of the 2.405 MeV gamma-ray. From the previous stripping works (Ar 65, Ob 67, Cu 69), this level has been assigned as $\frac{1}{2}^-$.

(f) The 2.687 MeV level

This level decays to the ground state (52%), to the first excited state (26%) and to the second excited state (22%). The χ^2-plots and the angular distributions shown in Figs. 17 and 18 clearly indicate that the 2.687 MeV level has a spin of $\frac{7}{2}$ uniquely; this conclusion is also supported by the yield curve analysis (Fig. 11). The E2/M1 mixing ratio of $\delta = -0.46 \pm 0.2$ for the 2.687 → 0.0 MeV transition was obtained in the present work. Previously, no information about proton angular momentum

Table 3

Summary of angular distribution results. The energy levels, spin assignments, branching ratios and multipole mixing ratios are listed for the excited states of ^{53}Mn.

State (MeV)	Final state (MeV)	E_γ (MeV)	Branching ratio	Multipole mixing ratio δ
0.378 $\frac{5}{2}^-$	0.000 $\frac{7}{2}^-$	0.378	100	
1.288 $\frac{3}{2}^-$	0.000 $\frac{7}{2}^-$	1.288	57	E2
	0.378 $\frac{5}{2}^-$	0.910	43	
1.440 $\frac{11}{2}^-$	0.000 $\frac{7}{2}^-$	1.440	100	E2
1.619 $\frac{9}{2}^-$	0.000 $\frac{7}{2}^-$	1.619	90	$-3.2^{+1.5}_{-0.5}$ or $-0.6^{+0.1}_{-0.2}$
	0.378 $\frac{5}{2}^-$	1.241	10	E2
2.272 $\frac{7}{2}^-$	0.000 $\frac{7}{2}^-$	2.272	78	
	0.378 $\frac{5}{2}^-$	1.894	22	-1.2 ± 0.2
2.405 $\frac{3}{2}^-$	0.000 $\frac{7}{2}^-$	2.405	32	E2
	0.378 $\frac{5}{2}^-$	2.027	11	
	1.288 $\frac{3}{2}^-$	1.117	57	
2.572 $\frac{7}{2}^-$	0.000 $\frac{7}{2}^-$	2.572	34	$-0.46^{+0.5}_{-0.7}$
	0.378 $\frac{5}{2}^-$	2.194	66	$-1.2^{+0.5}_{-1.2}$
2.670 $\frac{1}{2}^-$	0.378 $\frac{5}{2}^-$	2.292		E2
	1.288 $\frac{3}{2}^-$	1.382		
2.687 $\frac{7}{2}^-$	0.000 $\frac{7}{2}^-$	2.687	52	-0.46 ± 0.2
	0.378 $\frac{5}{2}^-$	2.309	26	$+0.30^{+2.8}_{-0.2}$ or $+1.6 \pm 1.5$
	1.288 $\frac{3}{2}^-$	1.399	22	E2

Table 3 (continued)

State (MeV)	Final state (MeV)	E_γ (MeV)	Branching ratio	Multipole mixing ratio δ
2.705 $\frac{1}{2}^+$	1.288 $\frac{3}{2}^-$	1.417	100	
2.872	0.000 $\frac{7}{2}^-$	2.872	100	
2.876 $\frac{3}{2}^-$	0.000 $\frac{7}{2}^-$	2.876	13	E2
	0.378 $\frac{5}{2}^-$	2.498	87	
2.914 $\frac{3}{2}^-$	0.378 $\frac{5}{2}^-$	2.536	100	
2.947 $\frac{9}{2}^-$	0.000 $\frac{7}{2}^-$	2.947		$-1.0^{+0.3}_{-1.1}$
	1.440 $\frac{11}{2}^-$	1.507		
3.005 $\frac{5}{2}^-$	0.000 $\frac{7}{2}^-$	3.005	16	
	0.378 $\frac{5}{2}^-$	2.627	23	
	1.288 $\frac{3}{2}^-$	1.717	61	$-0.70^{+0.7}_{-0.4}$
3.095	0.000 $\frac{7}{2}^-$	3.095	35	
	0.378 $\frac{5}{2}^-$	2.717	65	
3.125	0.378 $\frac{5}{2}^-$	2.747	100	
3.183	0.000 $\frac{7}{2}^-$	3.183	11	
	0.378 $\frac{5}{2}^-$	2.803	89	
3.193	0.000 $\frac{7}{2}^-$	3.193	32	
	0.378 $\frac{5}{2}^-$	2.815	31	
	1.288 $\frac{3}{2}^-$	1.905	37	
3.250	0.000 $\frac{7}{2}^-$	3.250	100	

transfer for this level has been reported from the stripping and pickup reactions.

(g) The 2.705 MeV level

This level seems to decay to the second excited state only, indicating a very low spin of the level. The isotropic angular distribution of the 2.705 → 1.288 MeV transition could not yield any information about the spin of this level. Transfer reactions (Ob 67, Ne 68, Gl 66) indicating $\ell_p = 0$ for this level indicate the assignment of a $\frac{1}{2}^+$ spin.

(h) The 2.872 and 2.876 MeV levels

The angular distributions for both of these levels do not give any information on the level spins in the present work. From the (^{3}He,d) reactions (Cu 69, Ob 67) momentum transfer $\ell_p = 1$ has been obtained. The spin of the 2.876 MeV level should be concluded to be $\frac{3}{2}^-$ (see Ma 70).

(i) The 2.914 MeV level

The 2.914 MeV level decays to the first excited state only. The values of a_2 and a_4 for the 2.914 → 0.378 MeV angular distribution are given in table 2. Weak anisotropic angular distribution of this transition has yielded no information on the level spin. From the previous (d,n) reaction (Nu 70), momentum transfer $\ell_p = 1$ has been obtained. $J^\pi = \frac{3}{2}^-$ has been assigned by the previous (p,γ) reaction (Ma 70).

Fig. 17 The angular distribution and the χ^2 plot for the 2.687 → 0.378 MeV transition.

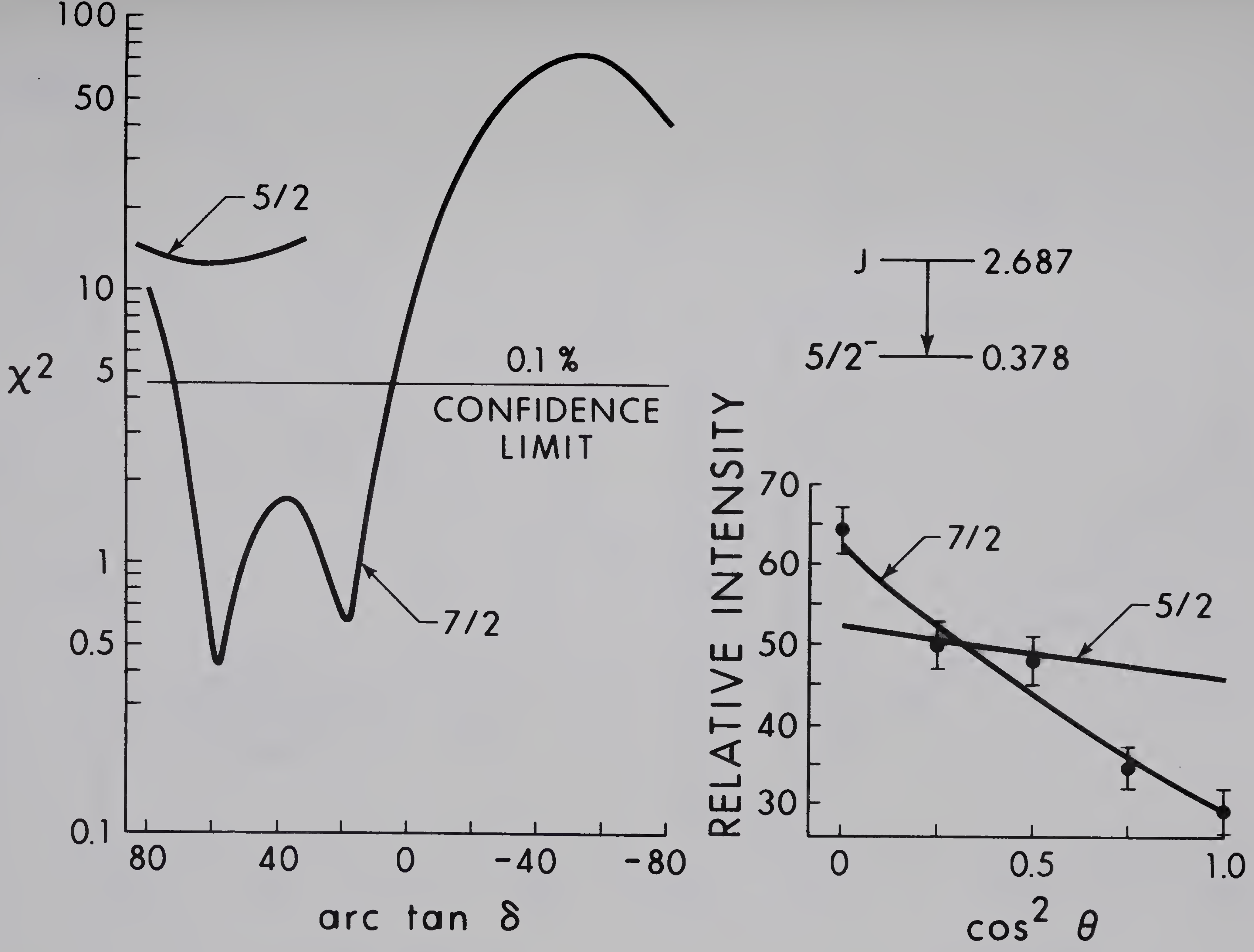
100
50
10
5
1
0.5
0.1
χ^2
5/2
7/2
0.1 %
CONFIDENCE
LIMIT
80
40
0
-40
-80
arc tan δ
J
2.687
5/2⁻
0.378
RELATIVE INTENSITY
70
60
50
40
30
7/2
5/2
0
0.5
1.0
$\cos^2\theta$

Fig. 18 The angular distribution and the χ^2 plot for the 2.687 → 0.0 MeV transition.

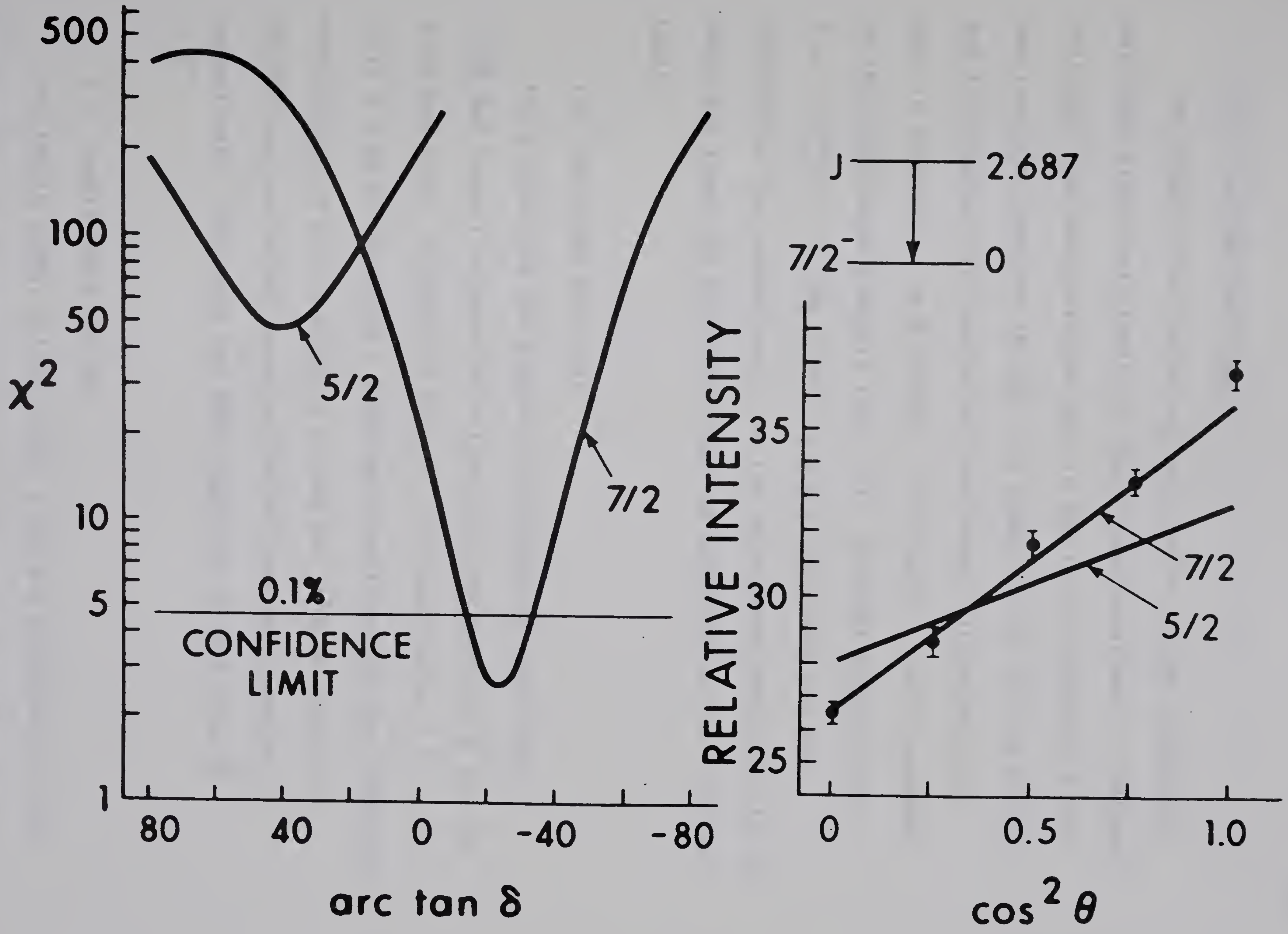
500
100
50
10
5
1
χ^2
5/2
7/2
0.1%
CONFIDENCE
LIMIT
80
40
0
-40
-80
arc tan δ
J
2.687
7/2⁻
0
RELATIVE INTENSITY
35
30
25
7/2
5/2
0
0.5
1.0
$\cos^2\theta$

(j) The 2.947 MeV level

The angular distribution of the 2.947 → 0.0 MeV transition was found highly anisotropic in the present experiment. Previously this level had been observed only in the (p,n) reaction (Ta 70) and the (p,α) reaction (Br 66). As shown in Fig. 19, the χ^2-plot and the angular distribution for this level indicate that the spin is assigned to be $\frac{9}{2}$ uniquely. The result is also supported by the yield curve analysis (Fig. 11). An E2/M1 mixing ratio, $\delta = -1.0^{+0.3}_{-1.1}$, for the 2.947 → 0.0 MeV transition has been obtained in the present work. In the coincidence spectrum (Fig. 8) there was found the transition from the 2.947 MeV to the 1.440 MeV level.

(k) The 3.005 MeV level

The χ^2-plot and the angular distribution of the 3.005 → 1.288 MeV transition show the unique spin assignment of $\frac{5}{2}$ for the 3.005 MeV level, as shown in Fig. 20. A mixing ratio, $\delta = +0.70 \pm 0.36$ of the 3.005 → 1.288 MeV transition has been obtained. Previously $\ell_p = 2$ or 3 and $\ell_p = 2$ from the (^{3}He,d) reaction (Ob 67) and the (d,^{3}He) reaction (Ne 68) have been measured, respectively. The level has been suggested (Gl 66) to be $\frac{3}{2}^+$ or $\frac{5}{2}^+$.

(l) Levels above 3.0 MeV

The levels 3.095, 3.125, 3.183, 3.193 and 3.250 MeV in ^{53}Mn have been seen in the present work. All angular distributions

from these levels are isotropic within statistical error.

Fig. 19 The angular distribution and the χ^2 plot for the 2.947 → 0.0 MeV transition

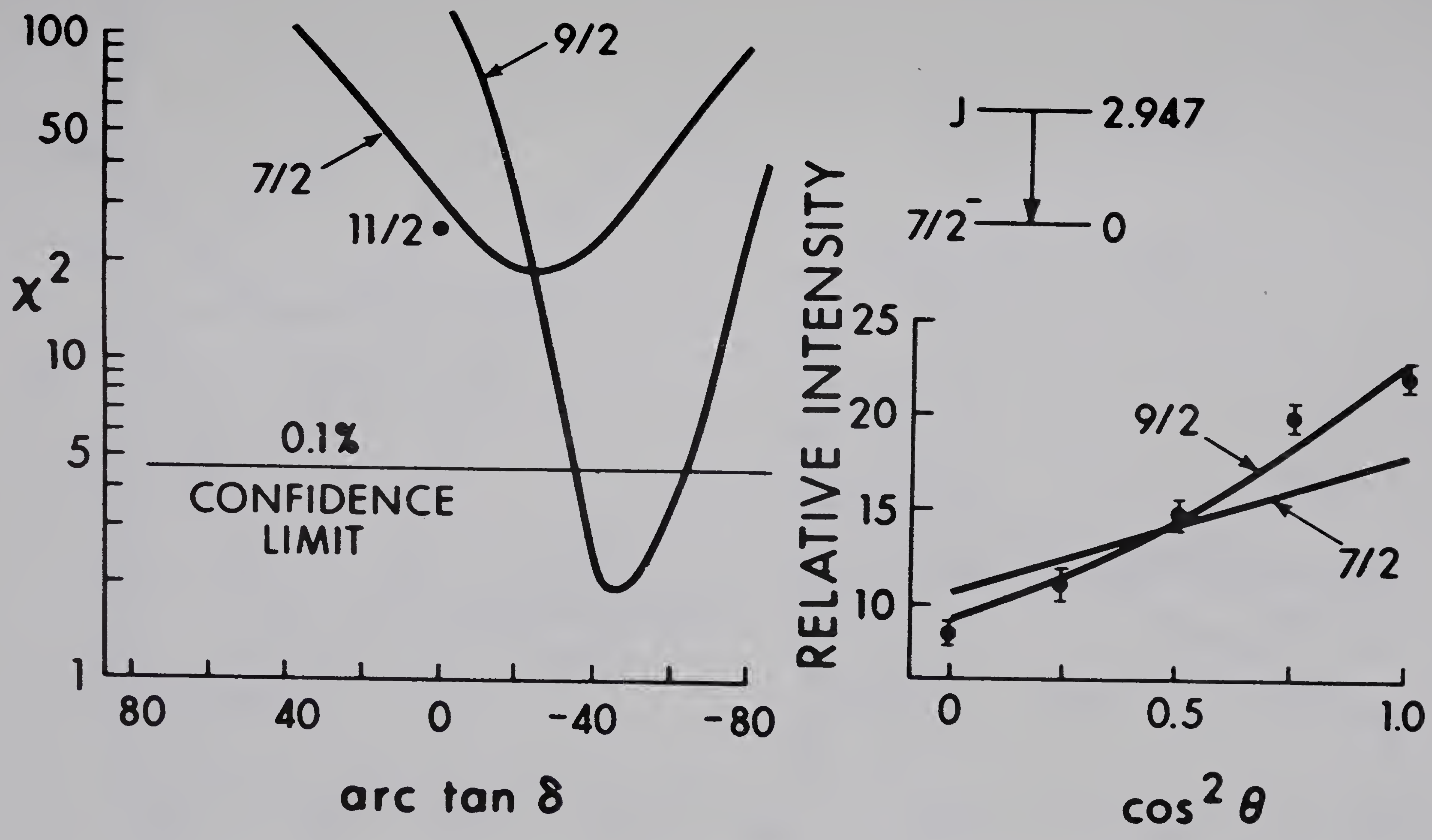
100
50
χ^2
10
5
1
80
40
0
-40
-80
arc tan δ
9/2
7/2
11/2
0.1%
CONFIDENCE
LIMIT
J
2.947
7/2⁻
0
RELATIVE INTENSITY
25
20
15
10
9/2
7/2
0
0.5
1.0
cos² θ

Fig. 20 The angular distribution and the χ^2 plot for the 3.005 → 1.288 MeV transition.

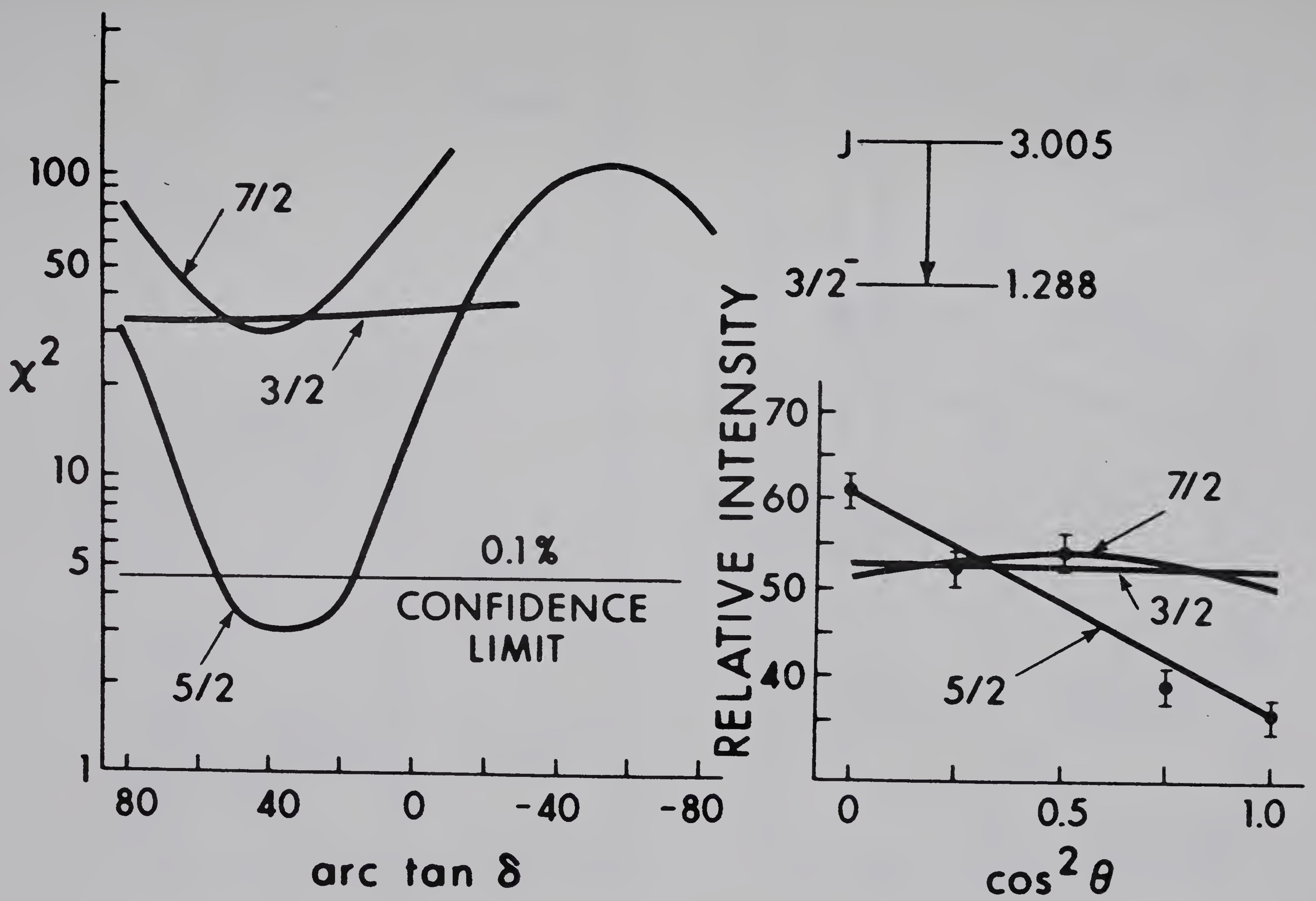
100
50
χ^2
10
5
1
80
40
0
-40
-80
arc tan δ
7/2
3/2
5/2
0.1%
CONFIDENCE
LIMIT
J
3.005
$3/2^-$
1.288
RELATIVE INTENSITY
70
60
50
40
0
0.5
1.0
$\cos^2\theta$
7/2
3/2
5/2

Fig. 21 Angular distributions for the gamma-ray transitions of the 0.378, 1.288, 1.440, 1.619, 2.272, 2.405 and 2.670 MeV levels.

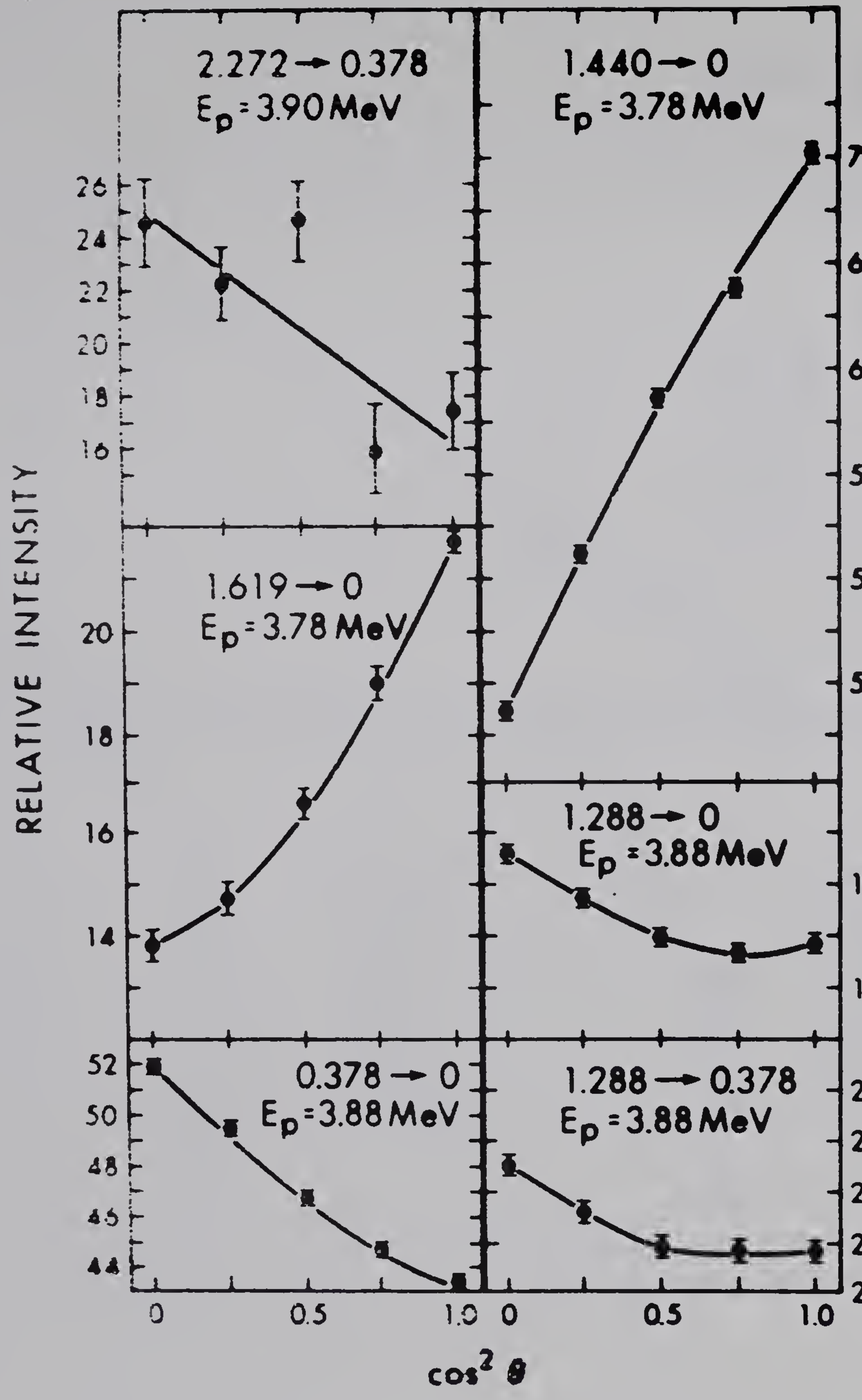
RELATIVE INTENSITY
2.272 → 0.378
$E_p = 3.90$ MeV
26
24
22
20
18
16
1.619 → 0
$E_p = 3.78$ MeV
20
18
16
14
0.378 → 0
$E_p = 3.88$ MeV
52
50
48
46
44
1.440 → 0
$E_p = 3.78$ MeV
70
66
62
58
54
50
1.288 → 0
$E_p = 3.88$ MeV
18
17
1.288 → 0.378
$E_p = 3.88$ MeV
26
25
24
23
22
0
0.5
1.0
0
0.5
1.0
$\cos^2\theta$

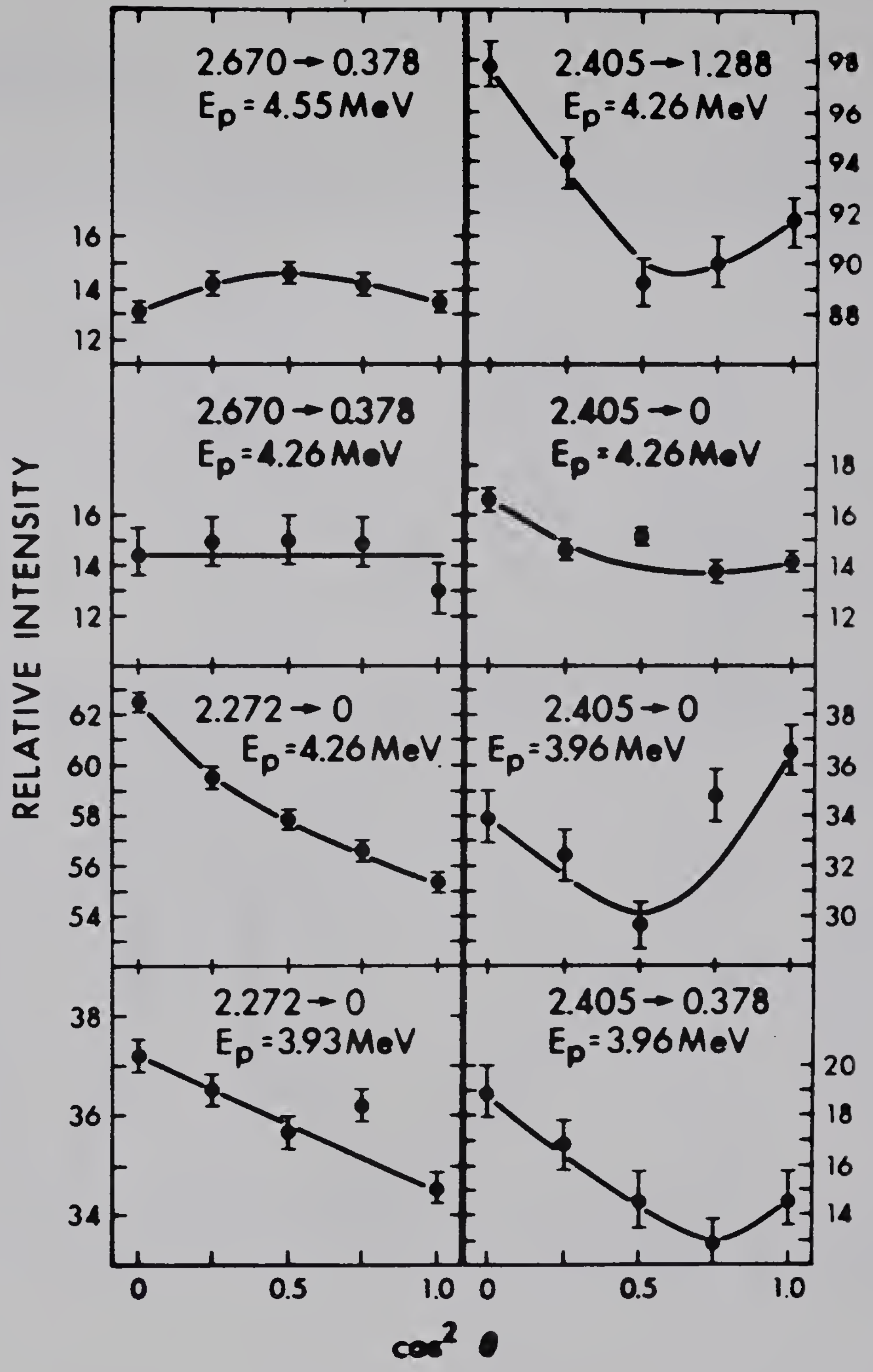
RELATIVE INTENSITY
2.670 → 0.378
$E_p = 4.55$ MeV
16
14
12
2.670 → 0.378
$E_p = 4.26$ MeV
16
14
12
2.272 → 0
$E_p = 4.26$ MeV
62
60
58
56
54
2.272 → 0
$E_p = 3.93$ MeV
38
36
34
2.405 → 1.288
$E_p = 4.26$ MeV
98
96
94
92
90
88
2.405 → 0
$E_p = 4.26$ MeV
18
16
14
12
2.405 → 0
$E_p = 3.96$ MeV
38
36
34
32
30
2.405 → 0.378
$E_p = 3.96$ MeV
20
18
16
14
0
0.5
1.0
0
0.5
1.0
$\cos^2\theta$

Fig. 22 Angular distributions for the gamma-ray transitions of the 2.876, 2.914, 2.947 and 3.005 MeV levels.

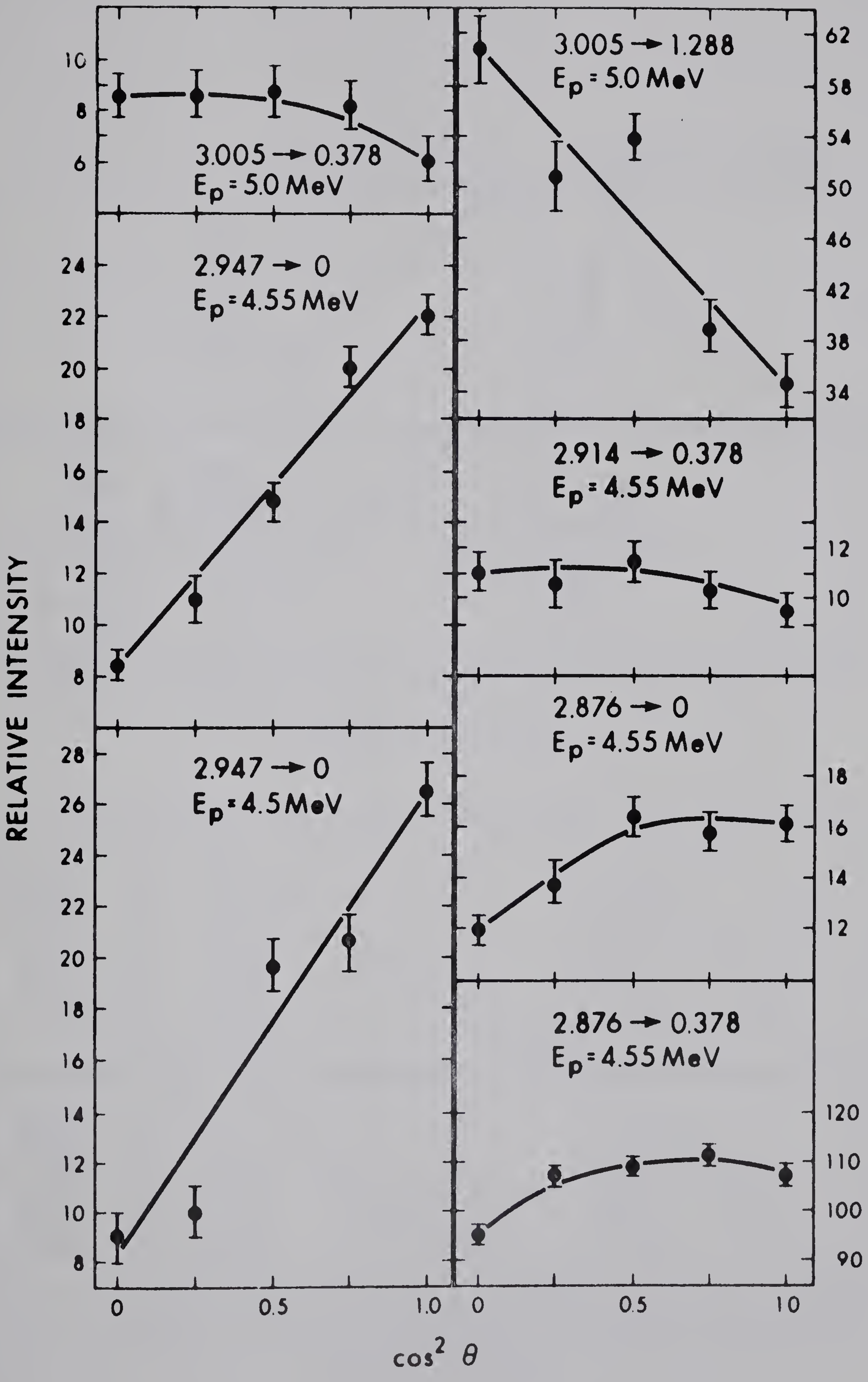
RELATIVE INTENSITY
$\cos^2\theta$
3.005 → 0.378
E_p = 5.0 MeV
3.005 → 1.288
E_p = 5.0 MeV
2.947 → 0
E_p = 4.55 MeV
2.914 → 0.378
E_p = 4.55 MeV
2.876 → 0
E_p = 4.55 MeV
2.947 → 0
E_p = 4.5 MeV
2.876 → 0.378
E_p = 4.55 MeV
6
8
10
8
10
12
14
16
18
20
22
24
8
10
12
14
16
18
20
22
24
26
28
62
58
54
50
46
42
38
34
10
12
12
14
16
18
90
100
110
120
0
0.5
1.0
0
0.5
1.0

Fig. 23 Angular distributions for the gamma-ray transitions of the 2.572, 2.687, 2.705, 3.095 and 3.125 MeV levels.

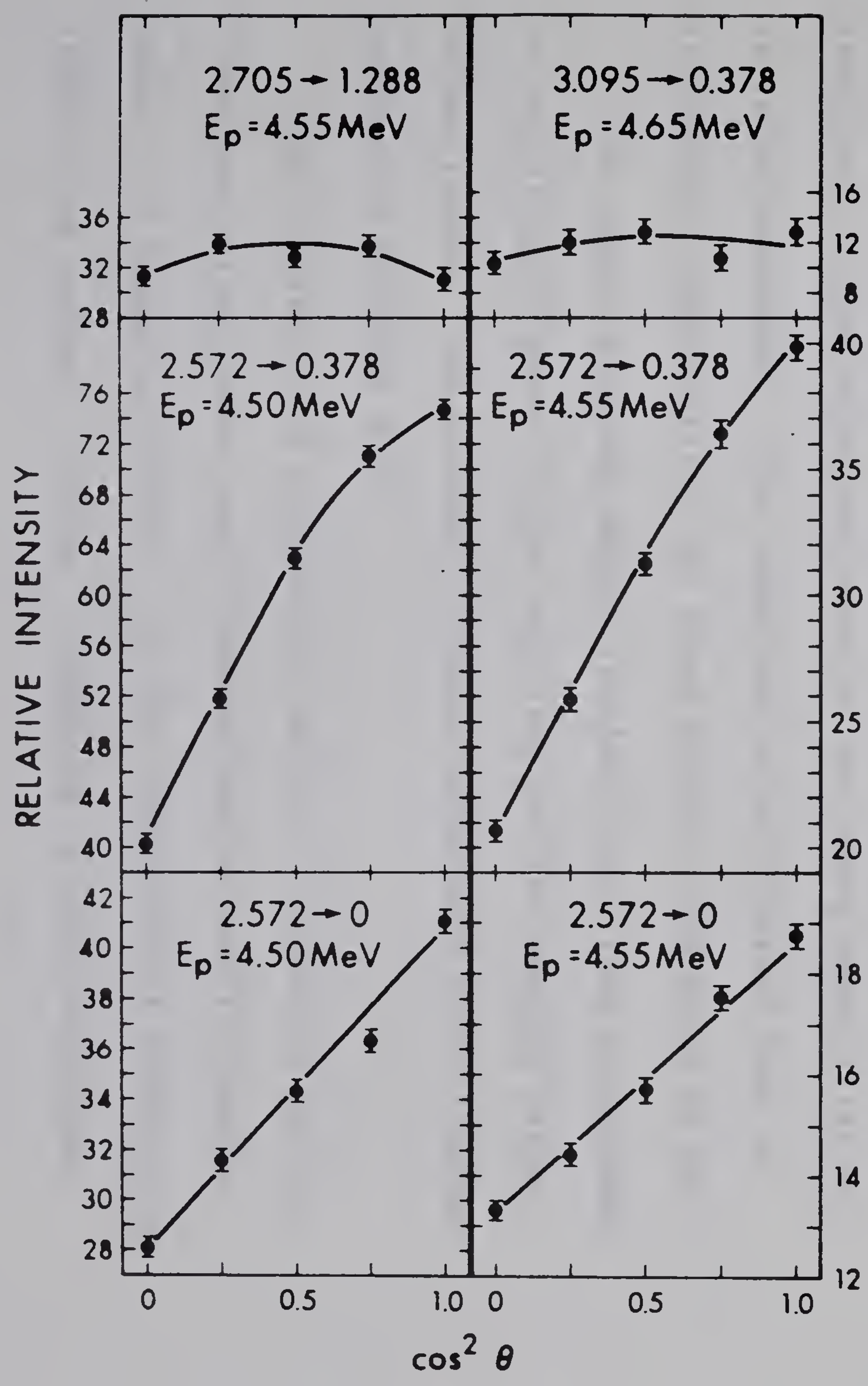
2.705 → 1.288
E_p = 4.55 MeV
3.095 → 0.378
E_p = 4.65 MeV
2.572 → 0.378
E_p = 4.50 MeV
2.572 → 0.378
E_p = 4.55 MeV
2.572 → 0
E_p = 4.50 MeV
2.572 → 0
E_p = 4.55 MeV
RELATIVE INTENSITY
36
32
28
76
72
68
64
60
56
52
48
44
40
42
40
38
36
34
32
30
28
16
12
8
40
35
30
25
20
18
16
14
12
0
0.5
1.0
0
0.5
1.0
cos² θ

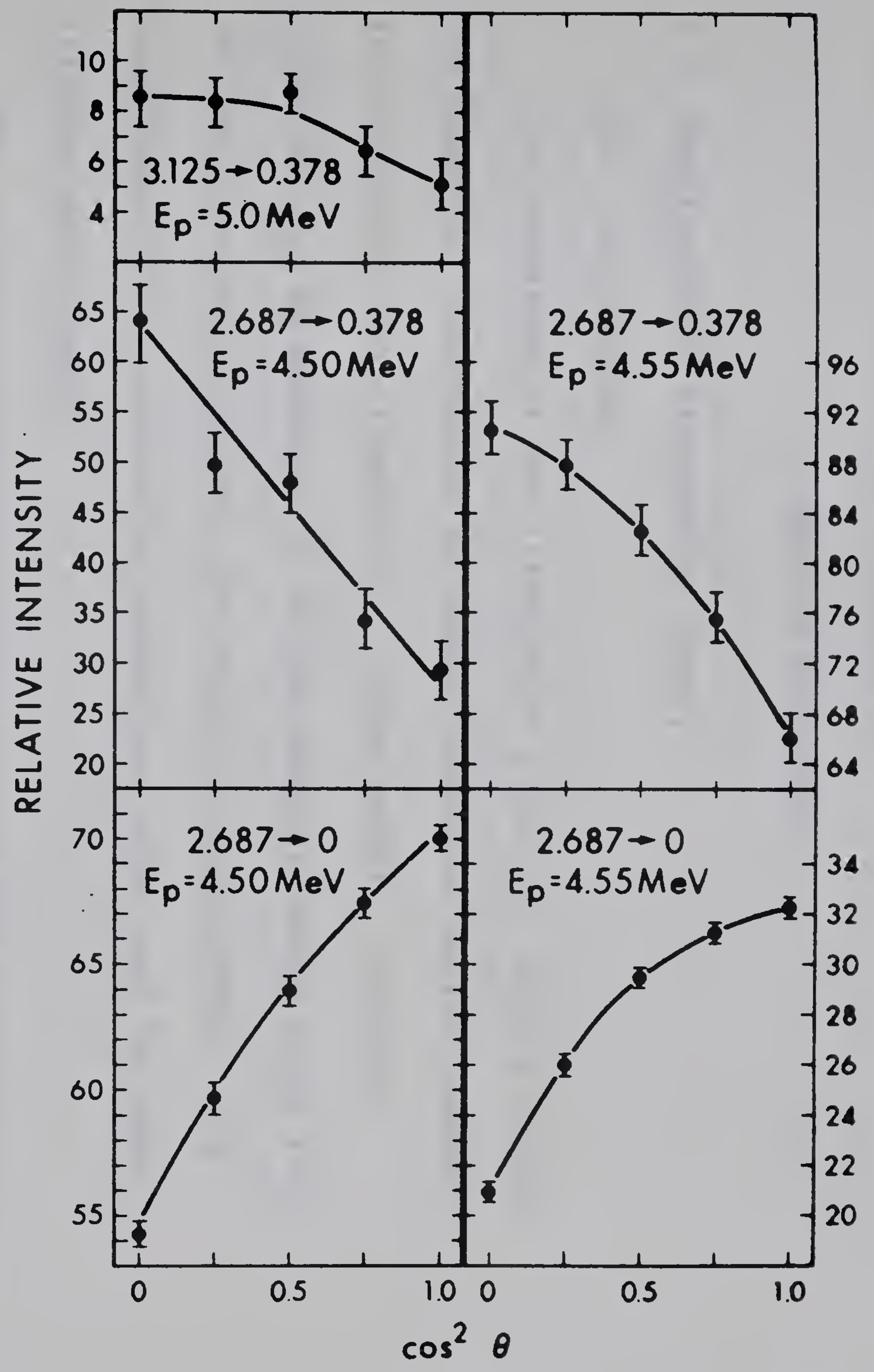
3.125 → 0.378
E_p = 5.0 MeV
2.687 → 0.378
E_p = 4.50 MeV
2.687 → 0.378
E_p = 4.55 MeV
2.687 → 0
E_p = 4.50 MeV
2.687 → 0
E_p = 4.55 MeV
RELATIVE INTENSITY
10
8
6
4
65
60
55
50
45
40
35
30
25
20
70
65
60
55
96
92
88
84
80
76
72
68
64
34
32
30
28
26
24
22
20
0
0.5
1.0
0
0.5
1.0
cos² θ

CHAPTER III

NUCLEAR LIFETIMES

3.1 Doppler-Shift Attenuation Theory

(a) Introduction

The knowledge of the lifetime of a nuclear state provides the essential information to obtain transition matrix elements for comparison with theoretical nuclear models. Nuclear lifetimes can be measured by various methods, among which the delayed-coincidence method, the recoil-distance method, and the Doppler-shift attenuation method are often used for short lifetime measurements.

The delayed-coincidence method involves the detection of the times of population and decay of the state whose lifetime is to be determined. The importance of this method lies in its general applicability for times greater than about 50 ps.

The recoil-distance method involves the direct measurement of the distance moved by the recoiling excited nucleus before de-excitation. The shortest lifetime measurable by this method appears to be about 5 ps.

The Doppler-shift attenuation method of measuring nuclear lifetimes relies on the rapid slowing down of swiftly moving atoms in a stopping material. In the Doppler-shift attenuation (DSAM), the nuclear lifetime is compared to the slowing-down

time of the recoiling excited nuclei. This time is of the order of 0.5 ps in a solid and about 500 ps in a gas, so that the DSAM may be used over a range of lifetimes from about 10 to 0.005 ps in the former case and from about 10,000 ps to 5 ps in the latter (Wa 67).

The principal methods and estimates of the range of applicability for each are listed in table 4 (Ol 68).

Table 4

Methods and estimated ranges for measuring lifetimes of states formed in nuclear reactions.

Method	Range in τ (ps)
Delayed-coincidence	$\tau \gtrsim 50$
Recoil-distance	$5 \lesssim \tau \lesssim 5{,}000$
DSAM	$0.005 \lesssim \tau \lesssim 10$

In the present work, only the Doppler-shift attenuation method, which has in the recent years become a general method for measuring short nuclear lifetimes, will be treated below. Elliott and Bell (El 48) carried out the first Doppler-shift measurement to deduce a lifetime for the first excited level of ^{7}Li from the ^{10}B(n,α) Li reaction. The Doppler-shift attenuation method was first exploited by Devons and his collaborators (De 55) and has been fully developed into an

extremely valuable method for the determination of short nuclear lifetimes by many investigators (Wa 63, Li 63, Bl 66).

(b) The Doppler-shift attenuation

A gamma-ray emitted from a nucleus recoiling freely in vacuum with a velocity V_0 has an energy $E(\theta)$ given by

$$E(\theta) = E_0[1 + \frac{V_0}{c} \cos \theta], \qquad V_0 << c , \qquad (III.1)$$

where E_0 is the gamma radiation energy for nuclei at rest, θ the angle of gamma emission relative to the recoil direction, and c the velocity of light. The average (or centroid) energy of the de-excitation gamma-rays emitted by an ensemble of recoil nuclei slowed down and stopped in a solid is given by (Es 65)

$$\bar{E}(\theta) = E_0 [1 + F(\tau) \frac{V_0}{c} \cos \theta] , \qquad (III.2)$$

where V_0 is the initial velocity of the recoil nucleus, and $F(\tau)$ is the attenuation factor related to the nuclear lifetime τ and slowing-down properties of the recoil nuclei in the stopping material.

In essence, the general problem involved in obtaining nuclear lifetimes τ based on the Doppler-shift attenuation method is the determination of the attenuation factor, $F(\tau)$,

theoretically and experimentally.

For any given lifetime, the value of $F(\tau)$ can be calculated if the slowing-down properties of the ion are known (Bl 66, Si 67, Ro 69):

$$F(\tau) = \frac{\int_0^\infty V(t)\ \overline{\cos\phi(t)}\ \exp(-t/\tau)\ dt}{\int_0^\infty V_0 \exp(-t/\tau)\ dt}$$

$$= \frac{1}{V_0\tau} \int_0^\infty V(t)\ \overline{\cos\phi(t)}\ \exp(-t/\tau)\ dt, \qquad (\text{III}.3)$$

where $\phi(t)$ is the angle between the recoil direction at time t and the initial recoil direction, $\overline{\cos\phi\ (t)}$ denotes an ensemble average over the observed nuclei which are scattered at the angle $\phi(t)$ relative to their initial direction.

The experimental attenuation factor, $F(\tau)_{exp}$, is the ratio of the observed (average) Doppler shift to the maximum possible shift and can be expressed by (Es 65)

$$F(\tau)_{exp} \equiv \frac{\text{observed average shift}}{\text{maximum possible shift}}$$

$$= \frac{\Delta E}{E_0 \frac{V_0}{c} (\cos\theta_1 - \cos\theta_2)}, \qquad (\text{III}.4)$$

where θ_1 and θ_2 are two different gamma-ray detector angles, and $\Delta E = \bar{E}\ (\theta_1) - \bar{E}\ (\theta_2)$.

Thus, comparison of the experimentally determined value of $F(\tau)$ with the calculated values will yield the nuclear lifetimes, τ.

(c) The attenuation factor, $F(\tau)$

In the formula of the attenuation factor (eq. III.3), $V(t)$ and $\overline{\cos\phi(t)}$ are related to the stopping power $\frac{dE}{dx}$ and the scattering of the recoil ions, respectively, i.e.,

$$\frac{dE}{dx} = M_1 \frac{dV(t)}{dt} , \tag{III.5}$$

where M_1 is the mass of the recoil ion (Li 63).

Therefore, the essence of determining the attenuation factor, $F(\tau)$, consists of using the slowing-down properties, i.e. the stopping power and the scattering of the recoil ions.

The slowing down of the recoil ion is due to two types of collision processes, electronic collisions and nuclear collisions. In the electronic collisions, the recoil ion interacts inelastically with the outer electrons in the stopping material and loses energy, and in the nuclear collisions the ion interacts elastically with an atom as a whole, thereby losing energy and perhaps being scattered away from the original direction of motion. Therefore, the stopping power is described as the sum of two distinct processes:

$$\frac{dE}{dx} = \left(\frac{dE}{dx}\right)_e + \left(\frac{dE}{dx}\right)_n , \qquad (III.6)$$

where e and n denote electronic and nuclear, respectively.

The stopping process: The stopping process of the recoil ion has been described in detail in a review article of Northcliffe (No 63).

At high velocities of the recoil ion ($V \gg \frac{c}{137} z_1$, where z_1 is the atomic number of the recoil ion), the electronic stopping power, $\left(\frac{dE}{dx}\right)_e$, increases with decreasing velocity roughly as $\frac{c^2}{v^2}$, and at intermediate velocities ($v \approx \frac{c}{137} z_1^{\frac{2}{3}}$) the electronic stopping power goes through a maximum. However, collisions with the nuclei of the medium will be relatively rare at these high velocities and will play no significant role in the energy loss process. As the decrease in recoil ion velocity continues, the electronic stopping power decreases, eventually falling to zero.

In the limit of very low velocities ($v < \frac{c}{137}$), i.e. lower than velocities of the orbital electron of the recoil ion, the nuclear stopping power is rapidly increasing approximately as $\frac{c^2}{v^2}$, while the electronic stopping power is declining to zero with decreasing ion velocity $\frac{v}{c}$. Below a certain critical velocity ($v_c \ll \frac{c}{137}$) the nuclear stopping power exceeds the electronic stopping power and goes through a maximum, and then also declines to zero.

The electronic stopping power : The theory of the electronic stopping power has been developed by many authors (Bo 48, Bl 33, Be 53, Fi 59, Li 63a). The theoretical formula for the electronic stopping power is given in a conventional form (No 63):

$$-\left(\frac{dE}{dx}\right)_e \quad \left(\frac{\mathrm{MeV}}{\mathrm{mg/cm^2}}\right) = 3.072 \times 10^{-4} \left(\frac{\gamma^2 z_1^2}{\beta^2 M_2}\right) \; B \tag{III.7}$$

with

$\beta \equiv \frac{v}{c}$, M_2 : amu ,

where γz_1 denotes the instantaneous net charge of the ion, M_2 the mass of an atom of the stopping medium (the suffixes 1 and 2 will be used throughout to denote the recoiling and stopping nucleus, respectively), B a dimensionless multiplier called the stopping number.

The stopping number B in the formula is in the form of a logarithmic function and has been calculated on the basis of various theories (Bl 33, Bo 48, Be 53).

Bethe (Be 30, Be 53) obtained the first purely wave-mechanical solution to the problem through use of the Born approximation. The stopping number given by Bethe's theory is

$$B = z_2 \left(\log \frac{2m_e v^2}{I} + \Delta L\right), \tag{III.8}$$

where z_2 is the atomic number of an atom of the medium, m_e is the mass of the electron, I is the mean excitation energy of the atomic electrons, and ΔL corresponds to the relativistic correction term.

Bloch (Bl 33) took into account the perturbation of the wave functions of the atomic electrons caused by the presence of the incident particle (also see No 63). Bloch (Bl 33) showed that, in stopping media consisting of atoms adequately described by the Thomas-Fermi atomic model, the mean excitation energy I is expected to be approximately proportional to z_2 :

$$I = k\, z_2 \qquad (III.9)$$

where k is the "Bloch constant". The empirically determined values of the Block constant k turn out to be ~ 10 keV for a wide range of z_2 values (see table 1 in ref. Fa 63).

Substituting Bloch's relation, $I = k\, z_2$, and Bethe's formula (III.8) into eq. (III.7), the Bethe-Bloch formula for the electronic stopping power will be obtained:

$$-\left(\frac{dE}{dx}\right)_e = 3.072 \times 10^{-4} \frac{\gamma^2 z_1{}^2}{\beta^2 M_2} z_2 \, (L + \Delta L), \qquad (III.10)$$

with

$$B \equiv z_2 \, (L + \Delta L) , \qquad (III.11)$$

$$L = \log 2 m_e \left[\left(\frac{c}{137}\right)^2 \Big/ k \right] + \log\left[\frac{(137\beta)^2}{z_2}\right], \qquad \text{(III.12)}$$

$$\Delta L = - \log (1 - \beta^2) - \beta^2 \qquad \text{(III.13)}$$

where the logarithmic function L is the nonrelativistic stopping number per atomic electron.

Lindhard and Scharff (Li 53) chose to regard L as an unknown universal function of $(137\beta)^2/z_2$, the form of which could be determined empirically by plotting the L values calculated from experimental stopping power data (using eq. (III.12)) vs. $\log \frac{(137\beta)^2}{z_2}$. The result is a smooth curve (almost a straight line) with little dependence of z_2 (see Fig. 5 in ref. Fa 63).

The Bethe-Bloch formula applies to the electronic stopping power in the high velocity region, but for low velocities it is no longer valid even if shell effects are taken into consideration (Fa 68).

Lindhard, Scharff and Schiott (Li 61a, Li 63 -- referred to as LSS) have treated the electronic stopping at low velocities ($0 < v < \frac{c}{137} z_1^{\frac{2}{3}}$) by using a Thomas-Fermi model of the interaction between heavy ions. In LSS, they introduced dimensionless variables ε for the energy and ρ for the range:

$$\varepsilon = \frac{a M_2}{z_1 z_2 e^2 (M_1 + M_2)} E ,$$

$$\rho = 4\pi a^2 N \frac{M_1 M_2}{(M_1 + M_2)^2} R , \qquad (\text{III}.14)$$

where z is the atomic number, M the atomic mass, N the number of scattering atoms per unit volume, E the kinetic energy of the moving atom, R the distance traveled along its path, and a the screening parameter in the Thomas-Fermi potential. That is, in a screen potential,

$$U(\gamma) = \frac{z_1 z_2 e^2}{\gamma} \phi_0 \left(\frac{\gamma}{a}\right) , \qquad (\text{III}.15)$$

$$a = 0.8853 \frac{1}{(z_1^{\frac{2}{3}} + z_2^{\frac{2}{3}})^{\frac{1}{2}}} \cdot \frac{\hbar^2}{m_e e^2} , \qquad (\text{III}.16)$$

where m_e and e are the mass and charge of the electron, ϕ_0 is the Fermi function.

For low recoil velocities ($0 < v < \frac{c}{137} z_1^{\frac{2}{3}}$), the electronic stopping power is given in ε-ρ units by (Li 63):

$$\left(\frac{d\varepsilon}{d\rho}\right)_e = k\, \varepsilon^{\frac{1}{2}} , \qquad (\text{III}.17)$$

$$k = z_1^{\frac{1}{6}} \frac{0.0793\, z_1^{\frac{1}{2}} z_2^{\frac{1}{2}} (A_1 + A_2)^{\frac{3}{2}}}{(z_1^{\frac{2}{3}} + z_2^{\frac{2}{3}})^{\frac{3}{4}} A_1^{\frac{3}{2}} A_2^{\frac{1}{2}}} , \qquad (\text{III}.18)$$

where $k \sim 0.1 - 0.2$: normal case
$k > 1$: $z_1 << z_2$
$k = 0.133\, z_2^{\frac{2}{3}} A_2^{-\frac{1}{2}}$: $z_1 = z_2$, $A_1 = A_2$.

The LSS formula gives a good over-all fit to experimental results at low velocities ($v < \frac{c}{137}$) (Sc 66). Oscillations around the theoretical k-value, due to atomic shell effects, have been observed, especially for low atomic numbers (Fa 68).

The nuclear stopping power : The role of nuclear collisions in the penetration process was first discussed by Bohr (Bo 48). Bohr employed the simple power potential based on the classical Rutherford scattering. Bohr's formula for the nuclear stopping power is given by (Gu 70):

$$\left(\frac{dE}{dx}\right)_n = N\, B_n \log \left[\frac{2E\, M_2 \hbar^2}{(M_1+M_2)\, z_1 z_2 e^4 m_e\, (z_1^{\frac{2}{3}} + z_2^{\frac{2}{3}})^{\frac{1}{2}}}\right], \qquad (\text{III}.19)$$

$$B_n = \frac{2\pi\, z_1^2 z_2^2 M_1 e^4}{M_2\, E}, \qquad (\text{III}.20)$$

where N is the number of atoms per cc in the stopping medium.

Bohr's ideas have been developed and refined by Lindhard, Scharff and Schiott (Li 61, Li 63). They have derived a universal curve for the nuclear stopping power using the Thomas-Fermi model. In LSS, the nuclear stopping power is given by (Li 63)

$$\left(\frac{d\varepsilon}{d\rho}\right)_n = \frac{1}{\varepsilon} \int_0^{\varepsilon} f(x)\ dx, \qquad (\text{III}.21)$$

$$\text{with} \quad f\,(t^{\frac{1}{2}}) = \frac{1}{\pi a^2}\, 2t^{\frac{3}{2}} \frac{d\sigma}{dt}, \qquad (\text{III}.22)$$

$$t^{\frac{1}{2}} = \varepsilon \cdot \sin \frac{1}{2}\,\text{Ⓗ}, \qquad \text{(III.23)}$$

where $d\sigma$ is a universal differential cross section, and Ⓗ is the deflection angle in the center of mass system. The function $f(t^{\frac{1}{2}})$ and the nuclear stopping power $(\frac{d\varepsilon}{d\rho})_n$ are given in Figs. 24 and 25, respectively.

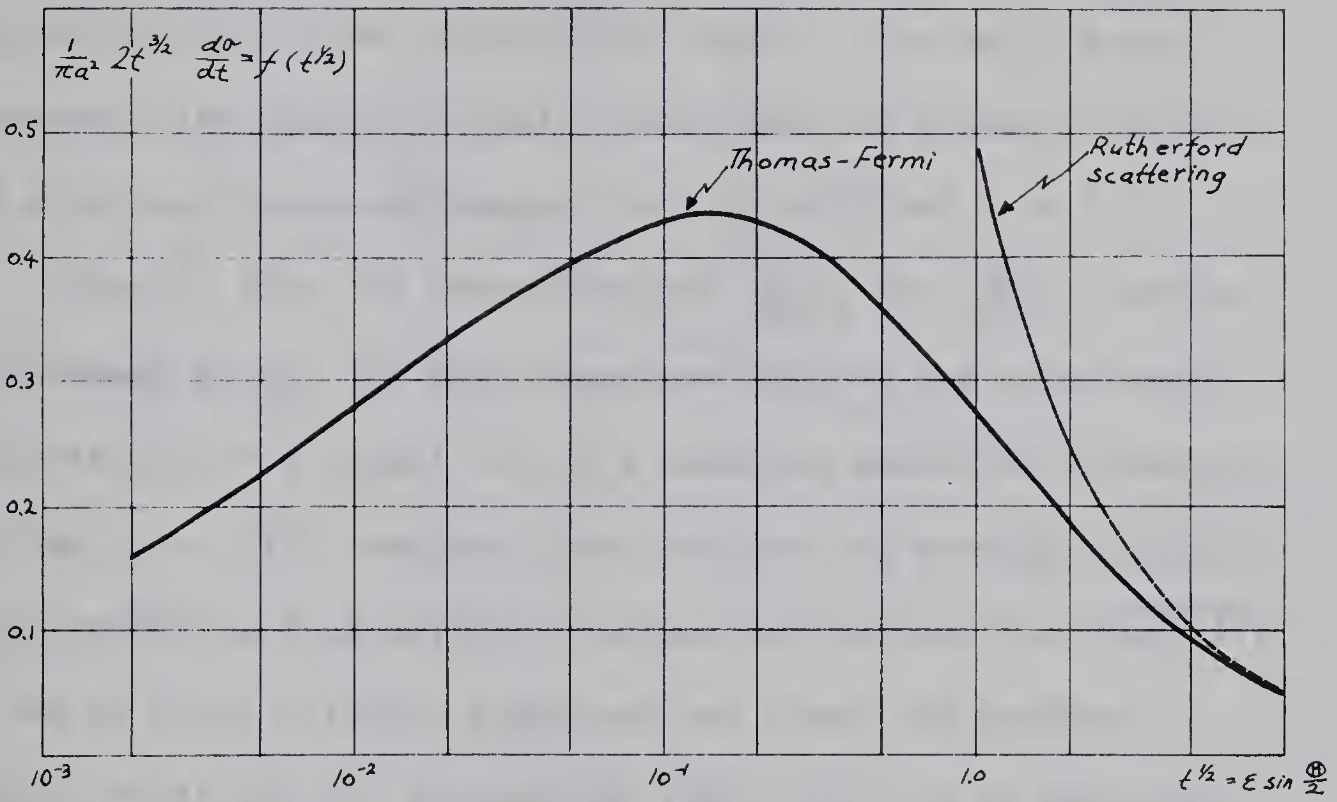

Fig. 24

Universal differential cross section for elastic nuclear collisions (taken from ref. Li 63). At high values of $t^{\frac{1}{2}}$ it smoothly joins Rutherford scattering.

The attenuation factor: As mentioned above, at the high velocities of the recoil ion ($v > \frac{c}{137} z_1^{\frac{2}{3}}$), only the electronic stopping power plays a significant role in the energy loss process, and at the low velocities ($0 < v < \frac{c}{137} z_1^{\frac{2}{3}}$) the nuclear stopping power is dominant, but both may play significant roles. At high

velocities, the Bethe-Bloch formula may be applied in the electronic stopping power. At low velocities Lindhard, Scharff and Schiott (Li 63) have derived the electronic and nuclear stopping power formulae using the Thomas-Fermi model, which give a good over-all fit to experimental data.

Fig. 25 shows nuclear and electronic stopping powers derived by LSS in the low velocity region. The solid curve represents the nuclear stopping power and the broken lines are the electronic stopping powers for $k = 0.15$ and $k = 1.5$.

Starting from the expression for $(\frac{d\varepsilon}{d\rho})_e$ and $(\frac{d\varepsilon}{d\rho})_n$, derived by Lindhard _et al_. (Li 63), Blaugrund (Bl 66) has calculated the velocity of a recoil ion in a stopping medium as a function of time, i.e. V(t), and has first derived the average scattering angle resulting from multiple nuclear collisions, i.e. $\overline{\cos \phi (t)}$. By use of these effects, Blaugrund has given the average Doppler shift and the attenuation factor $F(\tau)$ in an analytical form.

The nuclear specific energy loss function calculated by LSS from a Thomas-Fermi ion-atom potential has been published in graphical form (see Fig. 25), and has been tabulated by Schiott (Sc 66). This function has been approximated using various expressions, by Blaugrund (Bl 66),

$$(\frac{d\varepsilon}{d\rho})_n = (\frac{1}{2}\varepsilon)^{-1}\{0.3 + \log [(0.6 + \varepsilon^2)/\varepsilon]\} \quad : \quad \varepsilon > 1 \qquad (\mathrm{III}.24)$$

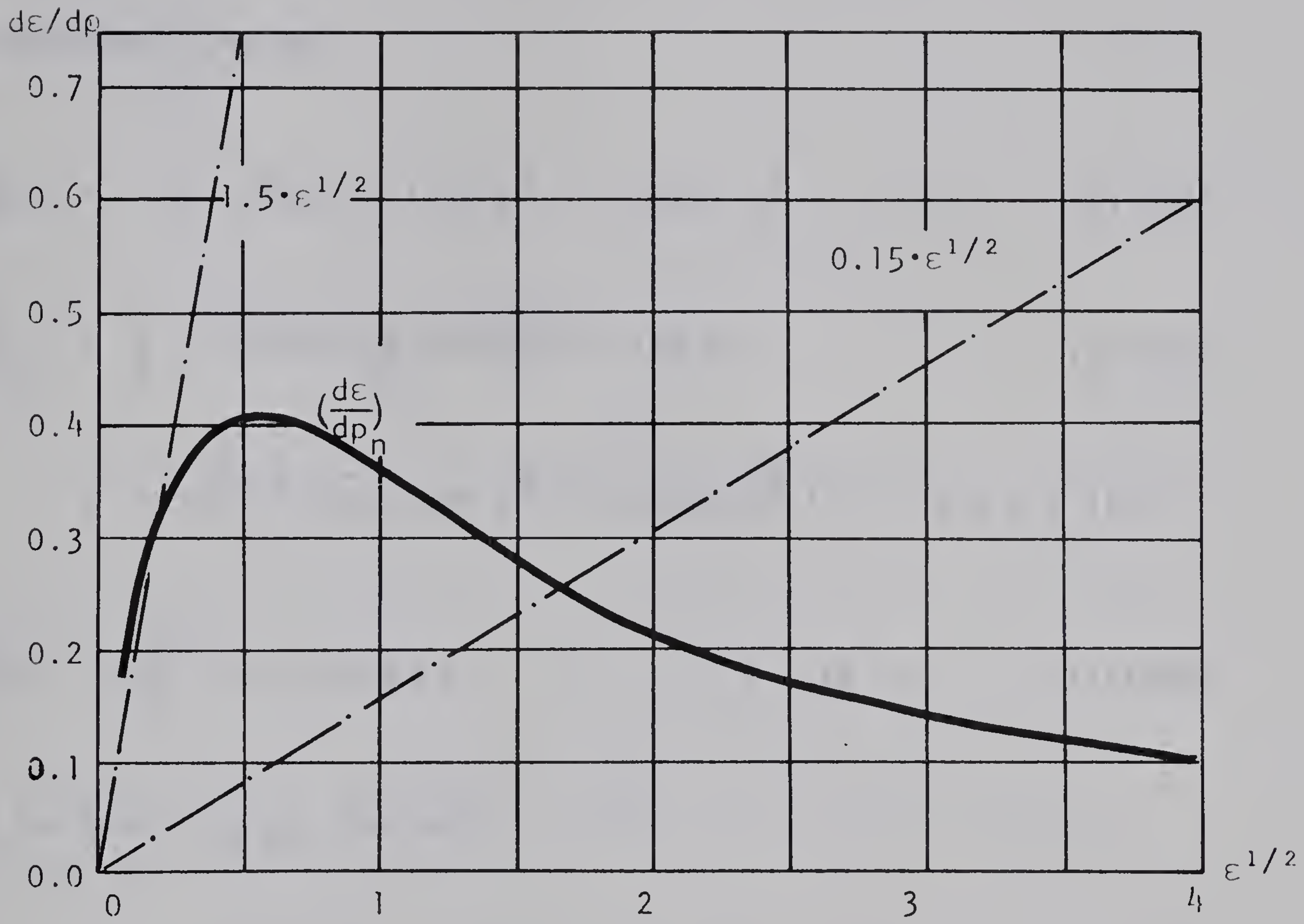

Fig. 25

Nuclear and electronic stopping powers (taken from ref. Li 63) in the low velocity region,

$$0 < v < \frac{c}{137} \ z_1^{\frac{2}{3}}.$$

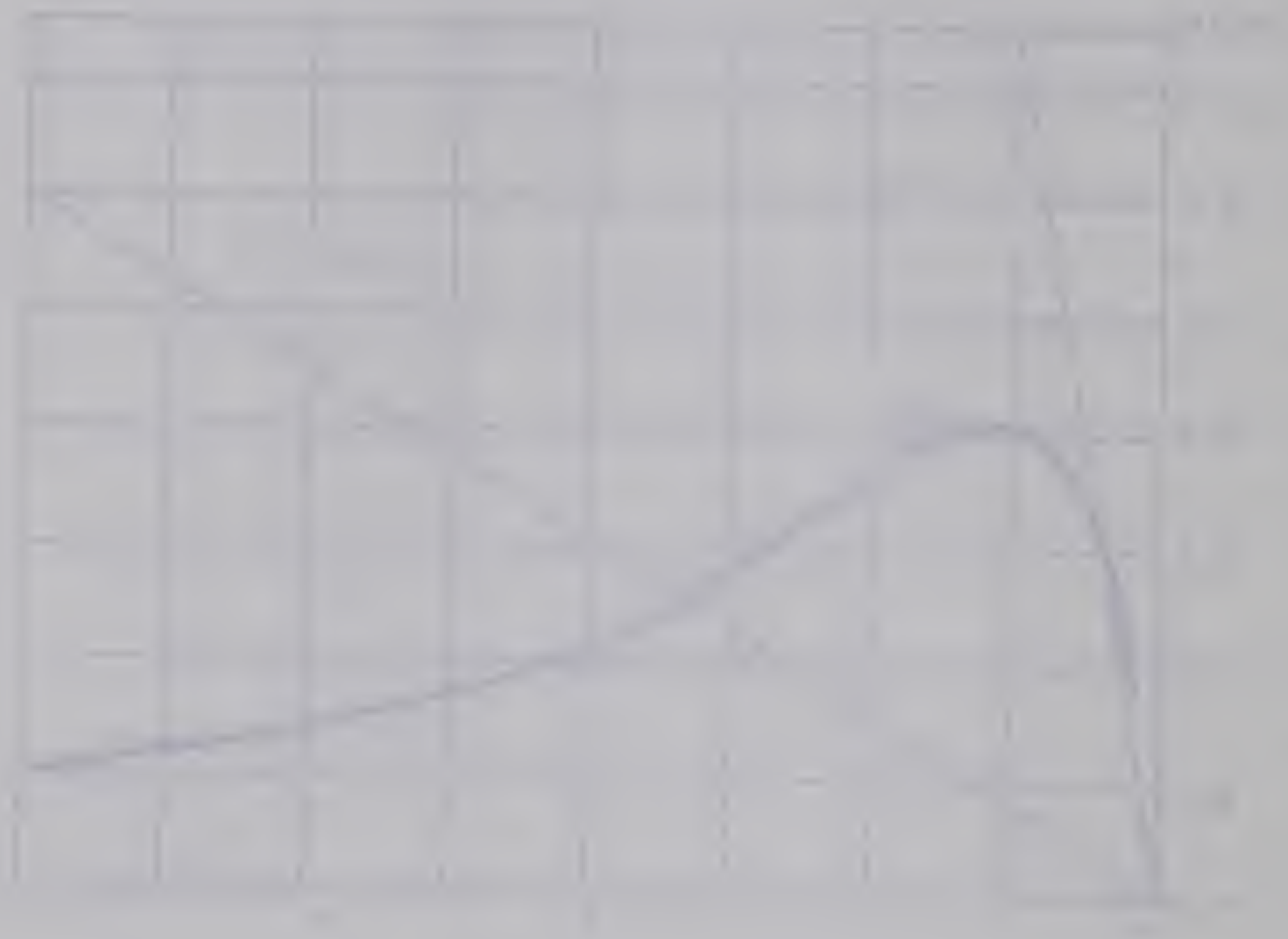

[illegible]

$$\left(\frac{d\varepsilon}{d\rho}\right)_n = 0.4\ \varepsilon^{-\frac{1}{2}} \quad : \quad 1.2 < \varepsilon < 20\ ; \qquad \text{(III.25)}$$

by Robertson (Ro 69),

$$\left(\frac{d\varepsilon}{d\rho}\right)_n = 1.97\ \varepsilon^{\frac{1}{2}} \exp\ (-1.82\ \varepsilon^{\frac{1}{2}}) + 0.0225\ \varepsilon^{\frac{1}{2}} \quad : \varepsilon < 14 \qquad \text{(III.26)}$$

$$\left(\frac{d\varepsilon}{d\rho}\right)_n = \frac{1}{4}\ \left\{\frac{(\varepsilon-14)\ \log\ (2.259\varepsilon)}{2\varepsilon} + (18-\varepsilon) \right. \qquad \text{(III.27)}$$

$$\left. \times\ (1.97\ \varepsilon^{\frac{1}{2}} \exp(-1.82\ \varepsilon^{\frac{1}{2}}) + 0.0225\ \varepsilon^{\frac{1}{2}})\right\} \quad : \quad 14 \leq \varepsilon \leq 18$$

$$\left(\frac{d\varepsilon}{d\rho}\right)_n = \frac{1}{2\varepsilon}\ \log\ (2.259\ \varepsilon) \quad : \quad \varepsilon > 18\ ; \qquad \text{(III.28)}$$

and by Bertin _et al_. (Be 69),

$$\left(\frac{d\varepsilon}{d\rho}\right)_n = \frac{\varepsilon^{\frac{1}{2}}}{0.67 + 2.07\,\varepsilon + 0.03\,\varepsilon^2}\ . \qquad \text{(III.29)}$$

In order to account for the scattering effect in the Doppler shift, $\overline{\cos\phi}$ has to be calculated as a function of time. The multiple scattering theory was developed by Goudsmit and Saunderson (Go 40) and extended by Lewis (Le 50).

For the particular case of the scattering law given by LSS, $\overline{\cos\phi}$ is given by (Bl 66)

$$\overline{\cos\phi} = \exp\ \left[-\ \frac{1}{2}\ \frac{A_2}{A_1}\ G\ (r)\ I\right]\ , \qquad \text{(III.30)}$$

with

$$I = \int_{\varepsilon}^{\varepsilon_0} \frac{(\frac{d\varepsilon}{d\rho})_n}{\varepsilon\,(\frac{d\varepsilon}{d\rho})}\, d\,\varepsilon, \qquad (III.31)$$

$$G\,(r) = 1 + \frac{2}{3}\,r - \frac{7}{15}\,r^2 + 8 \sum_{n=3}^{\infty} \frac{(-r)^n}{(2n+1)(2n-1)(2n-3)} : r < 1$$

$$= \frac{2}{3} + \frac{8}{15}\;\frac{1}{r} - 8 \sum_{n=3}^{\infty} \frac{(-\frac{1}{r})^{n-1}}{(2n+1)(2n-1)(2n-3)} : r > 1\,, \qquad (III.32)$$

where $r \equiv \frac{A_1}{A_2}$.

In the region $1.2 < \varepsilon < 20$, $(\frac{d\varepsilon}{d\rho})$ is fairly well approximated by (see eq. III.25)

$$\frac{d\varepsilon}{d\rho} = 0.4\,\varepsilon^{-\frac{1}{2}} + k\,\varepsilon^{\frac{1}{2}}, \qquad (III.33)$$

and $\overline{\cos\phi}$ is given by (Bl 66)

$$\overline{\cos\phi} = \left|\frac{1 + \frac{0.4}{k\varepsilon}}{1 + \frac{0.4}{k\varepsilon_0}}\right|^{-G/2r} . \qquad (III.34)$$

Once V(t) and $\overline{\cos\phi}$ are known as a function of the time t, the calculation of the attenuation factor, $F(\tau)$, is straightforward.

Ignoring the scattering term $\overline{\cos\phi}$ and assuming that for all

energies the stopping power in a medium is proportional to the ion velocity, i.e.,

$$\frac{dE}{dx} = M_1 \frac{dV(t)}{dt} = k\,V(t) \quad , \tag{III.35}$$

then the velocity, $V(t)$, will be given by

$$V(t) = V_0 \exp(-t/\alpha) \quad , \tag{III.36}$$

where $\alpha \equiv M_1/k$ is called the slowing-down time, k is a constant of proportionality, V_0 is the initial velocity. The attenuation factor, $F(\tau)$, is then given by

$$\begin{aligned} F(\tau) &= \frac{1}{V_0\tau}\int_0^\infty V(t)\exp(-t/\alpha)\,dt \qquad \text{(III.37)} \\ &= \frac{\alpha}{\alpha+\tau} \quad . \end{aligned}$$

The contribution of cascade gamma-rays to $F(\tau)$: In the cascade transitions, if the higher states have appreciable lifetimes, or significantly different initial velocities, the $F(\tau)$ observed for the lower state will be appreciably affected.

If several levels, each with lifetime τ_i and direct population ν_i $(i \geq 2)$, decay to a level with τ_1 and ν_1, then the observed Doppler shift for the latter level depends on (Be 69a)

$$\overline{F(\tau_1)} = \nu_1 F(\tau_1) + \sum_{i \geq 2} \frac{\nu_i}{\tau_i - \tau_1} [\tau_i F(\tau_i) - \tau_1 F(\tau_1)] , \qquad (III.38)$$

$$\text{where} \quad \nu_1 + \sum_{i \geq 2} \nu_i = 1 . \qquad (III.39)$$

Thus, assuming $F(\tau_i) = \dfrac{\alpha}{\alpha + \tau_i}$,

$$\overline{F(\tau_1)} = \nu_1 F(\tau_1) + \nu_2 F(\tau_2) F(\tau_1) \qquad (III.40)$$

for a single cascade,

$$\overline{F(\tau_1)} = \nu_1 F(\tau_1) + \nu_2 F(\tau_2) F(\tau_1) + \nu_3 F(\tau_3) F(\tau_1) \qquad (III.41)$$

for double cascades.

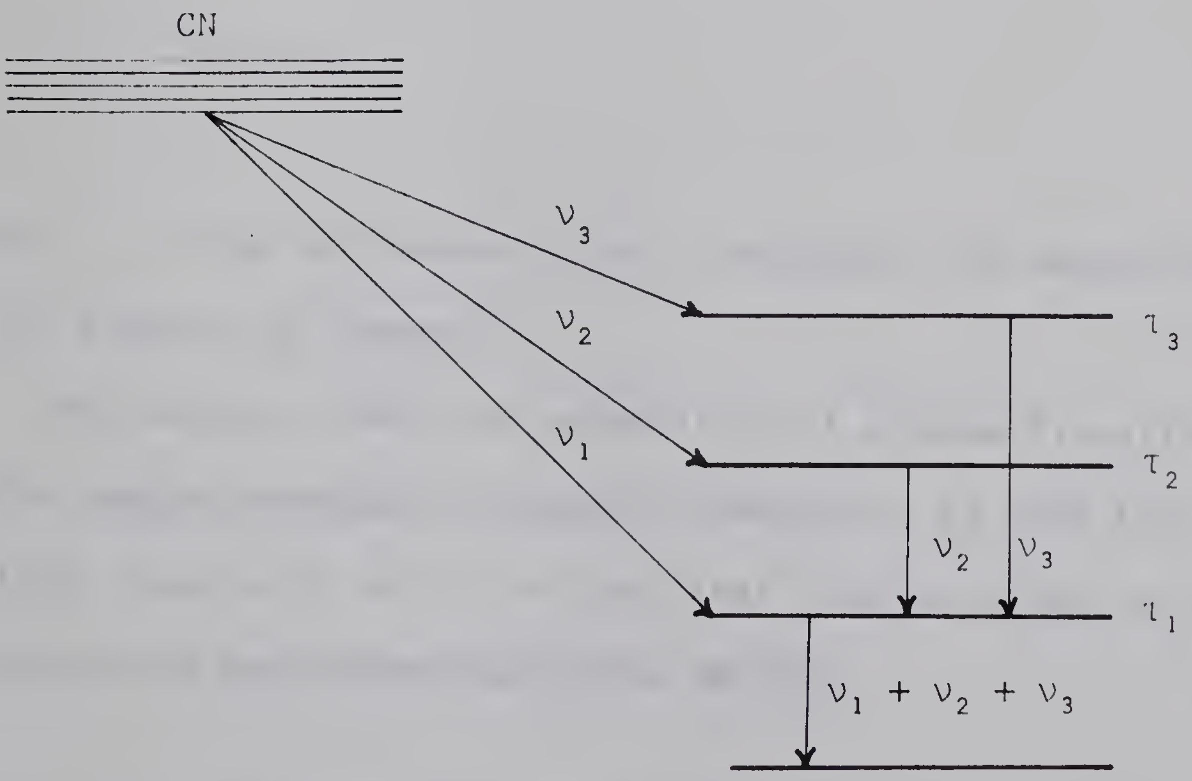
CN
ν_3
ν_2
ν_1
τ_3
τ_2
τ_1
ν_2
ν_3
$\nu_1 + \nu_2 + \nu_3$

Fig. 26

Cascade contribution to F (τ).

(d) Lifetimes and transition probabilities

By Heisenberg's uncertainty principle, the mean life, τ, may be expressed in terms of an energy width Γ of the level E_i:

$$\Gamma\tau = \hbar = 0.6582 \times 10^{-15} \text{ eV sec.} \tag{III.42}$$

The radiative transition probability is the reciprocal of the mean life τ of the level concerned, that is,

$$T = \frac{1}{\tau} = \frac{\Gamma}{\hbar} , \tag{III.43}$$

which is the sum of the partial transition probabilities,

$$T = \sum_{\sigma L} T (\sigma L) , \tag{III.44}$$

where L is the multipolarity and σ represents the decay mode, i.e., electric or magnetic.

The partial transition probability of a gamma transition (with angular momentum L, energy E, and parity π) from the initial level with spin J_i to the final level with spin J_f is given by the well-known expression (Bl 52):

$$T (\sigma L) = \frac{8\pi (L+1)}{L [(2L+1)!!]^2} \frac{1}{\hbar} \left(\frac{E}{\hbar c}\right)^{2L+1} B (\sigma L) , \tag{III.45}$$

with $J_i + J_f \geq L \geq |J_i - J_f|$

$$(2L+1)!! = 1.3.5 \ldots (2L+1) ,$$

where $B(\sigma L)$ is the reduced transition probability which is connected to the reduced matrix element by (Sk 66)

$$B(\sigma L) = \frac{1}{2J_i + 1} \left| \langle J_f \| M_{\sigma L} \| J_i \rangle \right|^2 , \tag{III.46}$$

where $M_{\sigma L}$ is the corresponding multipole operator.

$B(\sigma L)$ is usually expressed in units $[e^2 \cdot fm^{2L}]$ and $(n.m)^2$ for electric and magnetic transitions, respectively. Using convenient units,

$$\hbar = 6.582 \times 10^{22} \text{ MeV-sec}$$

$$\hbar c = 1.973 \times 10^{-11} \text{ MeV-cm}$$

$$e^2 = 1.440 \times 10^{-13} \text{ MeV-cm}$$

$$fm^4 = 10^{-52} \text{ cm}^4$$

$$M_p c^2 = 938.11 \text{ MeV}$$

$$(n.m)^2 = 0.1589 \times 10^{-40} \text{ MeV-cm}^3 \tag{III.47}$$

B(E2) and B(M1) may be expressed as

$$B(E2) = 8.1603 \times 10^{-10} \frac{T(E2)}{E^5} \; e^2\text{-}fm^4$$

$$= 1.2397 \times 10^{6} \frac{\Gamma(E2)}{E^5} \tag{III.48}$$

$$B(M1) = 56.9552 \times 10^{-15} \frac{T(M1)}{E^3} (n.m)^2$$

$$= 8.6531 \times 10^{1} \frac{\Gamma(M1)}{E^3} , \qquad (III.49)$$

where

$$T(\sigma L) = \frac{\Gamma(\sigma L)}{6.582 \times 10^{-16}}$$

$T(\sigma L)$: sec^{-1}

E : MeV

$\Gamma(\sigma L)$: eV

The E2/M1 multipole mixing ratio δ may be given by the relations,

$$\delta^2 = \frac{T(E2)}{T(M1)} = 0.03 \left(\frac{E}{\hbar c}\right)^2 \frac{B(E2)}{B(M1)} , \qquad (III.50)$$

$$T(M1) = \frac{1}{1+\delta^2} T , \qquad (III.51)$$

$$T(E2) = \frac{\delta^2}{1+\delta^2} T , \qquad (III.52)$$

$$T = T(M1) + T(E2) . \qquad (III.53)$$

Excited states sometimes have available two or more paths for decay, such as two nuclear transitions or beta-ray

emission in competition with a nuclear transition. Each path has its own characteristic partial mean life τ_1, τ_2 · · ·. Thus, the observed mean life, τ, of the state is given by

$$\frac{1}{\tau} = \frac{1}{\tau_1} + \frac{1}{\tau_2} + \cdots . \qquad (\text{III}.54)$$

Evidently, when one of the partial mean life values is much shorter than all of the others, it will be the main one to determine the observed mean life of the state.

Partial mean lives can never be measured directly and the decay rates of each of a number of competing radiations will be exactly equal to each other and to the overall mean life of the parent state. Partial mean life values may be inferred from the relative intensities of the competing radiations together with the observed mean life of the state.

If a considerable internal conversion is included, the lifetime must be corrected by

$$\tau = \tau_{total} (1 + \alpha_T) , \qquad (\text{III}.55)$$

where τ is the radiative decay lifetime, τ_{total} the total life time, α_T the total internal conversion coefficient.

3.2 Experimental Method

(a) Apparatus

Lifetime measurements were performed by means of the Doppler-shift attenuation method through the ^{53}Cr(p,nγ)^{53}Mn reaction at a proton energy of 4.9 MeV. The experimental method has been previously described in the earlier work (Gu 70). Fig. 27 shows a schematic diagram of the experimental arrangement.

A thick target (~ 3 mg/cm^2) was prepared by evaporation of Cr_2O_3 (enriched to 96.4% ^{53}Cr) onto 0.127 mm thick tantalum backing; the target itself was thick enough to stop more than 98% of the recoiling ^{53}Mn nuclei (see Gu 70).

The gamma-rays were detected in a 48 cc Ge(Li) crystal placed 10 cm from the target in coincidence with neutrons detected in an annular liquid organic scintillator (NE 218) located 15 cm upstream from the target at an angle of approximately 180° with respect to the beam direction.

The faces of the neutron detector were shielded with lead (about 1.5 cm thick) to reduce the gamma-ray flux into the scintillator, and the Ge(Li) crystal was shielded with lead (about 0.3 cm thick) to reduce significantly the counting rate produced by low energy gamma-rays.

A NaI crystal was placed directly above the Ge(Li) detector. Two sources, ^{60}Co and ^{88}Y, were situated midway between the detectors, and provided a continuous calibration during the

lifetime experiment by means of γ-γ coincidence spectra of the sources.

The electronics block diagram is shown in Fig. 28. The neutron detector was biased at -2150 volts and the discriminator was set just above the self-triggering level.

The slow and fast signals from the neutron detector are fed into the neutron identifier TAC. The gamma-ray slow signals (E) from the Ge(Li) detector are fed directly into the analog-to-digital converter (ADC) and into the coincidence units through an R-C amplifier and a single channel analyzer with a window set on the desired gamma spectrum.

The gamma-ray fast signals (T) from the Ge(Li) detector are fed into the starts of the n-γ TAC and γ-γ TAC, where the n-γ TAC is stopped by the neutron fast signals and the γ-γ TAC is stopped by the γ-ray pulses from the NaI detector. A timing SCA (TSCA) is used to put a window on the spectra of the ^{60}Co and ^{88}Y.

The true start signal of the n-γ TAC is delayed and then used to strobe three SCA's at the sides of the Ge(Li) detector, the n-ident. TAC and the n-γ TAC at the same time.

(b) n-γ coincidence spectrum

The beam current was approximately 30 nA and the counting rate in the Ge(Li) was maintained at about 6,000 counts/sec.

The n-γ coincidence spectra were taken at 0° and 120° and the runs were for about 8 and 6 hours, respectively.

Fig. 27 A schematic diagram of the experimental arrangement for the lifetime measurements (cross section in a vertical plane).

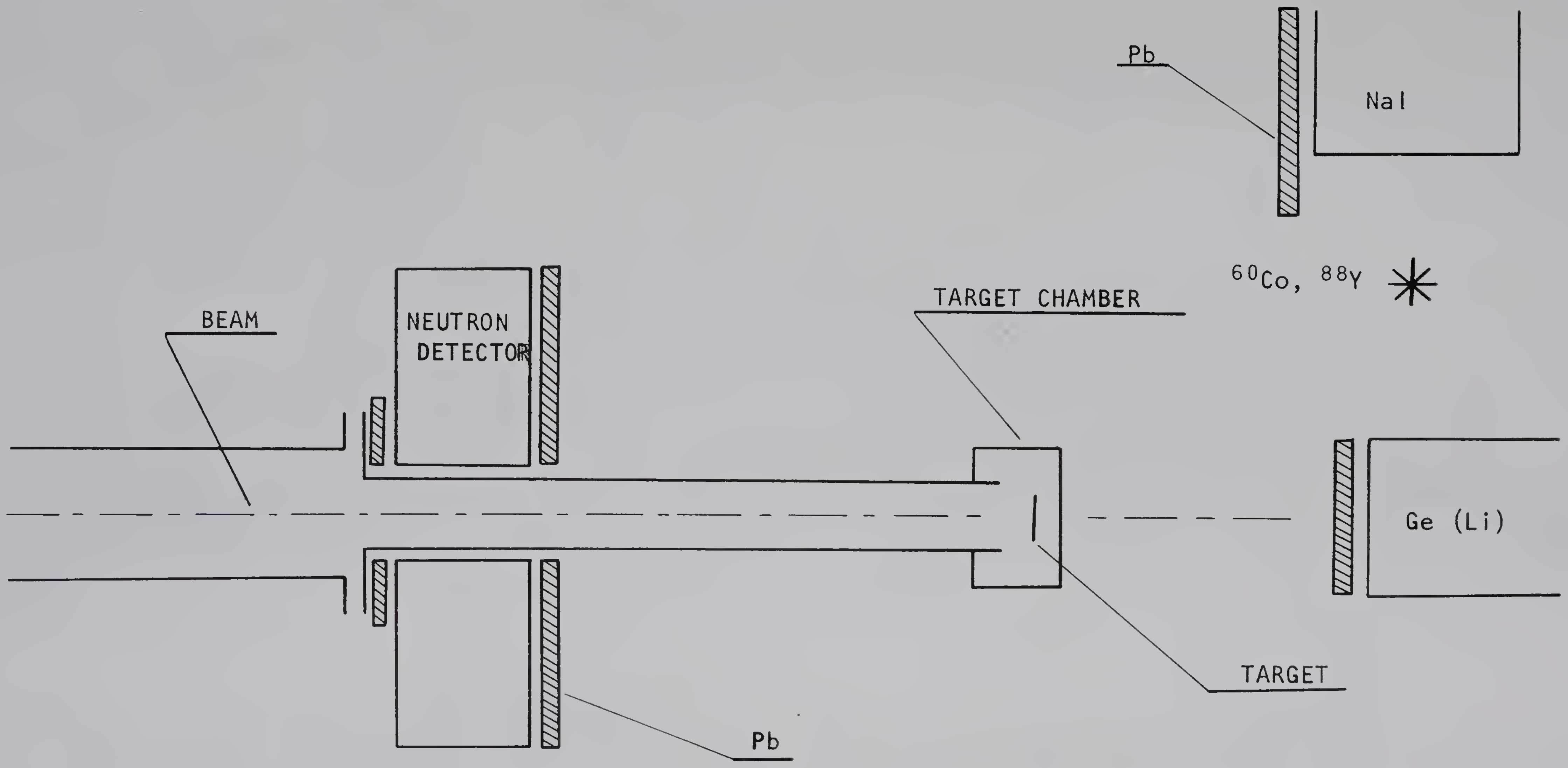
Pb
NaI
^{60}Co, ^{88}Y
BEAM
NEUTRON DETECTOR
TARGET CHAMBER
Ge (Li)
TARGET
Pb

Fig. 28 The electronics.

DDLA : Double delay line amplifier (Ortec model 410)

TPOC : Time pickoff control (Ortec model 403A)

R-CA : Research amplifier (Ortec model 450)

TFA : Timing filter amplifier (Ortec model 454)

G & D : Gate and delay generator (Ortec model 416)

TSCA : Timing single channel analyzer (Ortec model 455)

CFPHT : Constant fraction timing discriminator (Ortec model 453)

CI SCA : Single channel analyzer (Canberra model 1431)

Strobed SCA : Strobed single channel analyzer (Ortec model 413)

U.C. : Universal coincidence (Ortec model 418)

TAC : Time to amplitude converter (Ortec model 437)

FZCD : Fast zero crossing discriminator (Ortec)

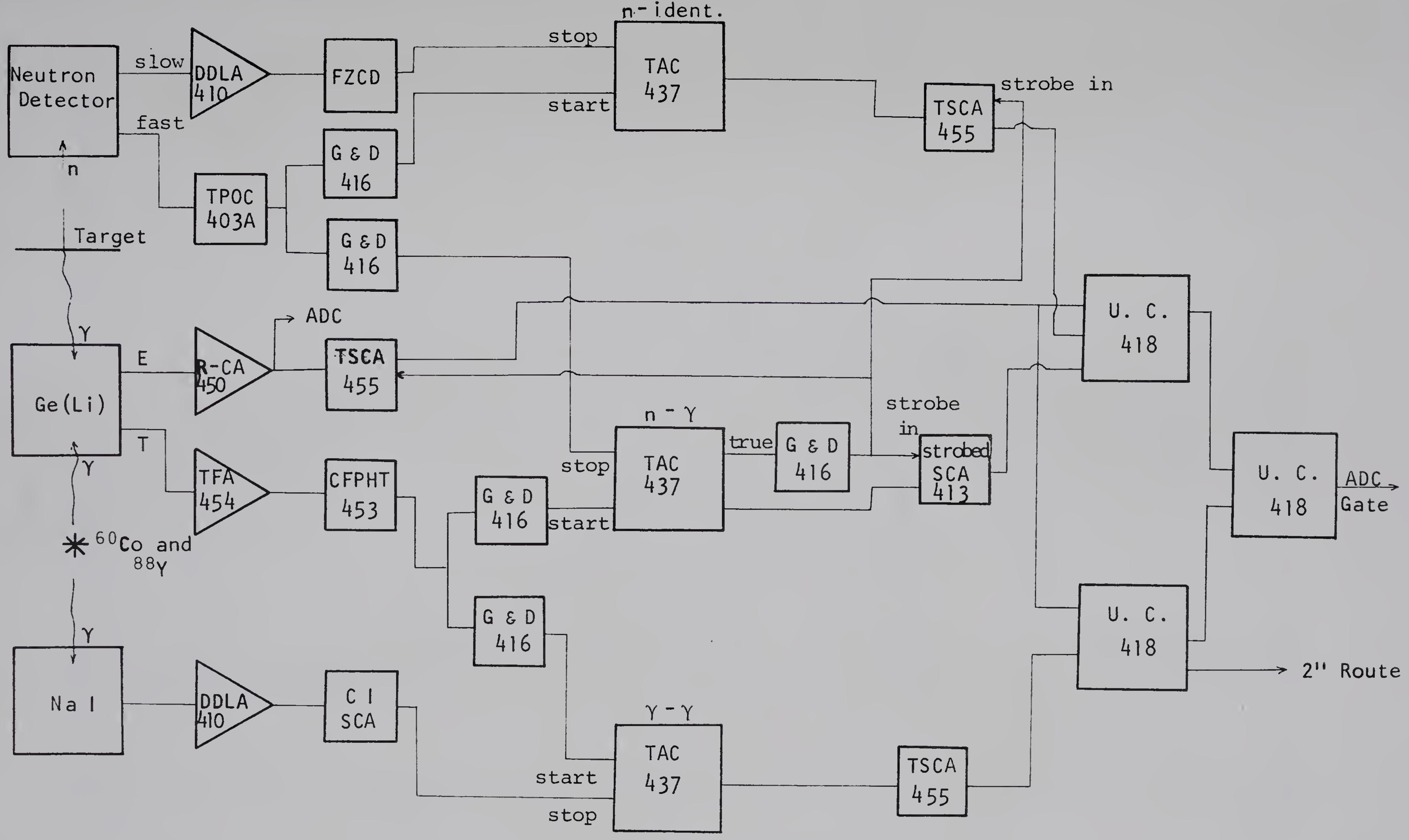
Neutron Detector
slow
fast
n
DDLA 410
FZCD
TPOC 403A
G & D 416
G & D 416
Target
γ
Ge(Li)
E
T
R-CA 450
ADC
TSCA 455
TFA 454
CFPHT 453
γ
60Co and 88Y
γ
Na I
DDLA 410
C I SCA
n-ident.
stop
start
TAC 437
TSCA 455
strobe in
n - γ
stop
start
TAC 437
true
G & D 416
strobe in
strobed SCA 413
G & D 416
G & D 416
γ - γ
start
stop
TAC 437
TSCA 455
U. C. 418
U. C. 418
U. C. 418
ADC Gate
2" Route

Fig. 29 A typical n-γ time spectrum.

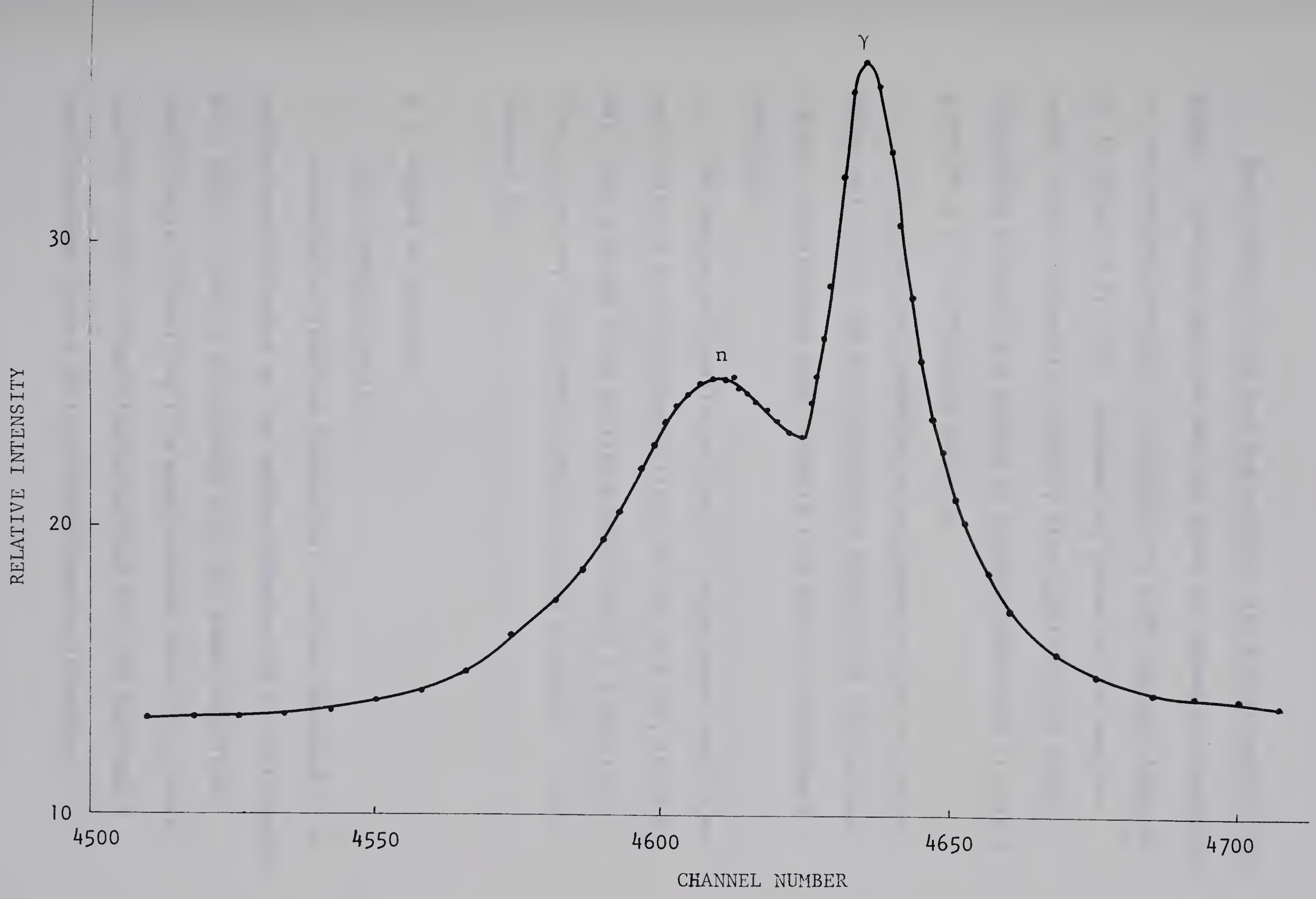
γ
n
30
20
10
RELATIVE INTENSITY
4500
4550
4600
4650
4700
CHANNEL NUMBER

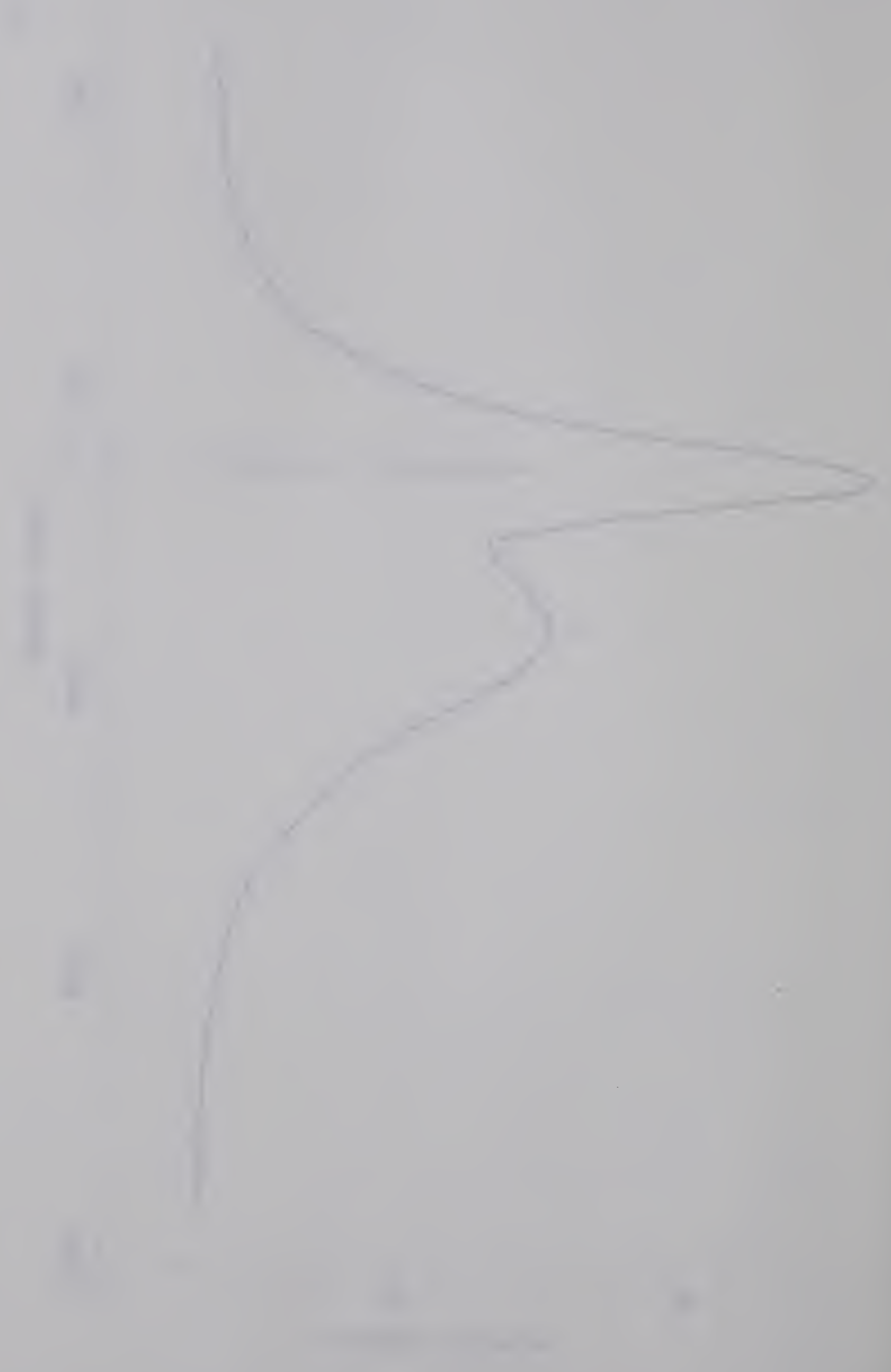

Each output of the n-γ and n-ident. TAC's will contain two peaks -- one for neutrons and the other for gamma rays detected in the neutron detector. A typical n-γ time spectrum taken at 0° is shown in Fig. 29. Windows are placed on the neutron peaks of the n-identifier and n-γ time spectra using TSCA's, the pulses of which are placed in a coincidence unit (I); this provides a n-γ coincidence spectrum.

By routing the kicksorter by an output of the γ-γ coincidence unit (II), the γ-γ coincidence spectrum of the sources is put into the next 2048 channels from the n-γ coincidence spectrum.

The energy calibration of the n-γ coincidence spectra was made with the γ-γ coincidence lines of ^{60}Co and ^{88}Y, the 0.511 MeV line, and the first excited state line ($\tau \approx 170$ ps) of ^{53}Mn in the n-γ coincidence spectra, using a quadratic least-squares fit.

3.3 Method of Analysis

(a) Kinematic shift

According to reaction kinematics, neutrons detected in a narrow cone subtended by the neutron detector (e.g., half-angle of ~ 20°) will be in coincidence with the gamma rays from recoil nuclei travelling in a much narrower cone (e.g., half-angle of ~ 4°). It was also calculated that the beam would lose less than 10 keV of its original energy in passing

through the target, giving very little uncertainty in the recoil nucleus initial velocity.

The kinematic (maximum possible) shift, from eq. (III.1), is given by

$$\text{Kinematic shift} = E_0 \frac{V_0}{c} (\cos\theta_1 - \cos\theta_2), \tag{III.56}$$

where θ_1 and θ_2 are two different gamma-ray detector angles, V_0 the initial velocity of the recoil nucleus, and E_0 the unshifted gamma-ray energy.

The ratios $\frac{V_0}{c}$ ($\equiv \beta_0$) for the excited levels to be considered were calculated by means of relativistic kinematics (Fortran program DSAM 1A), taking into account the finite detection angle of the neutron detector and incident beam energy loss through the target.

The unshifted gamma-ray energy E_0 can be determined, from eq. (III.2), by

$$E_0 = \frac{\bar{E}(\theta_1)\cos\theta_2 - \bar{E}(\theta_2)\cos\theta_1}{\cos\theta_2 - \cos\theta_1}, \tag{III.57}$$

where $\bar{E}(\theta)$ is the average (or centroid) energy of the de-excitation gamma-rays observed at the angle of θ.

(b) Centroid calculations

The centroid of a gamma-ray peak may be calculated by

$$\bar{i} = \frac{\sum_{i=1}^{I} (c_i - b_i) \cdot i}{\sum_{i=1} (c_i - b_i)} , \qquad (III.58)$$

where c_i and b_i are the total and background counts in channel i, and I is the total number of channels summed over.

The background in channel i may be given by

$$b_i = c_L - \frac{(c_L - c_R)}{I} \cdot i \quad , \qquad (III.59)$$

where c_L is the average channel count in the left background region, c_R the average channel count in the right background region.

The centroid calculations of the gamma-ray peaks in the n-γ and γ-γ coincidence spectra were performed using an APL program BACK (Gu 70).

(c) The attenuation factor, $F(\tau)$

In order to determine the observed shifts between $\theta_1 = 0°$ and $\theta_2 = 120°$, i.e., $\Delta E = \bar{E}(\theta_1) - \bar{E}(\theta_2)$, centroids of the gamma-ray peaks to be considered were calculated and then calibrated with energies of the known standard peaks. The experimental attenuation factor, $F(\tau)_{exp}$, was obtained from eq. (III.4).

The theoretical attenuation factors, $F(\tau)_{theor}$, were calculated using an ALGOL program OXDS (Ro 69) which includes

the effects of the large-angle scattering and the nuclear stopping power, as well as the electronic stopping power based on the Lindhard theory. The results agree with Blaugrund's calculations to within 10% over most of the range of $F(\tau)$. Typical $F(\tau)$ versus τ curves are shown in Figs. 30 and 31. Contribution of cascade gamma-rays to $F(\tau)$ was taken into consideration by eq. (III.38).

(d) Nuclear lifetimes and transition probabilities

Lifetimes τ for the excited states in ^{53}Mn under investigation were extracted from the $F(\tau)$ versus τ curves and the measured $F(\tau)$ values.

Two types of errors contribute to the lifetime obtained from the Doppler-shift measurement. The first of these is simply the error in the measured $F(\tau)$, which arises primarily from the statistical uncertainty in the determination of the centroid shift, ΔE. Uncertainties in the initial recoil velocity, V_0, and detector angles make small contributions to this error. The second type of error is associated with uncertainties in the stopping powers used to evaluate the theoretical attenuation factor. Under the present considerations, it can be expected that the accuracy of experimental $F(\tau)$ determinations is ~ 10% and the accuracy of an $F(\tau)$ calculation is approximately 15 to 20%.

The total transition probabilities T can be obtained from the measured lifetimes τ using eq. (III.43) and the partial

Fig. 30 A typical $F(\tau)$ versus τ curve for the 1.440 MeV level of ^{53}Mn (E_p = 4.9 MeV).

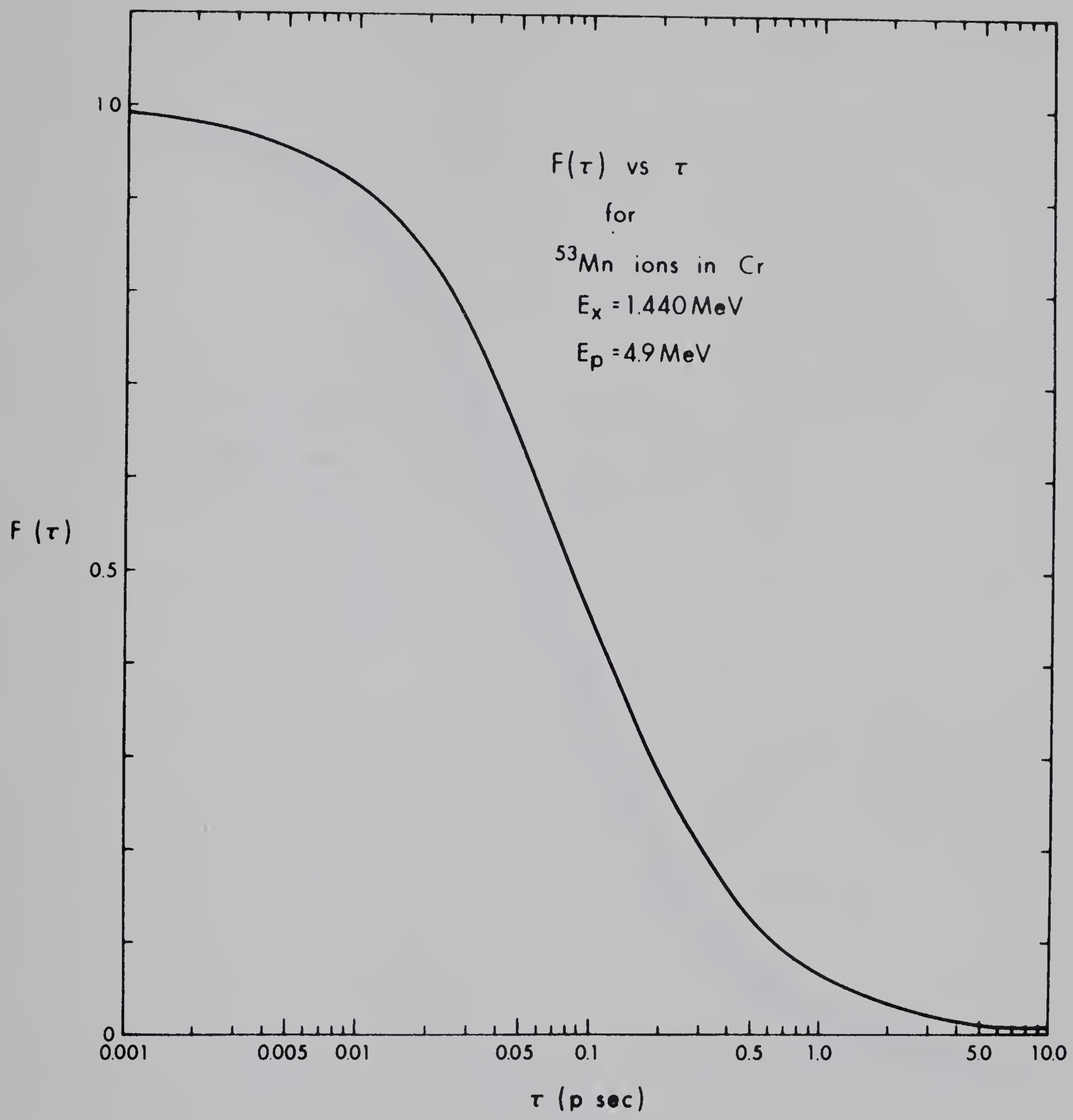

1.0
0.5
0
F (τ)
F(τ) vs τ
for
^{53}Mn ions in Cr
E_x = 1.440 MeV
E_p = 4.9 MeV
0.001
0.005
0.01
0.05
0.1
0.5
1.0
5.0
10.0
τ (p sec)

Fig. 31 $F(\tau)$ curves corresponding to ^{53}Mn ions recoiling with various initial velocities. Numbers indicate energies (in MeV) of excited states in ^{53}Mn.

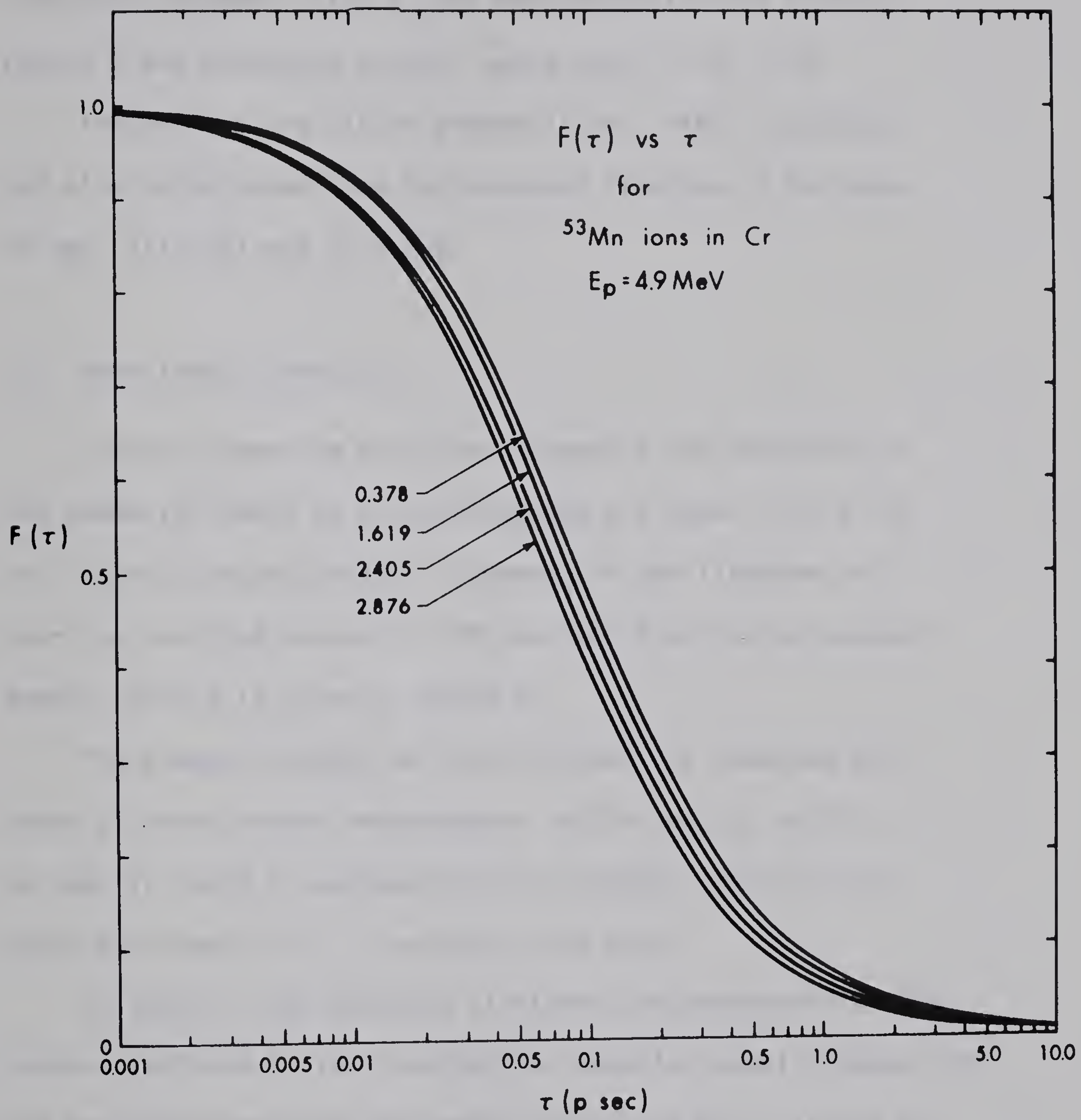
F(τ) vs τ
for
^{53}Mn ions in Cr
E$_p$=4.9 MeV
0.378
1.619
2.405
2.876
F (τ)
1.0
0.5
0
0.001
0.005
0.01
0.05
0.1
0.5
1.0
5.0
10.0
τ (p sec)

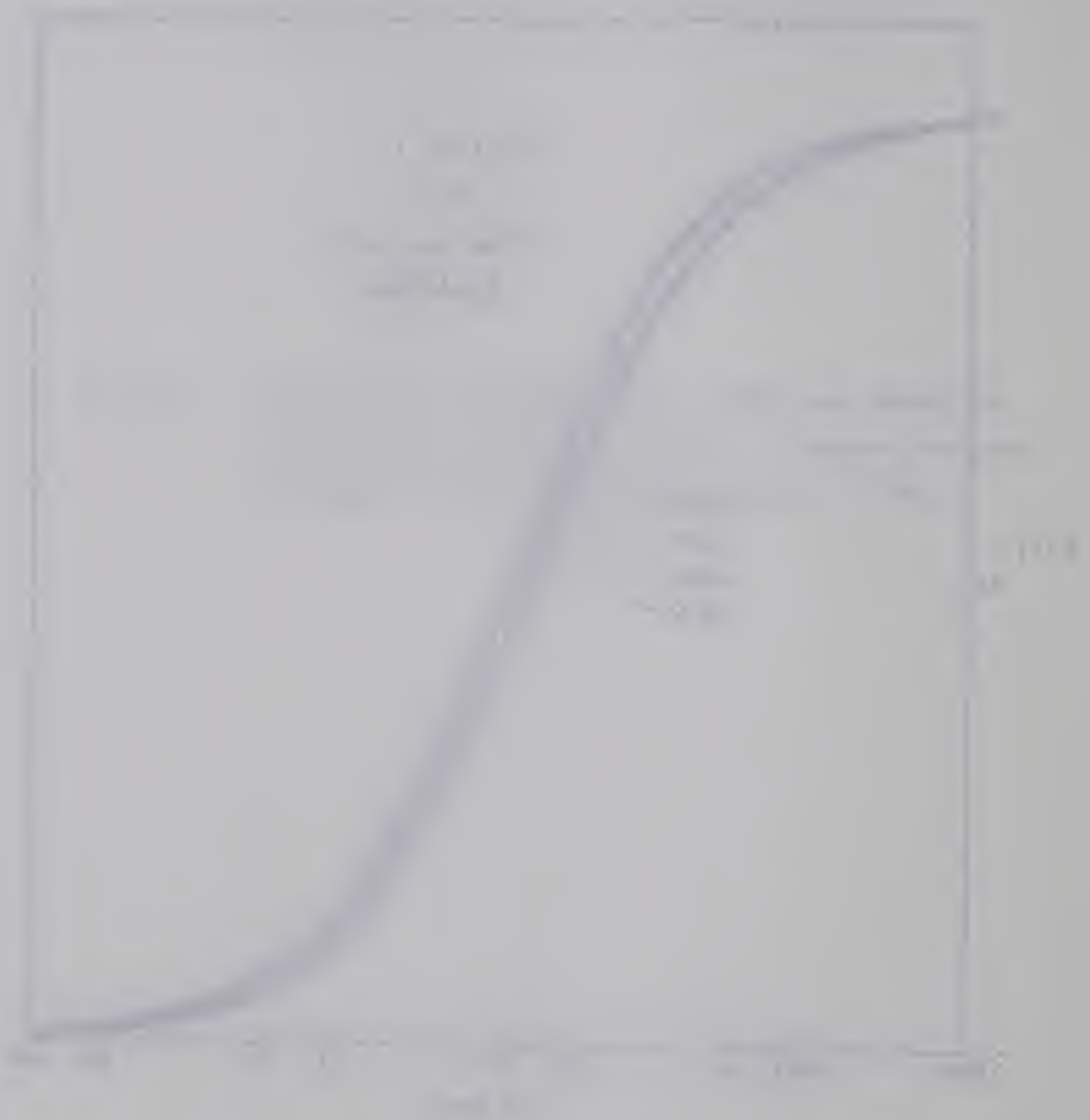

transition probabilities $T(\sigma L)$ are deduced from the total transition probabilities T, the measured multipole mixing ratios δ and branching ratios, using eqs. III.51 - 54.

The reduced transition probabilities, B(M1) and B(E2) can also be obtained from the measured lifetimes τ by means of eqs. (III.48) and (III.49).

3.4 Experimental Results

Typical gamma-ray coincidence spectra and centroids of the gamma-ray peaks to be investigated are shown in Fig. 32 and table 5, respectively. A summary of the lifetimes of low-lying excited states in ^{53}Mn derived from the attenuated Doppler shifts is given in table 6.

The present results of the lifetimes are compared with those of other recent measurements (Go 66, Gu 70, Ma 70). As seen in table 6, agreement of the present results with other experiments is, in general, very good.

In table 7, the measured lifetimes are compared with the values predicted by the Intermediate Coupling model (Chapter IV) and the single-particle estimates (Bl 52, Mo 66). It may be seen from table 7 that there is good agreement between the lifetimes obtained in the present experiment and those predicted by the Intermediate-Coupling model. It is also found, in Chapter IV, that the experimental reduced transition probabilities, B(M1) and B(E2) are in good agreement with the

Fig. 32 Doppler shifted coincidence spectra of gamma-rays observed at 0° and 120°.

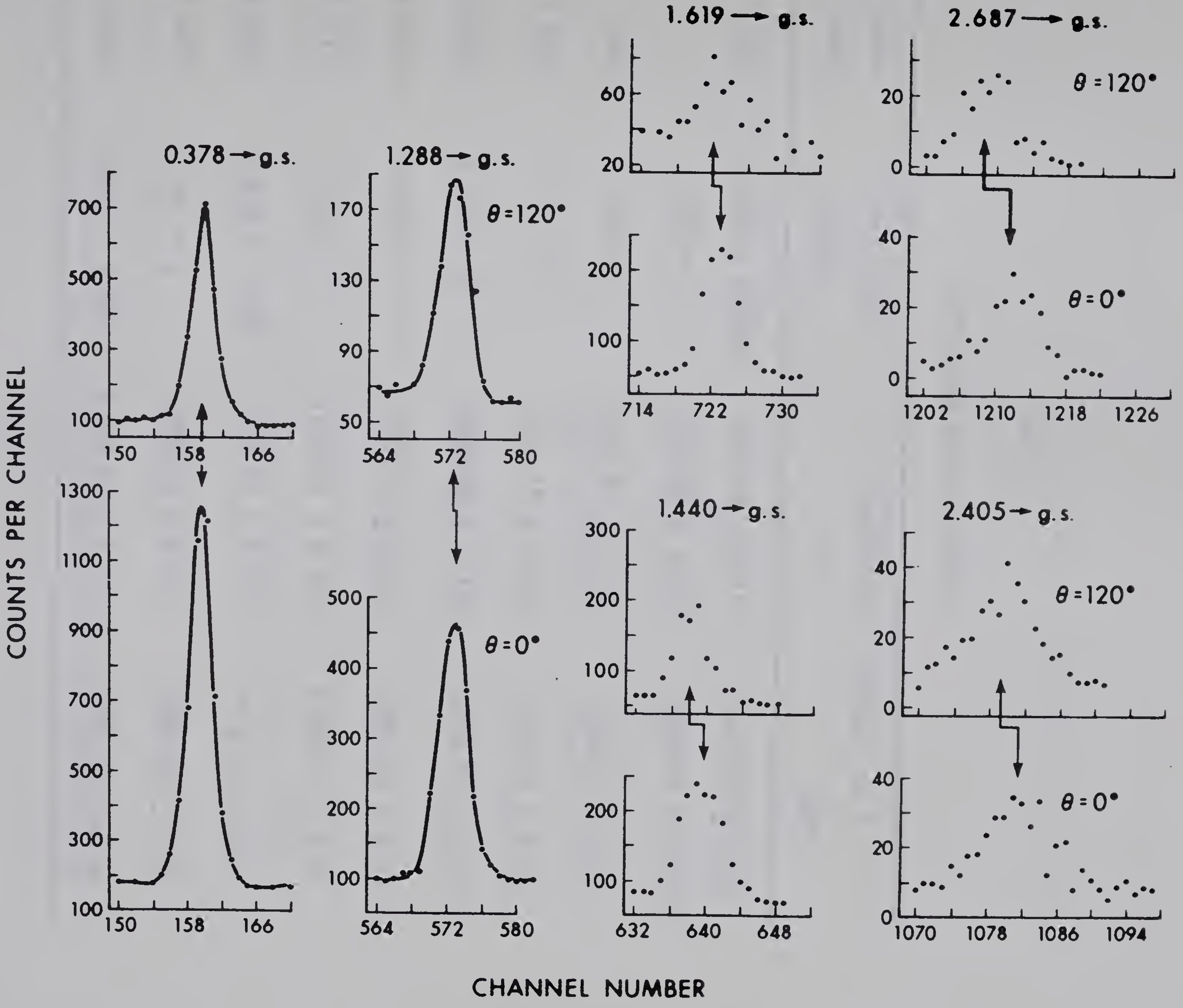
0.378 → g.s.
1.288 → g.s.
1.619 → g.s.
2.687 → g.s.
1.440 → g.s.
2.405 → g.s.
θ = 120°
θ = 0°
COUNTS PER CHANNEL
CHANNEL NUMBER
700
500
300
100
1300
1100
900
170
130
90
50
400
200
60
20
40
0
150
158
166
564
572
580
714
722
730
1202
1210
1218
1226
632
640
648
1070
1078
1086
1094

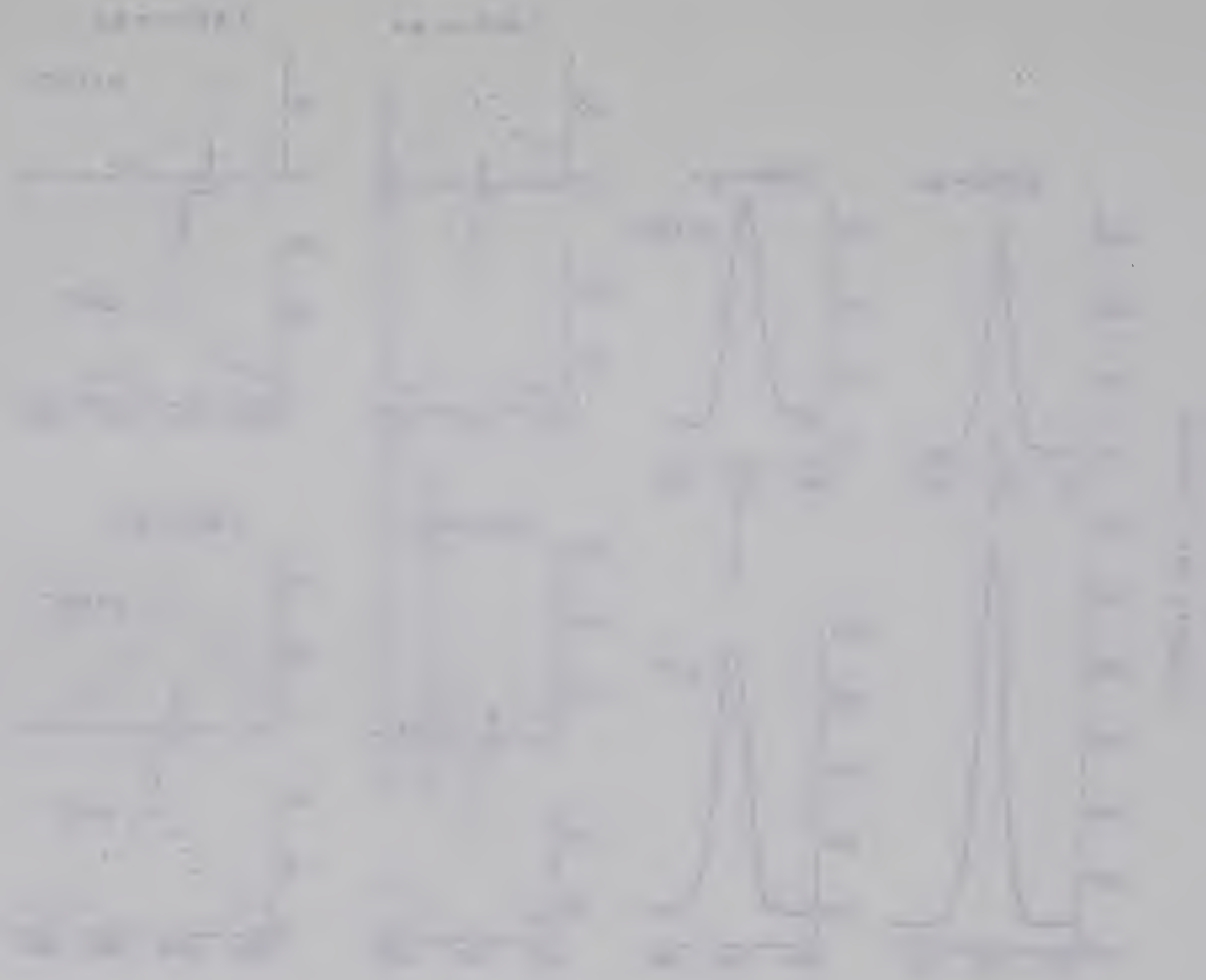

Table 5

Centroid calculations.

State (MeV)	Transition (MeV)	Centroids (channel no.) 0°	120°
1.288	1.288 → 0.378	401.28 ± 0.11	401.26 ± 0.29
	1.288 → 0	572.67 ± 0.13	572.44 ± 0.16
1.440	1.440 → 0	639.87 ± 0.15	639.05 ± 0.17
1.619	1.619 → 0	723.18 ± 0.15	722.50 ± 0.29
2.272	2.272 → 0	1020.86 ± 0.18	1019.70 ± 0.29
2.405	2.405 → 0	1081.72 ± 0.31	1079.46 ± 0.35
2.572	2.572 → 0	1157.84 ± 0.35	1154.24 ± 0.42
2.670	2.670 → 1.288	613.93 ± 0.35	613.01 ± 0.27
2.687	2.687 → 0	1209.97 ± 0.22	1206.79 ± 0.32
2.876	2.876 → 0.378	1123.02 ± 0.39	1120.36 ± 0.86

Intermediate-Coupling results.

(a) The 0.378 MeV level

The half-life of the 0.378 MeV state was measured with the delayed-coincidence technique, to be $\tau_{\frac{1}{2}} = 117 \pm 6$ ps, i,e., the mean life $\tau = 169 \pm 9$ ps (Go 66). In the present experiment, no Doppler shift was found for the gamma-ray from this level.

(b) The 1.288 MeV level

In the earlier work by Gutowski (Gu 70), the lifetimes of the 1.288 MeV state were found to be $\tau = 1.5^{+\infty}_{-1.3}$ ps (or $\tau > 0.2$ ps).

In the present experiment, there were found small Doppler shifts for the 1.288 MeV (1.288 → 0) and the 0.910 MeV (1.288 → 0.378) gamma rays. The lifetime results for the two transition gamma rays showed internal consistency. The average lifetime for this level was determined to be $\tau > 0.19$ ps; this is consistent with the value obtained by Gutowski. The experimental value is in agreement with the prediction of the Intermediate Coupling model, $\tau = 0.45$ ps.

(c) The 1.440 MeV level

The lifetime of this level was determined to be $0.21^{+0.31}_{-0.10}$ ps in the present experiment. The present value is in agreement with that of Gutowski, $\tau = 8.0^{+\infty}_{-7.7}$ ps (or $\tau > 0.3$ ps) within error, and also with the calculated value based on the Intermediate-Coupling model, 0.38 ps.

(d) The 1.619 MeV level

The lifetime of this level has not been previously reported. In the present experiment, the lifetime was determined to be $0.29^{+1.0}_{-0.2}$ ps. This value is consistent with the predicted value by the Intermediate-Coupling, $\tau = 0.10$ ps.

(e) The 2.272 MeV level

The lifetime of this level has been previously measured by Maripuu (Ma 70) to be $\tau > 0.12$ ps. The lifetime, $\tau = 0.31^{+0.49}_{-0.15}$ ps, obtained in the present work is consistent with the result of Maripuu. It is seen, in table 7, that the experimental value is in agreement with the predicted one.

(f) The 2.405 MeV level

The present lifetime, $\tau = 0.12^{+0.14}_{-0.05}$ ps, is consistent with $\tau > 0.12$ ps obtained by Maripuu (Ma 70). The Intermediate-Coupling model does not predict the experimental lifetime of the 2.405 MeV level which may be assumed to be a single-particle state.

(g) The 2.572 MeV level

The lifetime of this level has been previously reported by Maripuu (Ma 70) to be $\tau = 0.060^{+0.090}_{-0.030}$ ps. The value, $\tau = 0.042^{+0.058}_{-0.035}$ ps, obtained in the present experiment is in agreement with the result of Maripuu.

(h) The 2.670 MeV level

Previously, Maripuu (Ma 70) reported the lifetime of this level from the (p,γ) reaction to be $\tau = 0.030^{+0.024}_{-0.014}$ ps. This value is in agreement with the present result, $\tau = 0.1^{+0.13}_{-0.07}$ ps within error.

(i) The 2.687 MeV level

The lifetime of this level has not been previously reported. In the present work, the value $\tau = 0.072^{+0.05}_{-0.03}$ ps has been obtained. In table 7, it is seen that the experimental value is in good agreement with the Intermediate-Coupling prediction, $\tau = 0.06$ ps. It is also, in Chapter IV, found that the experimental values of B(M1) and B(E2), $17.5^{+14.6}_{-8.37}$ (in $10^{-3} \times$ n.m^2) and $0.072^{+0.06}_{-0.04}$ (in $10^2 \times e^2\cdot fm^4$), are in excellent agreement with those predicted by the Intermediate-Coupling model, 18.3 (in $10^{-3} \times$ n.m^2) and 0.056 (in $10^2 \times e^2\cdot fm^4$), respectively.

(j) The 2.876 MeV level

The lifetime of this level has been previously reported by Maripuu (Ma 70) to be $\tau = 0.040 \pm 0.07$ ps. The value of $\tau = 0.065^{+0.090}_{-0.044}$ ps obtained in the present work is consistent with the result of Maripuu.

Table 6

Summary of lifetimes in ^{53}Mn.

Transition (MeV)	F(τ)	State (MeV)	(ps) Present work	(ps) Maripuu (Ma 70)	(ps) Gutowski (Gu 70)	(ps) Gorodetzky (Go 66)
0.378 → 0		0.378				169 ± 9
1.288 → 0	0.16 ± 0.17	1.288	> 0.19		$1.5^{+\infty}_{-1.3}$	
1.288 → 0.378	0.15 ± 0.19					
1.440 → 0	0.33 ± 0.18	1.440	$0.21^{+0.31}_{-0.10}$		$8.0^{+\infty}_{-7.7}$	
1.619 → 0	0.25 ± 0.19	1.619	$0.29^{+1.0}_{-0.2}$			
2.272 → 0	0.23 ± 0.13	2.272	$0.31^{+0.49}_{-0.15}$	> 0.12		
2.405 → 0	0.44 ± 0.17	2.405	$0.12^{+0.14}_{-0.05}$	> 0.12		
2.572 → 0	0.68 ± 0.20	2.572	$0.042^{+0.058}_{-0.035}$	$0.060^{+0.090}_{-0.030}$		
2.670 → 1.288	0.45 ± 0.26	2.670	$0.10^{+0.13}_{-0.07}$	$0.030^{+0.024}_{-0.014}$		
2.687 → 0	0.57 ± 0.20	2.687	$0.072^{+0.05}_{-0.03}$			
2.876 → 0.378	0.54 ± 0.27	2.876	$0.065^{+0.090}_{-0.044}$	0.040 ± 0.07		

Table 7

Comparison of theoretical and experimental lifetimes in ^{53}Mn.

State	τ (ps)		
(MeV)	Experiment	Intermediate Coupling	Weisskopf estimates
1.288	> 0.19	0.45	0.023
1.440	$0.21^{+0.31}_{-0.10}$	0.38	7.2
1.619	$0.29^{+1.0}_{-0.2}$	0.10	0.006
2.272	$0.31^{+0.49}_{-0.15}$		
2.405	$0.12^{+0.14}_{-0.05}$	0.03	0.002
2.572	$0.042^{+0.058}_{-0.035}$		
2.670	$0.10^{+0.13}_{-0.07}$		0.006
2.687	$0.072^{+0.05}_{-0.03}$	0.06	0.0009
2.876	$0.065^{+0.090}_{-0.044}$		0.0011

CHAPTER IV

NUCLEAR MODEL CALCULATIONS

4.1 Introduction

The atomic nucleus is a system composed of many particles which interact with each other in a complicated and only partly understood fashion. It is not possible to obtain an exact theory of such a complicated structure with our present mathematical techniques. Therefore, in order to give some theoretical account of the nuclear properties, it is necessary to construct simple models of the nucleus which may approximate the true nuclear system as closely as possible. The success of a model is then judged by the extent to which theory and experiment are in agreement. The two most successful nuclear models are the shell model and the collective model, which will be considered in this chapter.

The shell model is based on the basic assumptions:

(i) the nucleus can be described in terms of particles moving in a spherically symmetric potential well,

(ii) there is a strong force coupling together the spin angular momentum and orbital angular momentum of each particle, and

(iii) there is a large pairing energy.

The consequences of the pairing energy assumption are that even-

even nuclei have zero angular momentum in the ground state, and that the properties of odd-even nuclei can be described in terms of the possible states available to the single odd nucleon.

The shell model (Ma 49, Ha 49) accounts for a number of experimental facts bearing on the ground states and low-lying excited states of nuclei. However, there remain a number of problems which are completely inexplicable in terms of the simple shell model, such as anomalously large nuclear quadrupole moments and radiative transition probabilities.

The collective model, also known as the unified model, is based on the combined ideas of the shell model and the liquid drop model. In the liquid drop model (Bo 39), the nucleus behaves in a manner similar to that of a liquid drop. It gives a good description only of the average behavior of the nucleus, for example, nuclear binding energies and the semi-empirical mass formula.

The collective model was first formulated by Bohr (Bo 52) and Bohr and Mottelson (Bo 53), following the suggestion by Rainwater (Ra 50) that the deformation of the nucleus from a spherical shape might be due to an interaction between the nucleons in the unfilled shell and the filled shells (or "core"). The model has been extended and developed in various ways by many authors, e.g., in strong-coupling by Nilsson (Ni 55) and in intermediate-coupling by Choudhury (Ch 54).

The nuclear shape depends on the configuration of the

nucleons. In the closed-shell regions where the nuclear shape is spherical, the shell model applies well. In the vicinity of closed shells, the equilibrium shape is approximately spherical, and the energy level scheme is expected to be vibrational. In regions far removed from closed shells where the nuclear equilibrium shape deviates strongly from spherical symmetry, the energy levels can be classified as being vibrational and rotational. In the mass regions $A \sim 25$, $150 < A < 190$, and $A > 220$, in particular, the nuclei are strongly deformed and strong-coupling rotational motion is predominant. Outside the rotational regions and excluding the closed shells, the intermediate-coupling approach has been applied successfully to nuclei in the mass regions $30 < A < 150$ and $190 < A < 220$.

4.2 The Nilsson Model

(a) Theory

The single-particle states in the deformed nuclear field were first introduced by Nilsson (Ni 55). The Nilsson model has been successfully applied to odd mass nuclei in the rotational regions by many authors (Li 58, Bi 60).

The nuclei in the medium weight region, $30 < A < 150$, are assumed to be spherical in shape and, away from closed shells, are expected to be collective vibrational in character. However, some recent nuclear studies (Go 62, So 69) have indicated that the nuclei in the transition region, e.g., chromium and iron

isotopes, possess permanently deformed shapes. Therefore, the strong coupling model of Nilsson might be also applicable for f-p shell nuclei in the medium weight region.

Nilsson's single-particle states

Nilsson's total Hamiltonian is given by (Ni 55)

$$H = \overset{\circ}{H}_o + H_\delta + C\bar{\ell}\cdot\bar{S} + D\bar{\ell}^2 \quad , \qquad \text{(IV.1)}$$

where $\overset{\circ}{H}_o + H_\delta \equiv H_o$ is the harmonic-oscillator Hamiltonian, $\overset{\circ}{H}_o$ a spherically symmetric term, H_δ the coupling of the particle to the axis of the deformation, $C\bar{\ell}\cdot\bar{S}$ the usual spin-orbit term and $D\bar{\ell}^2$ a correction to the oscillation potential.

Here,

$$H_o = -\frac{\hbar^2}{2M}\Delta' + \frac{M}{2}(\omega_x^2 x'^2 + \omega_y^2 y'^2 + \omega_z^2 z'^2)$$

$$\overset{\circ}{H}_o = \hbar\omega_o \frac{1}{2}(-\Delta + r^2) \qquad ; \omega_x^2 = \omega_o^2 (1 + \frac{2}{3}\delta) = \omega_y^2$$

$$H_\delta = -\delta\,\hbar\omega_o \frac{4}{3}\sqrt{\frac{\pi}{5}}\, r^2\, Y_{20} \; ; \omega_z^2 = \omega_o^2 (1 - \frac{4}{3}\delta) \qquad \text{(IV.2)}$$

$$\delta \simeq \frac{3}{2}\sqrt{\frac{5}{4\pi}}\,\beta \simeq 0.95\,\beta \qquad ; \omega_x\,\omega_y\,\omega_z = \text{const.}$$

$$x = \sqrt{\frac{M\omega_o}{\hbar}}\, x' \quad , \qquad ; \omega_o(\delta) = \overset{\circ}{\omega}_o (1 - \frac{4}{3}\delta^2 - \frac{16}{27}\delta^3)^{-\frac{1}{6}}$$

where x', y' and z' are the coordinates of a particle in a

coordinate system fixed in the nucleus ; the deformation parameter δ is related to the quantity β used in the paper by Bohr and Mottelson (Bo 53); $\overset{\circ}{\omega}_o$ is the value of $\omega_o(\delta)$ for $\delta = 0$.

The quantum numbers ℓ, Λ and Σ corresponding to $\bar{\ell}^2$, ℓ_z and S_z respectively for the single-particles, which all commute with $\overset{\circ}{H}_o$, are used as basic vectors:

$$\overset{\circ}{H}_o \,|\, N\ell\Lambda\Sigma > = (N + \tfrac{3}{2})\hbar\omega_o |N\ell\Lambda\Sigma > ,$$

$$\Lambda + \Sigma = \Omega \quad , \tag{IV.3}$$

where the quantum number N represents the total number of oscillator quanta, and Ω is the quantum number corresponding to the commuting operator $j_z = \ell_z + S_z$.

Nilsson introduced new parameters μ, κ, and η instead of C and D :

$$\kappa = -\frac{1}{2} \frac{C}{\hbar\overset{\circ}{\omega}_o}$$

$$\mu = 2\,\frac{D}{C}$$

$$\eta = \frac{\delta}{\kappa}\,\frac{\omega_o(\delta)}{\overset{\circ}{\omega}_o} = \frac{\delta}{\kappa}\left[1 - \frac{4}{3}\delta^2 - \frac{16}{27}\delta^3\right]^{-\frac{1}{6}} . \tag{IV.4}$$

It is then convenient to write :

$$\begin{aligned} H - \overset{\circ}{H}_0 &= H_\delta + C\bar{\ell}\cdot\bar{s} + D\bar{\ell}^2 \\ &= \kappa\hbar\overset{\circ}{\omega}_0 \left[-\frac{4}{3}\,\eta\sqrt{\frac{\pi}{5}}\; r^2\, Y_{20} - 2\,\bar{\ell}\cdot\bar{s} - \mu\bar{\ell}^2 \right] \\ &\equiv \kappa\hbar\overset{\circ}{\omega}_0\, R \end{aligned} \qquad \text{(IV.5)}$$

The eigenvalues $r_\alpha^{N\Omega}(\eta)$ and the expansion coefficients of the eigenvectors are obtained by diagonalizing the dimensionless matrix R in the representation chosen. The corresponding energy eigenvalues of the total H are then given as

$$E_\alpha^{N\Omega} = (N_\alpha + \tfrac{3}{2})\,\hbar\omega_0\,(\delta) + \kappa\hbar\overset{\circ}{\omega}_0\, r_\alpha^{N\Omega}(\eta) \qquad \text{(IV.6)}$$

In the above, κ and μ are used as free parameters varying from shell to shell.

A computer program NILSSON (Ch 71b) was used in the present Nilsson model calculations. In this program, the "asymptotic" quantum numbers $K[N\ n_z\ \Lambda]$ are used to distinguish the different single-particle states in a non-spherical field according to Mottelson and Nilsson's notations (Mo 59). Here K represents the component of the total angular momentum along the symmetry axis, N is the total number of nodes in the wave function, n_z is the number of nodal planes perpendicular to the symmetry axis, and Λ is the component of the particle's orbital angular momentum along the symmetry axis.

A description of spectra of a particular nucleus can now be attempted in terms of rotational bands built on intrinsic single-particle states.

Rotational spectra

The total Hamiltonian of the nuclear system can be written as (Ma 66)

$$H = H_p + \frac{\hbar^2}{2J} \vec{R}^{\,2}$$

$$= H_p + \frac{\hbar^2}{2J} \left[I^2 + j^2 - 2(\vec{I}\cdot\vec{j}) \right] \ , \qquad (IV.7)$$

where H_p represents the single-particle Hamiltonian and is usually the Nilsson Hamiltonian. The $(\vec{I}\cdot\vec{j})$ term is called Coriolis coupling or rotation-particle coupling term (RPC term). In the usual procedure, the coupling term $(\vec{I}\cdot\vec{j})$ and the term j^2 are either omitted or treated in the first order perturbation theory.

The total wave function describing the state of the nucleus is a product of the rotation wave function and the single particle wave function. It can be written as (Da 65) :

$$|EIMK> = \frac{1}{\sqrt{2}} \sum_j C_{j\Omega} \left[|IMK>|j\Omega> + (-)^{I-j} \, |IM-K>|j-\Omega> \right] . \qquad (IV.8)$$

In the even-even nucleus, the rotational energy spectrum is simply given by (Bo 54)

$$E_{rot} = \frac{\hbar^2}{2J} \; I \; (I+1) \qquad (IV.9)$$

with $I = 0, 2, 4 \ldots$,

where J is the effective moment of inertia of the nucleus undergoing collective rotations and I is the total angular momentum quantum number of the nucleus.

In the odd-A nucleus, the total angular momentum I is given by the sum of the angular momenta of the last odd particle and the rotational core, j and R, respectively:

$$\vec{I} = \vec{j} + \vec{R} \quad . \qquad (IV.10)$$

The rotational motion is then characterized by the quantum numbers I , M and K, representing the total angular momentum, its projection on the space fixed axis (z-axis), and its projection on the intrinsic nuclear axis (z'-axis), respectively. The nuclear coupling schemes are illustrated in Fig. 33.

The energy of a state with spin I belonging to a rotational band K is given by (Pr 62)

$$E_{IK} = E_K + \frac{\hbar^2}{2J} \; [I \; (I+1) - 2K^2 + \delta_{K,\frac{1}{2}} \; a(-)^{I+\frac{1}{2}} \; (I+\tfrac{1}{2})] \qquad (IV.11)$$

with $I = K, K+1, K+2, \ldots$,

where E_K is the energy of intrinsic motion, and a is the "decoupling parameter" resulting from the Coriolis coupling term. The decoupling parameter, a, may be expressed in terms of the expansion coefficients $C_{j\Omega}$ of the wave function (see eq. IV.8):

$$a = - \sum_j (-)^{j+\frac{1}{2}} (j + \tfrac{1}{2}) \, |C_{j\Omega}|^2 . \qquad \text{(IV.12)}$$

For K = ½, the sequence of energy levels depends on the decoupling parameter a (see Fig. 10-9 in ref. Pr 62).

In the ground state of each K band, R is perpendicular to z', i.e., K = Ω (Bo 53, Ni 55).

The energy difference in a rotational band between the excited level with spin I and the intrinsic state with spin K is given by

$$\Delta E_{IK} = \frac{\hbar^2}{2J} [I(I+1) + a (-)^{I+\frac{1}{2}} (I+\tfrac{1}{2}) \delta_{K,\frac{1}{2}}]$$

$$- \frac{\hbar^2}{2J} [K(K+1) + a (-)^{K+\frac{1}{2}} (K+\tfrac{1}{2}) \delta_{K,\frac{1}{2}}] . \qquad \text{(IV.13)}$$

At the edges of the rotational regions, there is a systematic deviation from the perfect rotational spectrum. This deviation can be fitted by a correction term (Li 58)

$$E_{IK} = \frac{\hbar^2}{2J} [I (I+1) + \delta_{K,\frac{1}{2}} \; a \; (-)^{I+\frac{1}{2}} (I + \tfrac{1}{2})]$$

$$+ \; B \; [I \; (I+1) + \delta_{K,\frac{1}{2}} \; a \; (-)^{I+\frac{1}{2}} (I + \tfrac{1}{2})]^2 \; , \qquad (IV.14)$$

where B is the vibration-rotation interaction parameter.

When there are two rotational spectra corresponding to the close configurations K and K + 1, the states with the same I of the bands will be mixed by the RPC (Ke 56). Malik and Scholz (Ma 66) have calculated level spectra of ^{53}Mn using the strong-coupling rotational model with band mixing.

The electromagnetic properties

Electromagnetic moments and transition probabilities of the rotating nucleus have been discussed by many authors (Bo 53, Bo 54, Ke 56, Ma 67) and will not be repeated here.

In the unified model, there is a selection rule for gamma-ray transitions which has been discussed by Alaga *et al*.(Al 55). For a transition of multipole order L from a level in a rotational band characterized by K_i to a level in a band characterized by K_f, the selection rule is

$$\Delta K \equiv |K_i - K_f| \leq L \; . \qquad (IV.15)$$

The degree of forbiddeness, ν, is given by

$$\nu = \Delta K - L \qquad (IV.16)$$

Fig. 33 The nuclear coupling scheme on an odd-A nucleus.

(a) shows the coupling in the ground state, and

(b) the coupling in the general case.

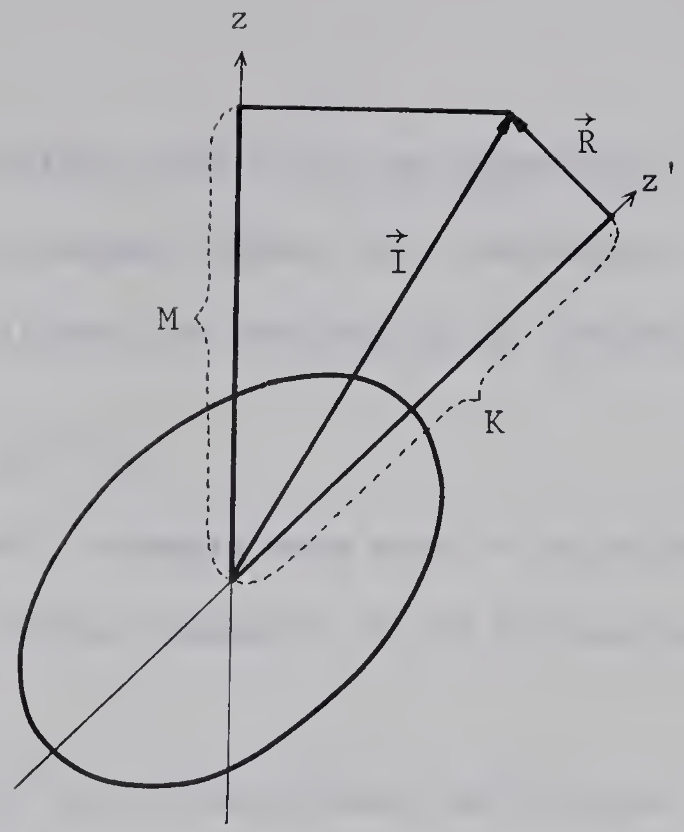
z
$\vec{R}$
z'
$\vec{I}$
M
K

(a)

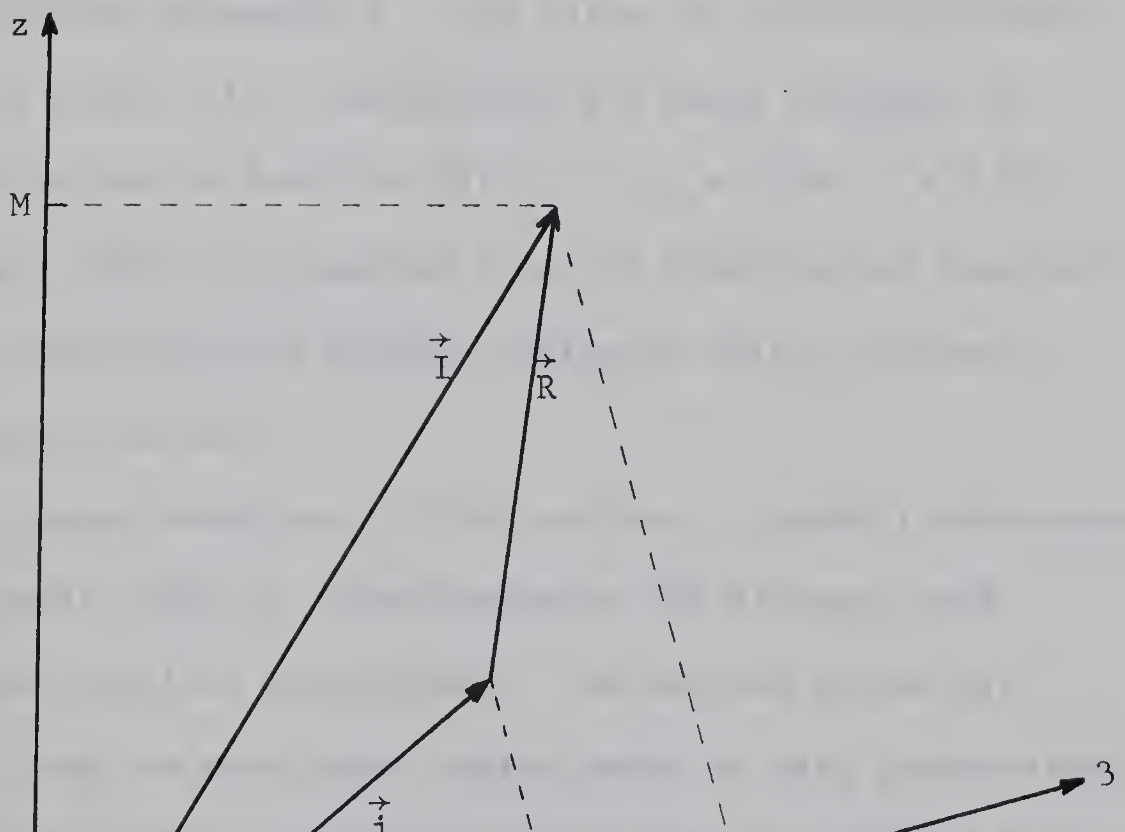
z
M
$\vec{I}$
$\vec{R}$
$\vec{j}$
3
Ω
K

(b)

For transitions that violate this rule, the transition probabilities will be retarded, rather than completely forbidden. Such transitions are referred to as K-forbidden.

(b) Application to ^{53}Mn

In the present work, attempts were made to calculate the energy levels of ^{53}Mn in the framework of the Nilsson model without band mixing.

The eigenvalues for the Nilsson-model Hamiltonian for the oscillator number $N = 3$ with the specified values of the parameters, μ and κ, are plotted in Fig. 34 as a function of the deformation parameter δ. The values of the Nilsson-model parameters used in this calculation are those obtained in this mass region by Sood (So 69), i.e., $\mu = 0.44$, $\kappa = 0.07$. This figure shows the expected relative ordering and spacing of various single-particle Nilsson states on which rotational levels are to be built.

The ground-state spin of the nucleus is usually determined by the lowest state of a band based on the Nilsson state occupied by the last odd nucleon. The excited states are obtained from the rotational states based on this ground-state band and from other rotational states built on particle bands and hole bands. Particle bands are constructed by placing the last unpaired nucleon in any of the unoccupied states and hole bands (or core-excited states) are constructed by lifting a core particle and pairing it with the odd nucleon.

Fig. 34 The Nilsson model energy diagram. Parameters used are $\mu = 0.44$ and $\kappa = 0.07$; the single-particle states are expressed in terms of the "asymptotic" quantum numbers $K\ [N\ n_z\ \Lambda]$.

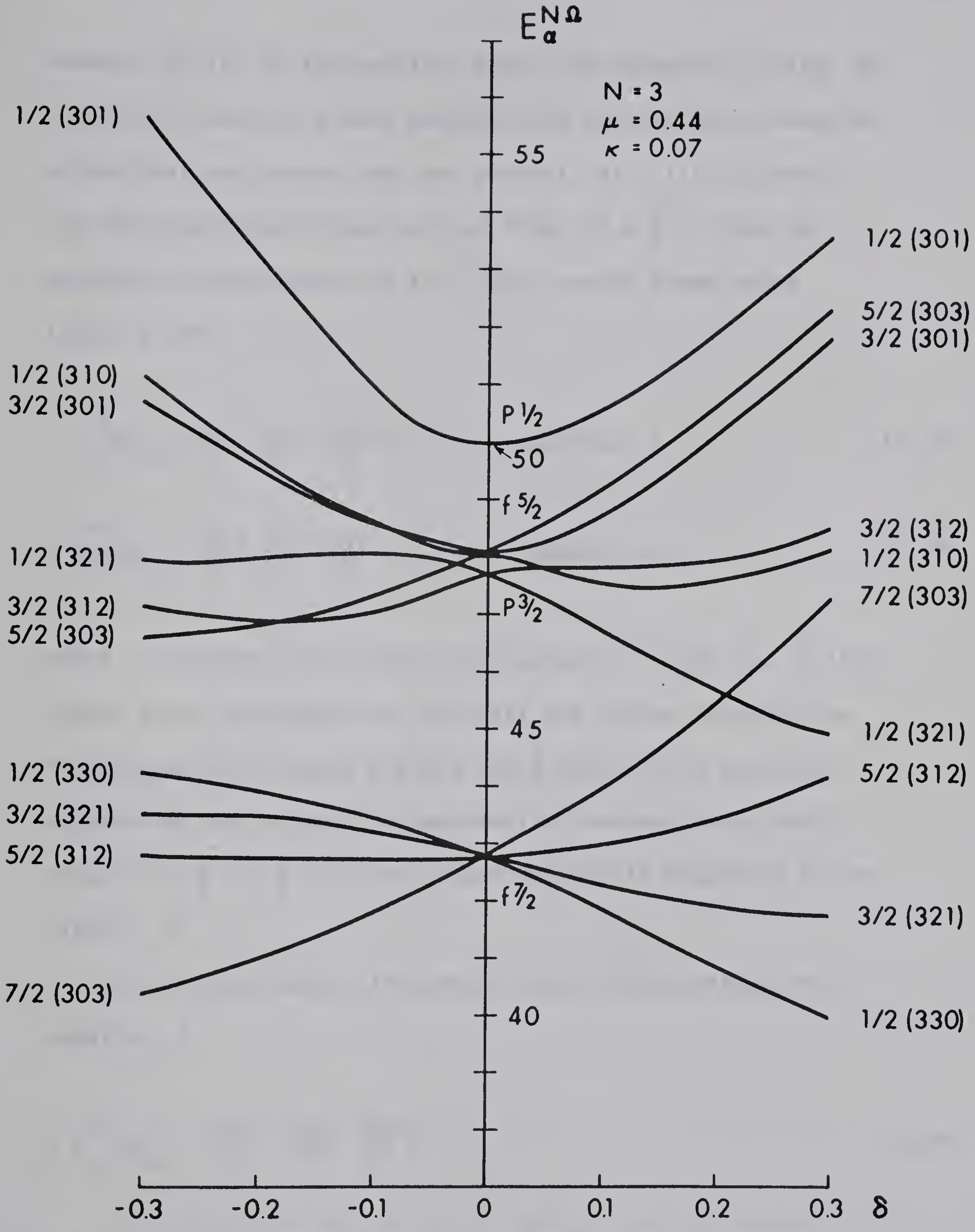
$E_\alpha^{N\Omega}$
N = 3
μ = 0.44
κ = 0.07
55
50
45
40
P 1/2
f 5/2
P 3/2
f 7/2
1/2 (301)
1/2 (310)
3/2 (301)
1/2 (321)
3/2 (312)
5/2 (303)
1/2 (330)
3/2 (321)
5/2 (312)
7/2 (303)
1/2 (301)
5/2 (303)
3/2 (301)
3/2 (312)
1/2 (310)
7/2 (303)
1/2 (321)
5/2 (312)
3/2 (321)
1/2 (330)
-0.3
-0.2
-0.1
0
0.1
0.2
0.3
δ

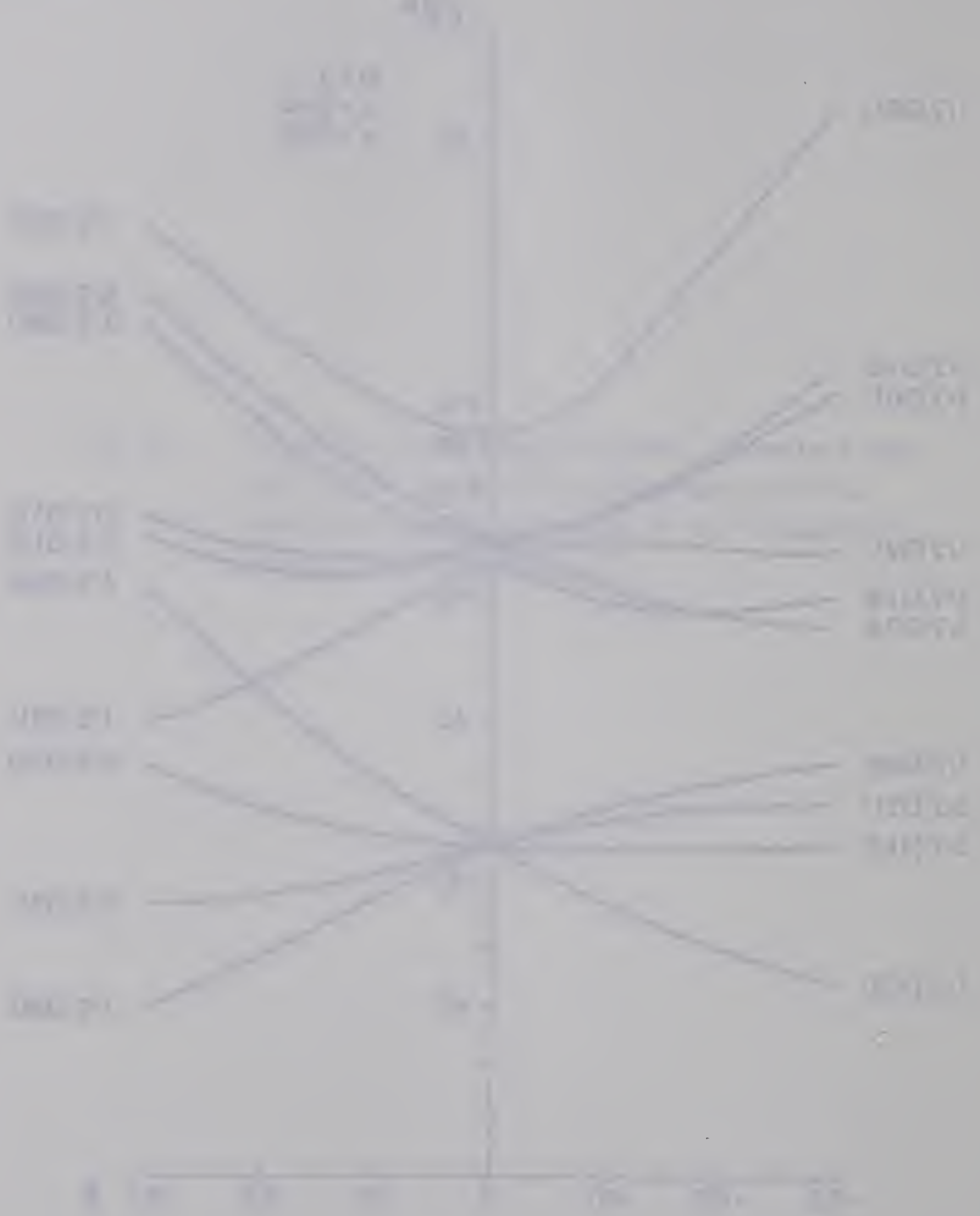

However, as far as the particle bands are concerned in Fig. 34, the lowest state of a band based on the Nilsson level occupied by the last odd proton does not predict, at a first glance, the observed ground-state spin of ^{53}Mn, $J^\pi = \frac{7}{2}^-$, since the ground state configuration for $^{53}_{25}\mathrm{Mn}_{28}$ may be taken to be (see Fig. 34)

$$\nu\ \{^{48}_{20}\mathrm{Ca}_{28};\ (\tfrac{1}{2})^2\ (\tfrac{3}{2})^2\ (\tfrac{5}{2})^1\}\quad \text{for a positive } \delta, \tag{IV.17}$$

$$\nu\ \{^{48}_{20}\mathrm{Ca}_{28};\ (\tfrac{7}{2})^2\ (\tfrac{5}{2})^2\ (\tfrac{3}{2})^1\}\quad \text{for a negative } \delta, \tag{IV.18}$$

where ν represents the proton configuration. That is, in the ground state configuration, the last odd proton occupies the Nilsson particle states $\frac{5}{2}$ [312] and $\frac{3}{2}$ [321] for a positive deformation and a negative deformation, respectively, indicating $J^\pi = \frac{5}{2}^-$ or $\frac{3}{2}^-$ for the ground-state spin depending on the sign of δ.

In the hole bands, the ground-state configuration for a negative δ,

$$\nu\ \{^{48}_{20}\mathrm{Ca}_{28};\ (\tfrac{7}{2})^{-1}\ (\tfrac{5}{2})^2\ (\tfrac{3}{2})^2\}\ , \tag{IV.19}$$

would reproduce the correct spin, $J^\pi = \frac{7}{2}^-$, for the ground state of ^{53}Mn. Therefore, in the present calculations, it was assumed that the rotational spectra in the levels of

^{53}Mn were built on the two hole bands $\frac{7}{2}$ [303] and $\frac{5}{2}$ [312], and on the two particle bands $\frac{3}{2}$ [321] and $\frac{1}{2}$ [330] for a negative δ.

The rotational constant $A = \frac{\hbar^2}{2J}$ is usually a free parameter. The present values of $A = 179.9$ keV and $a = -2.0$ were determined by the best fit of rotational levels to a given number of experimental levels. The parameters used in the present calculations are listed in table 8. The calculated energy levels of ^{53}Mn are shown in Fig. 35 and compared with the values computed with the band mixing by Malik and Scholz (Ma 66).

Table 8

Parameters used in the Nilsson model calculations in ^{53}Mn. The values of the Nilsson model parameters, μ and κ, are those obtained in this mass region by Sood (So 69).

μ	κ	δ	$A = \frac{\hbar^2}{2J}$	a
0.44	0.07	-0.1	179.9 keV	-2.0

In the band mixing, Malik and Scholz (Ma 66) included all bands based on the ten available single-particle and core-excited levels in the f-p shell and obtained the final spectra by diagonalizing the Coriolis interaction with rotational wave

Fig. 35 The calculated energy levels of ^{53}Mn based on the Nilsson model. The present calculated levels without band-mixing are compared with the observed levels and the computed levels with band-mixing by Malik and Scholz.

Nilsson model calculations

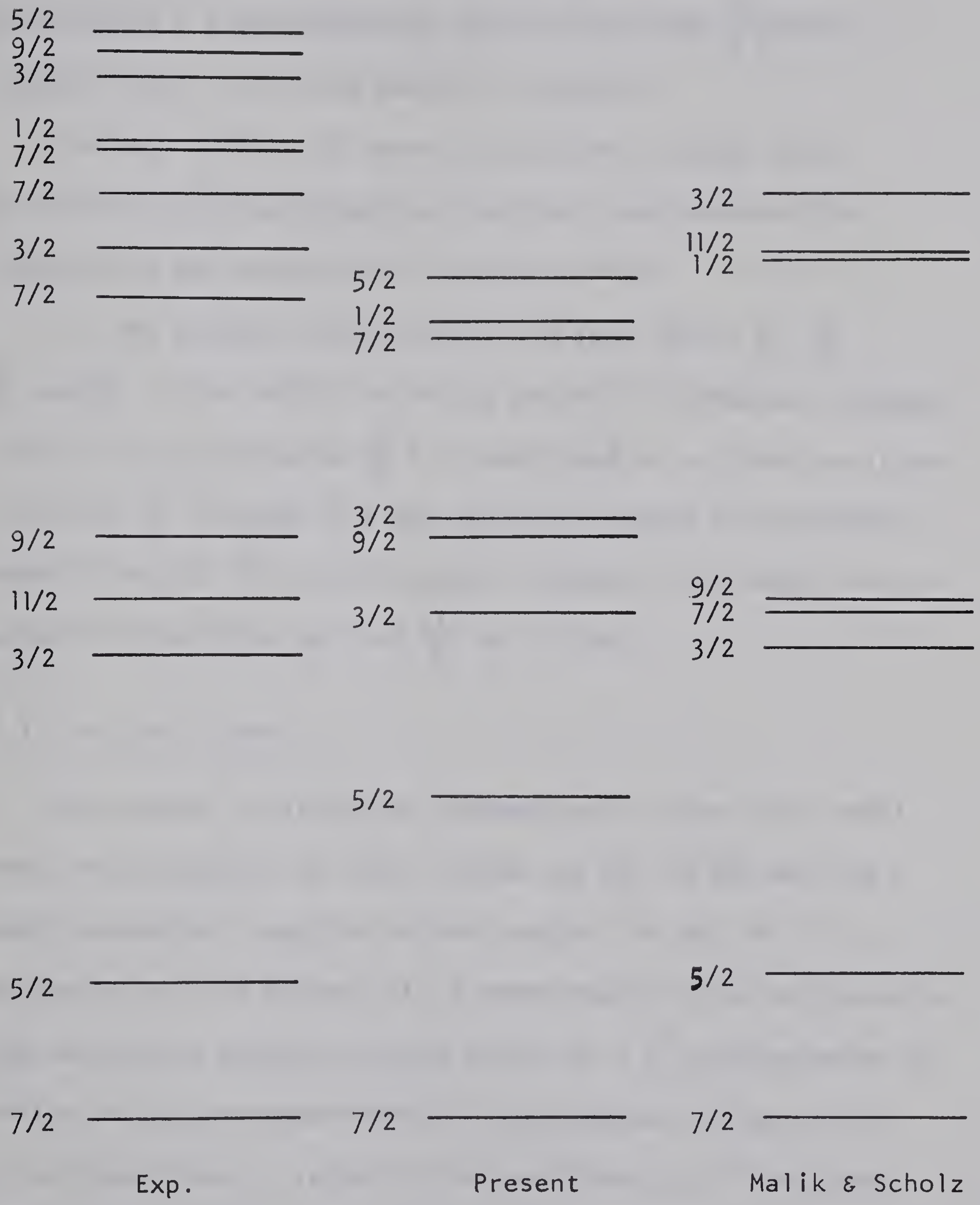
5/2
9/2
3/2
1/2
7/2
7/2
3/2
7/2
9/2
11/2
3/2
5/2
7/2
Exp.
5/2
1/2
7/2
3/2
9/2
3/2
5/2
7/2
Present
3/2
11/2
1/2
9/2
7/2
3/2
5/2
7/2
Malik & Scholz

^{53}Mn

functions. They attributed the ground-state spin in $\frac{7}{2}^-$ in ^{53}Mn to the occurrence of a low-lying $\frac{7}{2}^-$ state in the decoupled K = ½ band based on the Nilsson state $\frac{1}{2}$ [330] together with the strong Coriolis coupling.

As seen in Fig. 35, both calculations without band-mixing and with band-mixing are not very satisfactory for reproducing the experimental levels in ^{53}Mn.

In the present calculations, the four spins, $\frac{7}{2}^-$, $\frac{5}{2}^-$, $\frac{3}{2}^-$ and $\frac{9}{2}^-$ in the low-lying states are well reproduced, although the first excited state ($\frac{5}{2}^-$) is predicted at a higher position. A spin of $\frac{7}{2}^-$ at about 2.2 MeV would correspond to the experimental level of $\frac{7}{2}^-$ in this region. However, the model does not predict a low-lying spin of $\frac{11}{2}^-$ at 1.4 MeV.

4.3 The Shell Model

The method of effective interactions in the shell model was first suggested by Talmi (Go 56, La 57, Ta 58) and has been successfully applied to many nuclei (Ta 62, Ta 67). According to this method, it is sometimes possible to determine the excitation energies of the states of a j^n configuration by making use of the experimentally measured splittings of the j^2 configuration in terms of the coefficients of fractional parentage.

For a pure ($1f_{\frac{7}{2}}^3$) configuration, one obtains only six energy levels (La 57, Mc 64), i.e., 0.0 ($\frac{7}{2}^-$), 0.25 ($\frac{5}{2}^-$),

1.30 ($\frac{3}{2}^-$), 1.75 ($\frac{11}{2}^-$), 2.04 ($\frac{9}{2}^-$) and 3.10 ($\frac{15}{2}^-$). Another serious discrepancy in this model is that M1 transitions between the states are forbidden, which is in contradiction to observation of these transitions, indicating the use of configuration mixing.

Lips and McEllistrem (Li 70) carried out calculations with configuration mixing in the framework of the effective interaction method for the nuclei with N = 28 and 20 < z < 28, allowing states with proton configurations ($1f_{\frac{7}{2}}^{n-1}\ 2p_{\frac{3}{2}}$) and ($1f_{\frac{7}{2}}^{n-1}\ 1f_{\frac{5}{2}}$) as well as the pure ($1f_{\frac{7}{2}}^{n}$).

In the effective interaction method, the single particle energies and the two-particle matrix elements are used as free parameters for the best least-squares fit to experimental levels.

In their calculations, Lips and McEllistrem found that the ground state of ^{53}Mn was more than 98% ($1f_{\frac{7}{2}}^{n}$), the three lowest excited states in ^{53}Mn were more than 80% ($1f_{\frac{7}{2}}^{n}$), and the fourth excited state ($\frac{9}{2}^-$) was about 40% ($1f_{\frac{7}{2}}^{n}$). The order of the $\frac{11}{2}^-$ and $\frac{9}{2}^-$ levels was inverted, and the experimental values of the M1 transition rates, the mixing ratios and the branching ratios were not reproduced successfully. The calculated energy levels are shown in Fig. 39. However, the mixed-configurations, in general, provide a much improved model to describe the levels of ^{53}Mn over the pure configurations.

4.4 The Intermediate Coupling in the Unified Model

In the present calculations, the intermediate-coupling model has been applied to ^{51}V and ^{53}Mn, which are "equivalent" pair nuclei, i.e., the proton $(1f_{\frac{7}{2}})^{\pm 3}$ configurations.

The intermediate coupling model was first introduced by Bohr and Mottelson (Bo 53) and further developed by Choudhury (Ch 54), and has been successfully applied to account for properties of the low-lying levels in many nuclei in various mass regions (Gl 60, Ch 66, Ch 71, Ch 71a). In this model, an odd-mass nucleus is described by coupling one nucleon to an even-even vibrating core. In the present calculations of ^{51}V and ^{53}Mn each with 28 neutrons, the odd protons, having available the $f_{\frac{7}{2}}$, $f_{\frac{5}{2}}$ and $p_{\frac{3}{2}}$ states, are coupled to the quadrupole type collective surface vibrations of their even-even ^{50}Ti and ^{52}Cr cores.

(a) Theory

Since detailed descriptions of the intermediate coupling model have appeared in the original papers (Ch 54), only a brief survey of the required formulae is given here.

The total Hamiltonian for the core-particle system is of the following form:

$$H = H_c\,(\alpha_{2\mu}) + H_p(x) + H_{int}\,(\alpha_{2\mu}, x) \quad , \tag{IV.20}$$

where $\alpha_{2\mu}$ are the collective coordinates as defined by Bohr and Mottelson (Bo 53) and x the single particle coordinates. The core Hamiltonian H_c and the core-particle interaction Hamiltonian H_{int} are given by

$$H_c = \sum_{\mu} \{ \frac{1}{2} B \mid \dot{\alpha}_{2\mu} \mid^2 + \frac{1}{2} C \mid \alpha_{2\mu} \mid^2 \} , \tag{IV.21}$$

$$H_{int} = - K(r) \sum_{\mu} \sqrt{\frac{\hbar\omega}{2C}} \, (b_{\mu} + (-)^{\mu} b^{\dagger}_{-\mu}) \, Y_{2\mu} \, (\theta,\phi) \quad , \tag{IV.22}$$

where B is the mass parameter, C the nuclear deformability, K(r) is the strength function related to the radial dependence of the real potential for the extra nucleon, $\hbar\omega$ the phonon excitation energy of the doubly even core, b_{μ} and $b^{\dagger}_{\mu}$ the annihilation and creation operators, and $Y_{2\mu}$ the spherical harmonic operator.

Introducing the dimensionless coupling parameter ξ ,

$$\xi = K \sqrt{\frac{5}{2\pi\hbar\omega C}} \quad , \tag{IV.23}$$

where the coupling constant $K \equiv \langle K(r) \rangle$ is taken to be 40 MeV and the harmonic oscillator frequency ω is defined by

$$\omega = \sqrt{\frac{C}{B}} \quad , \tag{IV.24}$$

the interaction Hamiltonian, H_{int}, is rewritten as

$$H_{int} = -\xi \hbar\omega \sqrt{\frac{1}{5}\pi} \sum_{\mu} (b_{\mu} + (-)^{\mu} b^{\dagger}_{-\mu}) Y_{2\mu} (\theta,\phi) \quad . \qquad \text{(IV.25)}$$

The basis eigenvectors of the coupled system are denoted by

$$|j;\ NR;\ IM> = \sum_{m,m'} (j\ R\ mm' \mid j\ R\ IM) \mid jm> |NR\ m'> \quad , \qquad \text{(IV.26)}$$

where $(j\ R\ m\ m' \mid j\ R\ IM)$ is the Clebsch-Gordan coefficient, j the single particle angular momentum and N the number of phonons of the core angular momentum R. In the above definition it follows that:

$$(H_c + H_p)|j;\ NR;\ IM> = (N\hbar\omega + E_j)|j;\ NR;\ IM> \quad , \qquad \text{(IV.27)}$$

where E_j is the energy of the single particle. The matrix elements of H_{int} are calculated (Ca 71) :

$$<j';N'R';IM|H_{int}|j;NR;IM> = (-)^{R'+j'-I+1} \sqrt{\frac{\pi}{5}} \hbar\omega \xi$$

$$\times \sqrt{2j'+1} <j'||Y_2||j> \sqrt{2R+1} <N'R'||b||NR>$$

$$\times W(JJ'RR';2I) \quad \text{for} \quad N' < N \ , \qquad \text{(IV.28)}$$

where $W(jj'RR';2I)$ is the Racah coefficient (Ro 57) and $<N'R'||b||NR>$ and $<j'||Y_2||j>$ the reduced matrix elements

defined in Choudhury's paper (Ch 54). The selection rules resulting from eq. (IV.28) are $\Delta N = 1$, $\Delta R \leq 2$, $\Delta j \leq 2$ and $\Delta \ell = 0,2$. The eigenfunctions of the total Hamiltonian are a linear combination of the basis vectors :

$$|E;IM> = \sum_{j,NR} A_{j,NR}(E) \,|\, j;\ NR;\ IM> \quad , \qquad (IV.29)$$

where E and $A_{j,NR}(E)$ are the eigenvalues and the expansion coefficients, respectively, which are obtained by diagonalizing the total Hamiltonian H.

The multipole operators used in the calculation of electromagnetic transition rates are the following :

for the electric quadrupole (Ch 67) ,

$$M_e(2,\mu) = (e_p - \frac{Ze}{A^2})\, r^2\, Y_{2\mu}(\theta,\phi) + \frac{3}{4\pi}\, Ze\, R_0^{\,2}\, \alpha^{\dagger}_{2\mu} \quad , \qquad (IV.30)$$

and for the magnetic dipole

$$M_m(1,\mu) = \frac{e\hbar}{2Mc} \sqrt{\frac{3}{4\pi}}\, [g_\ell\, \ell_z + g_s\, S_z + g_R\, R_z] \quad , \qquad (IV.31)$$

where e_p is the electric charge, g_ℓ and g_s are the orbital and spin g-factors, g_R is the core g-factor taken to be Z/A and R_0 is the nuclear radius, $R_0 = 1.18\, A^{\frac{1}{3}}$ fm.

The results of the reduced transition probabilities and the moments are given as follows (Ch 67) :

for the electric quadrupole transitions,

$$\underset{I \to I'}{B(E2)} = (2I'+1) \Big| \sum_{\substack{jNR \\ j'N'R'}} A_{jNRI}(E)\, A_{j'N'R'I'}(E')$$

$$\times \{\eta_1 (-)^{I'+j-R} \sqrt{2j'+1} \langle j' \| Y_2 \| j \rangle\, W(jj'II';2R)\, \delta_{NN'} \delta_{RR'}$$

$$+ \eta_2 (-)^{I-j} [(-)^{R'} \sqrt{2R'+1} \langle N'R' \| b^{\dagger} \| NR \rangle + (-)^{R} \sqrt{2R+1}$$

$$\times \langle N'R' \| b \| NR \rangle]\, W(R'RI'I;2j)\, \delta_{jj'} \delta_{\ell\ell'} \} \Big|^2 , \qquad \text{(IV.32)}$$

where

$$\eta_1 = (e_p - \frac{Ze}{A^2}) \langle r^2 \rangle = \frac{3}{5} (e_p - \frac{Ze}{A^2})\, R_0^{\,2}$$

$$\eta_2 = \frac{3}{4\pi} \sqrt{\frac{\hbar\omega}{2C}}\, Ze\, R_0^{\,2} \; ; \qquad \text{(IV.33)}$$

for the magnetic dipole transitions,

$$\underset{I \to I'}{B(M1)} = \frac{3}{4\pi} (\mu_N)^2 (2I'+1) \Big| \sum_{jj'NR} A_{jNRI}(E)\, A_{j'NRI'}(E')$$

$$\times \{ (-)^{I'+R+\ell-\frac{1}{2}} \sqrt{(2J+1)(2j'+1)}\, [g_{\ell} (-)^{j+j'} \sqrt{\ell(\ell+1)(2\ell+1)}$$

$$\times W(j'j\,\ell\ell;\, 1\,\tfrac{1}{2}) + g_s \sqrt{\frac{3}{2}}\, W(jj'\,\tfrac{1}{2}\,\tfrac{1}{2};\, 1\ell)]$$

$$\times \; W(j'j\; I'I;\; 1R)\; \delta_{\ell\ell'} + g_R(-)^{I+j+R} \sqrt{R(R+1)(2R+1)}$$

$$\times \; W(RR\; I'I;\; 1j)\; \delta_{\ell\ell'}\; \delta_{jj'}\}|^2 \;, \qquad \text{(IV.34)}$$

where μ_N is the nuclear magneton $\frac{e\hbar}{2Mc}$;

for the electric quadrupole moment,

$$Q(E;I) = \frac{3}{5} R_0^{\,2} \sqrt{\frac{I(2I+1)(2I-1)}{(I+1)(2I+3)}} \sum_{\substack{jNR \\ j'N'R'}} A_{jNRI}(E)\, A_{j'N'R'I}(E)$$

$$\times \sqrt{\frac{16\pi}{5}}\; (e_p - \frac{Z}{A^2})\; (-)^{I+j-R}\; \delta_{NN'}\; \delta_{RR'} \sqrt{2j'+1} <j'\,\|\, Y_2 \,\|\, j>$$

$$\times \; W(jj'\; II;2R) + Z\, \frac{\hbar\omega}{K}\; \xi(-)^{I-j}\; \delta_{jj'}\; \delta_{\ell\ell'}$$

$$\times \; [(-)^{R'} \sqrt{2R'+1} <N'R'\,\|b^{\dagger}\|\,NR> + (-)^{R} \sqrt{2R+1}$$

$$\times \; <N'R'\,\|\,b\,\|\,NR>\,]\;\; W(RR'\; II;2j) \qquad \text{(IV.35)}$$

setting $<r^2>$ equal to $\frac{3}{5} R_0^{\,2}$;

for the dipole moment,

$$\mu(E;I) = \mu_N \sqrt{\frac{I(2I+1)}{I+1}} \sum_{\substack{jNR \\ j'N'R'}} A_{jNRI}(E)\; A_{j'N'R'I}(E)$$

$$\times \; \{g_R(-)^{I+j-R}\; \delta_{NN'}\; \delta_{RR'}\; \delta_{jj'}\; \delta_{\ell\ell'} \sqrt{R(R+1)(2R+1)}$$

$$\times \ W(RR\ II;1j) + g_{\ell}(-)^{R-\ell+\frac{1}{2}+j+j'-1}\ \delta_{NN'}\ \delta_{RR'}\ \delta_{\ell\ell'}$$

$$\times \ \sqrt{(2j+1)(2j'+1)}\ \sqrt{\ell(\ell+1)(2\ell+1)}\ \ W(jj'\ II;1R)$$

$$\times \ W(\ell\ell\ jj';1\tfrac{1}{2}) + g_s(-)^{\ell+\frac{1}{2}+R-1}\ \delta_{NN'}\ \delta_{RR'}\ \delta_{\ell\ell'}$$

$$\times \ \frac{3}{2}\ \sqrt{(2j+1)(2j'+1)}\ \ W(jj'\ II;1R)\ \ W(jj'\ \tfrac{1}{2}\tfrac{1}{2};\ 1\ell) \qquad (IV.36)$$

The wave functions obtained by the diagonalization of the total Hamiltonian have been used to calculate the reduced transition probabilities and nuclear moments. A computer program CORPAR (Ca 70) was used in the present calculations.

(b) Application to ^{51}V and ^{53}Mn

(i) Energy levels

In the present calculation, it was assumed that the ^{51}V and ^{53}Mn nuclei could be described as doubly even cores $(N = 28)$ of 22 and 24 protons, respectively, with the last odd protons occupying the $1f_{\frac{7}{2}}$, $1f_{\frac{5}{2}}$, and $2p_{\frac{3}{2}}$ single particle states. The effective spacing parameters, $\varepsilon_1 = f_{\frac{5}{2}} - f_{\frac{7}{2}}$ and $\varepsilon_2 = p_{\frac{3}{2}} - f_{\frac{7}{2}}$, the phonon energy $\hbar\omega$, and the coupling parameter ξ, which enter the calculations, are considered to be adjustable parameters. The best fit was determined by comparison with all the available experimental data.

The phonon energy $\hbar\omega$ was first taken from the energy of

the first 2^+ state in the even core as the starting value and then adjusted to within a reasonable range (Ca 71). It was found that the parameters were best adjusted by the procedure suggested by Heyde and Brussaard (He 67). In their analysis of various odd-proton nuclides, they found a systematic dependence of ξ and $\hbar\omega$ on the mass number A. The final best value of $\hbar\omega$ is between the values of $\hbar\omega$ of the two neighbouring even isotones, A $\pm$ 1. In intermediate coupling, the coupling parameter ξ could be expected in a neighbourhood of $\xi = 3$, and the starting value of the effective spacing parameters ε_1 and ε_2 are taken directly from the spacings of the two lowest states of the nucleus itself. The number of phonons is assumed to be $N \leq 3$.

The total Hamiltonian is diagonalized for the final values of the ε_1, ε_2, and ξ for each I, $\frac{1}{2} \leq I \leq \frac{11}{2}$. The highest order of the matrix is 23 x 23 for $I = \frac{7}{2}$. The parameters which give the best fit are listed in table 9. The energy eigenvalues were plotted as a function of the coupling parameter in Figs. 36 and 37, and the predicted energy spectra were compared with the experimental and other theoretical results for ^{51}V and ^{53}Mn in Figs. 38 and 39. In general, fairly good agreement is obtained between the experimental and the theoretical values for the energy spectra.

The ^{51}V nucleus : Fig. 38 is a comparison of the experimental spectrum of ^{51}V with intermediate coupling and other theoretical

calculations, i.e., the mixed configuration by Lips and McEllistrem (Li 70), the pure configuration shell model by McCullen et al. (Mc 64), and the strong coupling rotational model by Malik and Scholz (Ma 66). Table 10 lists the expansion coefficients of the basic states for five energy levels in ^{51}V. The experimental levels are taken from the recent $^{48}Ti(\alpha,p\gamma)^{51}V$ reaction by Horoshko et al. (Ho 70). As seen in Fig. 38, the intermediate coupling model reproduces all the states up to 1.8 MeV very well, and also shows a better agreement with the experimental levels than the other theoretical calculations.

The experimental level at 2.409 MeV ($\frac{3}{2}^-$) may correspond to the calculated level $\frac{3}{2}^-$ near 2.5 MeV. The positive parity states with spins $\frac{1}{2}^+$ and $\frac{3}{2}^+$ in the experimental levels are not reproduced by the intermediate coupling model, and probably are assumed to be proton hole states. It should be noted that the present model predicts four levels with spins $\frac{1}{2}^-$, $\frac{7}{2}^-$, $\frac{9}{2}^-$ and $\frac{5}{2}^-$ between 1.8 MeV and 2.5 MeV which are not observed experimentally. The predictions of this model for higher excited states may be doubtful.

The ^{53}Mn nucleus : Fig. 39 is a comparison of the experimental spectrum of ^{53}Mn with intermediate coupling and other theoretical calculations. The wave functions for the lowest five levels in ^{53}Mn are listed in table 11. The experimental

Table 9

Parameters used in the intermediate coupling calculations.

Nucleus	$\varepsilon_1 = f_{\frac{5}{2}} - f_{\frac{7}{2}}$ (MeV)	$\varepsilon_2 = p_{\frac{3}{2}} - f_{\frac{7}{2}}$ (MeV)	$\hbar\omega$ (MeV)	ξ
^{51}V	0.020	5.370	1.950	3.072
^{53}Mn	0.025	5.200	1.795	3.470

Fig. 36 Plot of E as a function of the coupling parameter ξ for ^{51}V.

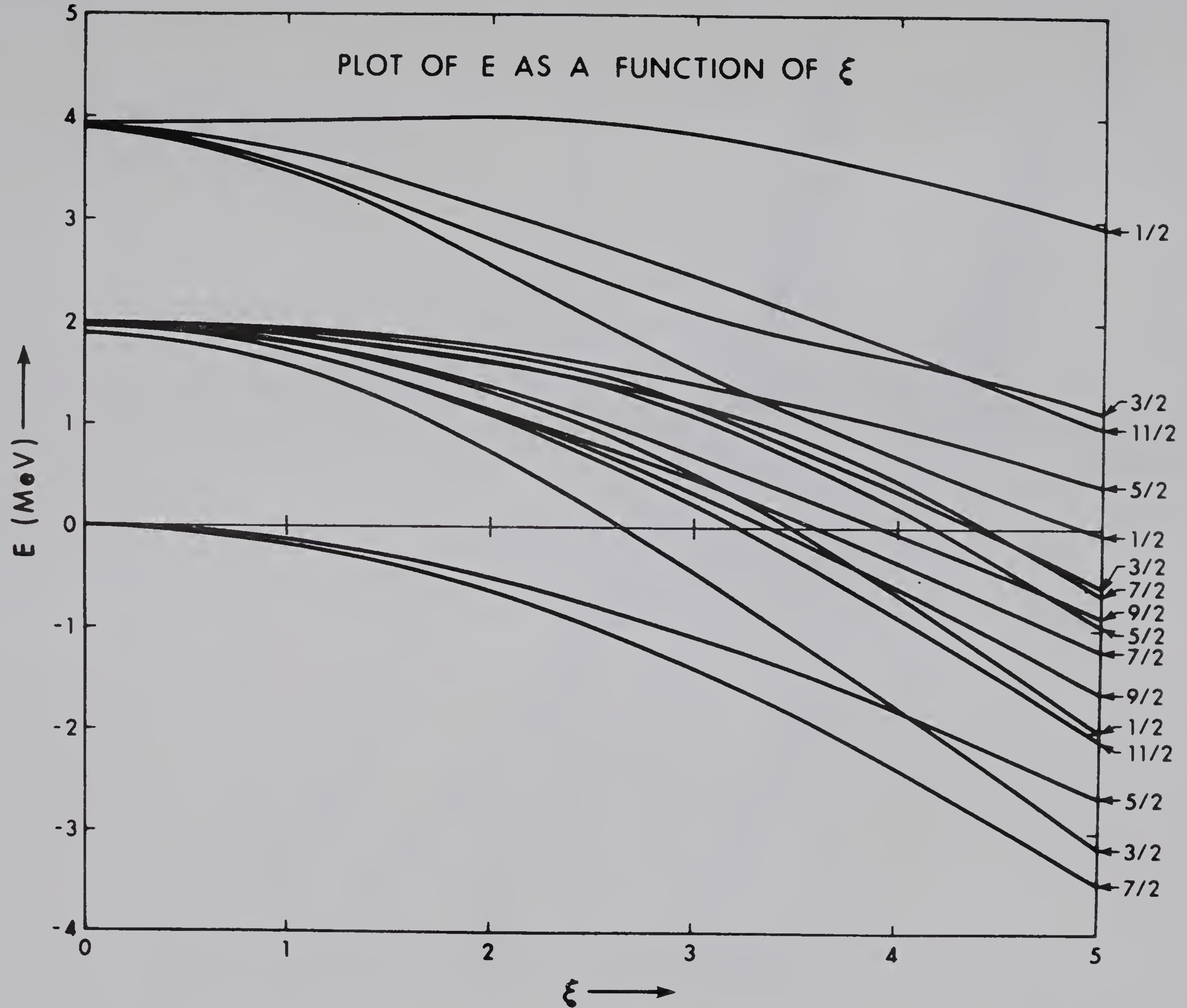

PLOT OF E AS A FUNCTION OF ξ

Fig. 37 Plot of E as a function of the coupling parameter ξ for ^{53}Mn.

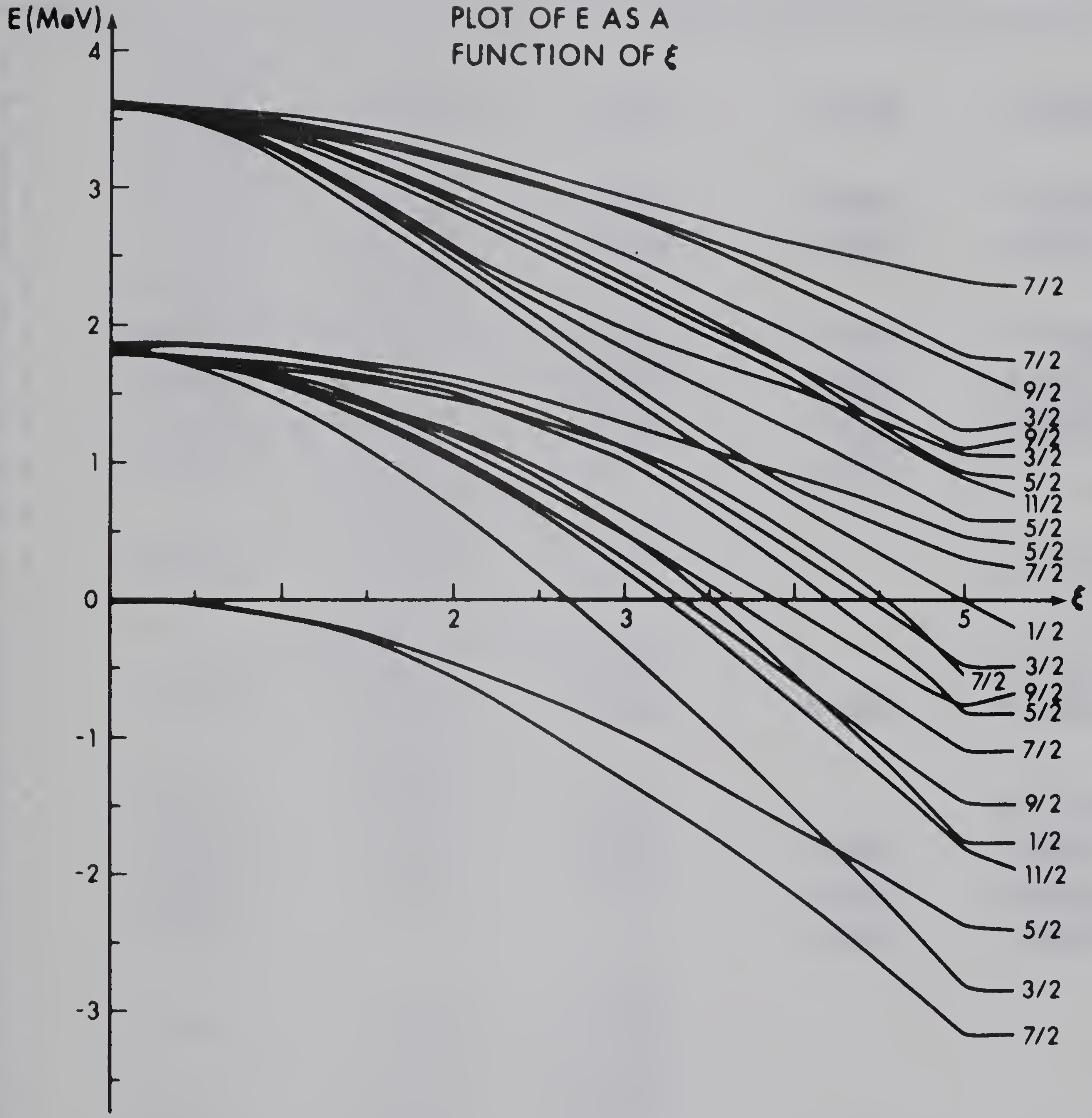
PLOT OF E AS A
FUNCTION OF ξ
E(MeV)
4
3
2
1
0
-1
-2
-3
2
3
5
ξ
7/2
7/2
9/2
3/2
9/2
3/2
5/2
11/2
5/2
5/2
7/2
1/2
3/2
7/2
9/2
5/2
7/2
9/2
1/2
11/2
5/2
3/2
7/2

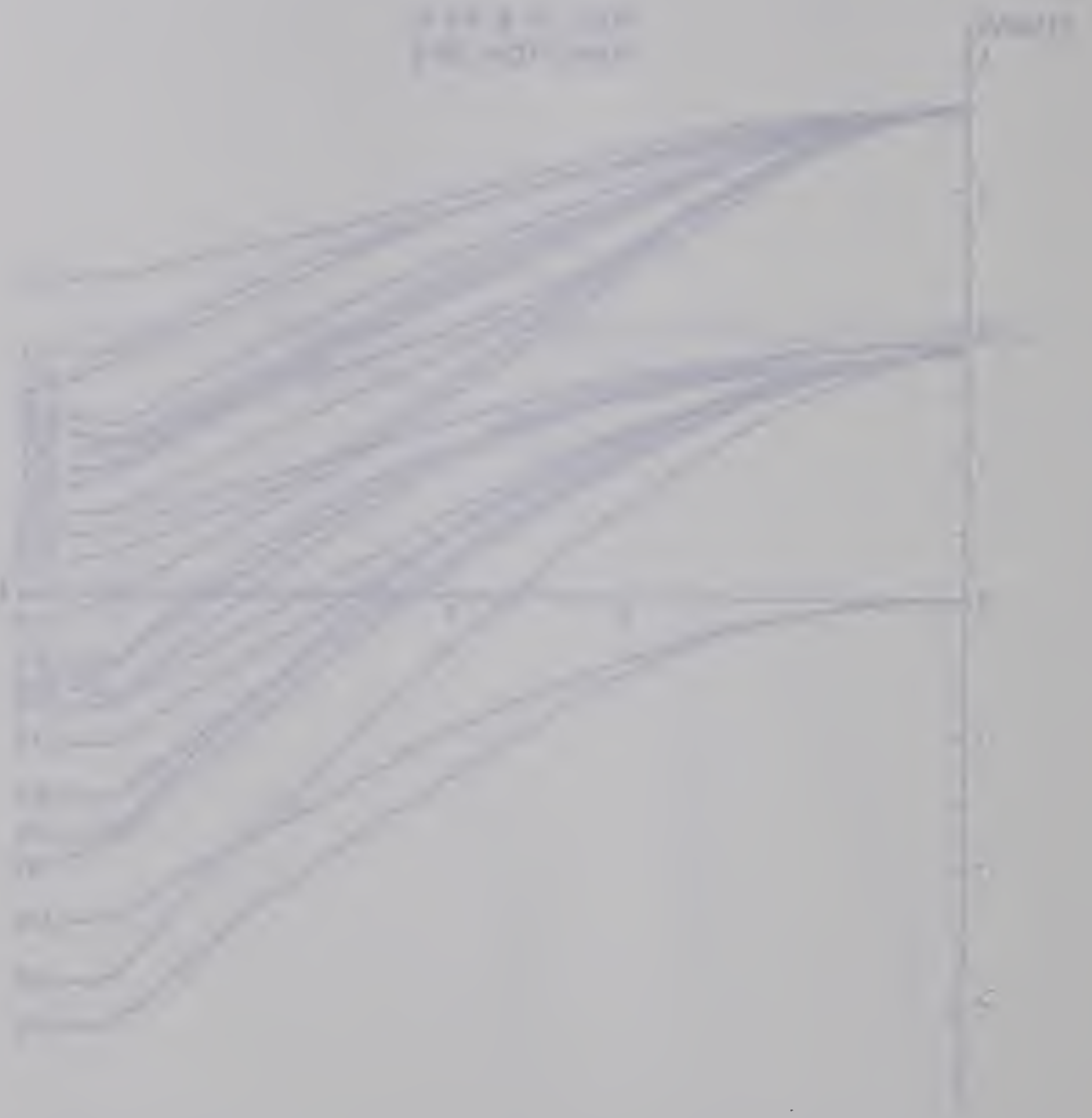

Table 10

Expansion coefficients corresponding to states $|E(\mathrm{MeV});\ I^{\pi}>$ of ^{51}V.

Basic states $\vert NR;\ j>$	$\vert 0;\ \frac{7}{2}^- >$	$\vert 0.320;\ \frac{5}{2}^- >$	$\vert 0.930;\ \frac{3}{2}^- >$	$\vert 1.609;\ \frac{11}{2}^- >$	$\vert 1.813;\ \frac{9}{2}^- >$
$\vert 00;\ \frac{7}{2}>$	0.7679				
$\vert 12;\ \frac{7}{2}>$	-0.5100	0.2363	0.7169	0.7760	0.7560
$\vert 20;\ \frac{7}{2}>$	0.1700				
$\vert 22;\ \frac{7}{2}>$	-0.0190	0.0040	-0.4056	-0.2549	0.3103
$\vert 24;\ \frac{7}{2}>$	0.1603	-0.1466	-0.1802	-0.4229	-0.4610
$\vert 30;\ \frac{7}{2}>$	-0.0155	0.0107			
$\vert 32;\ \frac{7}{2}>$	-0.0734	0.0298	0.1387	0.1303	0.1206
$\vert 33;\ \frac{7}{2}>$	-0.0049	-0.0020	-0.0796	0.0337	-0.0420
$\vert 34;\ \frac{7}{2}>$	-0.0204	0.0136	0.0720	0.0351	-0.0860
$\vert 36;\ \frac{7}{2}>$	-0.0272	0.0317		0.1418	
$\vert 00;\ \frac{5}{2}>$		0.7950			
$\vert 12;\ \frac{5}{2}>$	-0.1559	0.4898	0.2282		-0.0746
$\vert 20;\ \frac{5}{2}>$		0.1380			
$\vert 22;\ \frac{5}{2}>$		-0.0874	-0.1002		0.1510
$\vert 24;\ \frac{5}{2}>$	0.1000	0.0824	-0.0928	-0.1695	-0.0982
$\vert 30;\ \frac{5}{2}>$		0.0107			
$\vert 32;\ \frac{5}{2}>$	-0.0204	-0.0525	0.0435		-0.0120
$\vert 33;\ \frac{5}{2}>$	-0.0078	0.0001	-0.0411	0.0066	-0.0287
$\vert 34;\ \frac{5}{2}>$	-0.0099	0.0148	0.0437	0.0179	-0.0595
$\vert 36;\ \frac{5}{2}>$	-0.0201			0.1147	0.0694
$\vert 00;\ \frac{3}{2}>$			0.3340		
$\vert 12;\ \frac{3}{2}>$	0.1881	-0.0916	-0.1689		
$\vert 20;\ \frac{3}{2}>$			0.1769		
$\vert 22;\ \frac{3}{2}>$	-0.1142	0.0425	0.0541		
$\vert 24;\ \frac{3}{2}>$	-0.0479	0.0349		0.2395	0.1303
$\vert 30;\ \frac{3}{2}>$			-0.0681		
$\vert 32;\ \frac{3}{2}>$	0.0376	-0.0156	-0.0570		
$\vert 33;\ \frac{3}{2}>$	0.0251	-0.0136	0.0019		-0.1050
$\vert 34;\ \frac{3}{2}>$	0.0194	-0.0157		-0.1113	-0.0317
$\vert 36;\ \frac{3}{2}>$				-0.0503	-0.0230

Table 11

Expansion coefficients corresponding to states $|E(\mathrm{MeV});\ I^{\pi}>$ of ^{53}Mn.

Basic states $\vert NR;\ j>$	$\vert 0;\ \frac{7}{2}^{-}>$	$\vert 0.378;\ \frac{5}{2}^{-}>$	$\vert 1.288;\ \frac{3}{2}^{-}>$	$\vert 1.440;\ \frac{11}{2}^{-}>$	$\vert 1.619;\ \frac{9}{2}^{-}>$
$\vert 00;\ \frac{7}{2}>$	0.7294				
$\vert 12;\ \frac{7}{2}>$	-0.5313	0.2535	0.6958	0.7498	0.7288
$\vert 20;\ \frac{7}{2}>$	0.1963				
$\vert 22;\ \frac{7}{2}>$	-0.0187	0.0017	-0.4179	-0.2663	0.3217
$\vert 24;\ \frac{7}{2}>$	0.1839	-0.1718	-0.1998	-0.4374	-0.4767
$\vert 30;\ \frac{7}{2}>$	-0.0197	0.0131			
$\vert 32;\ \frac{7}{2}>$	-0.0908	0.0378	0.1539	0.1434	0.1328
$\vert 33;\ \frac{7}{2}>$	-0.0054	-0.0036	-0.0877	0.0367	-0.0467
$\vert 34;\ \frac{7}{2}>$	-0.0256	0.0181	0.0828	0.0401	-0.0935
$\vert 36;\ \frac{7}{2}>$	-0.0349	0.0410		0.1561	0.1534
$\vert 00;\ \frac{5}{2}>$		0.7601			
$\vert 12;\ \frac{5}{2}>$	-0.1569	-0.5104	0.2155		-0.0753
$\vert 20;\ \frac{5}{2}>$		0.1608			
$\vert 22;\ \frac{5}{2}>$	0.0025	-0.0998	-0.0963		0.1563
$\vert 24;\ \frac{5}{2}>$	0.1104	0.0923	-0.0997	-0.1724	-0.0996
$\vert 30;\ \frac{5}{2}>$		0.0131			
$\vert 32;\ \frac{5}{2}>$	-0.0246	-0.0661	0.0474		-0.0138
$\vert 33;\ \frac{5}{2}>$	-0.0098		-0.0429	0.0067	-0.0312
$\vert 34;\ \frac{5}{2}>$	-0.0128	0.0186	0.0490	0.0206	-0.0650
$\vert 36;\ \frac{5}{2}>$	-0.0246			0.1249	0.0764
$\vert 00;\ \frac{3}{2}>$			0.3289		
$\vert 12;\ \frac{3}{2}>$	0.2006	-0.0999	-0.1833		
$\vert 20;\ \frac{3}{2}>$			0.1893		
$\vert 22;\ \frac{3}{2}>$	-0.1304	0.0492	0.0588		
$\vert 24;\ \frac{3}{2}>$	-0.0571	0.0429		0.2521	0.1392
$\vert 30;\ \frac{3}{2}>$			-0.0744		
$\vert 32;\ \frac{3}{2}>$	0.0469	-0.0203	-0.0654		
$\vert 33;\ \frac{3}{2}>$	0.0306	-0.0167	0.0020		-0.1162
$\vert 34;\ \frac{3}{2}>$	0.0240	-0.0198		-0.1231	-0.0345
$\vert 36;\ \frac{3}{2}>$				-0.0563	-0.0261

Fig. 38 Comparison of energy levels of ^{51}V predicted from the intermediate-coupling calculations with experimental spectra, along with other predictions.

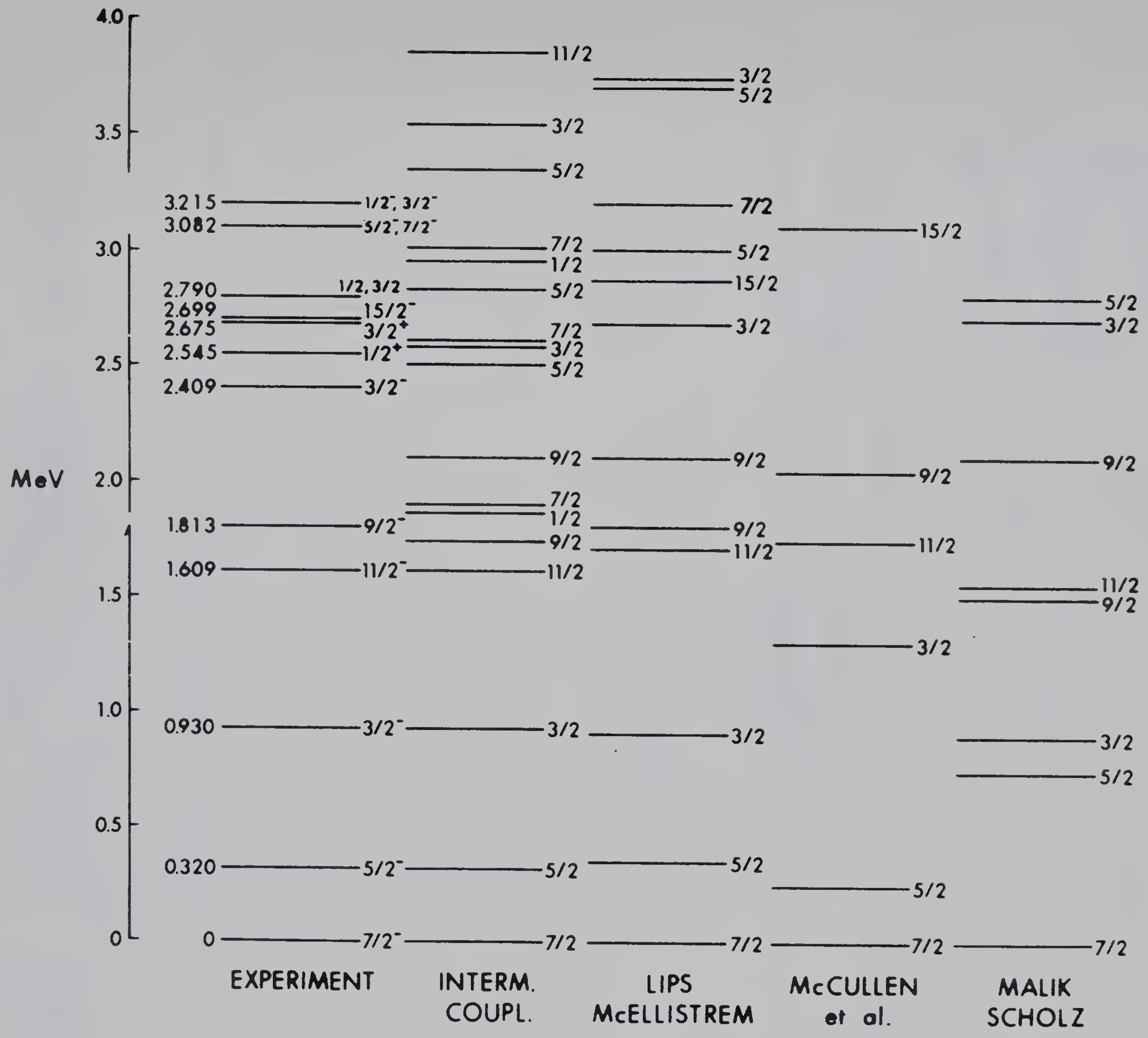
MeV
4.0
3.5
3.0
2.5
2.0
1.5
1.0
0.5
0
3.215 1/2⁻, 3/2⁻
3.082 5/2⁻, 7/2⁻
2.790 1/2, 3/2
2.699 15/2⁻
2.675 3/2⁺
2.545 1/2⁺
2.409 3/2⁻
1.813 9/2⁻
1.609 11/2⁻
0.930 3/2⁻
0.320 5/2⁻
0 7/2⁻
11/2
3/2
5/2
7/2
1/2
5/2
7/2
3/2
5/2
9/2
7/2
1/2
9/2
11/2
3/2
5/2
7/2
3/2
5/2
7/2
5/2
15/2
3/2
9/2
9/2
11/2
3/2
5/2
7/2
15/2
9/2
11/2
3/2
5/2
7/2
5/2
3/2
9/2
11/2
9/2
3/2
5/2
7/2
EXPERIMENT
INTERM. COUPL.
LIPS McELLISTREM
McCULLEN et al.
MALIK SCHOLZ

$^{51}_{23}V_{28}$

Fig. 39 Comparison of energy levels of ^{53}Mn predicted from the intermediate-coupling calculations with experimental spectra, along with other predictions.

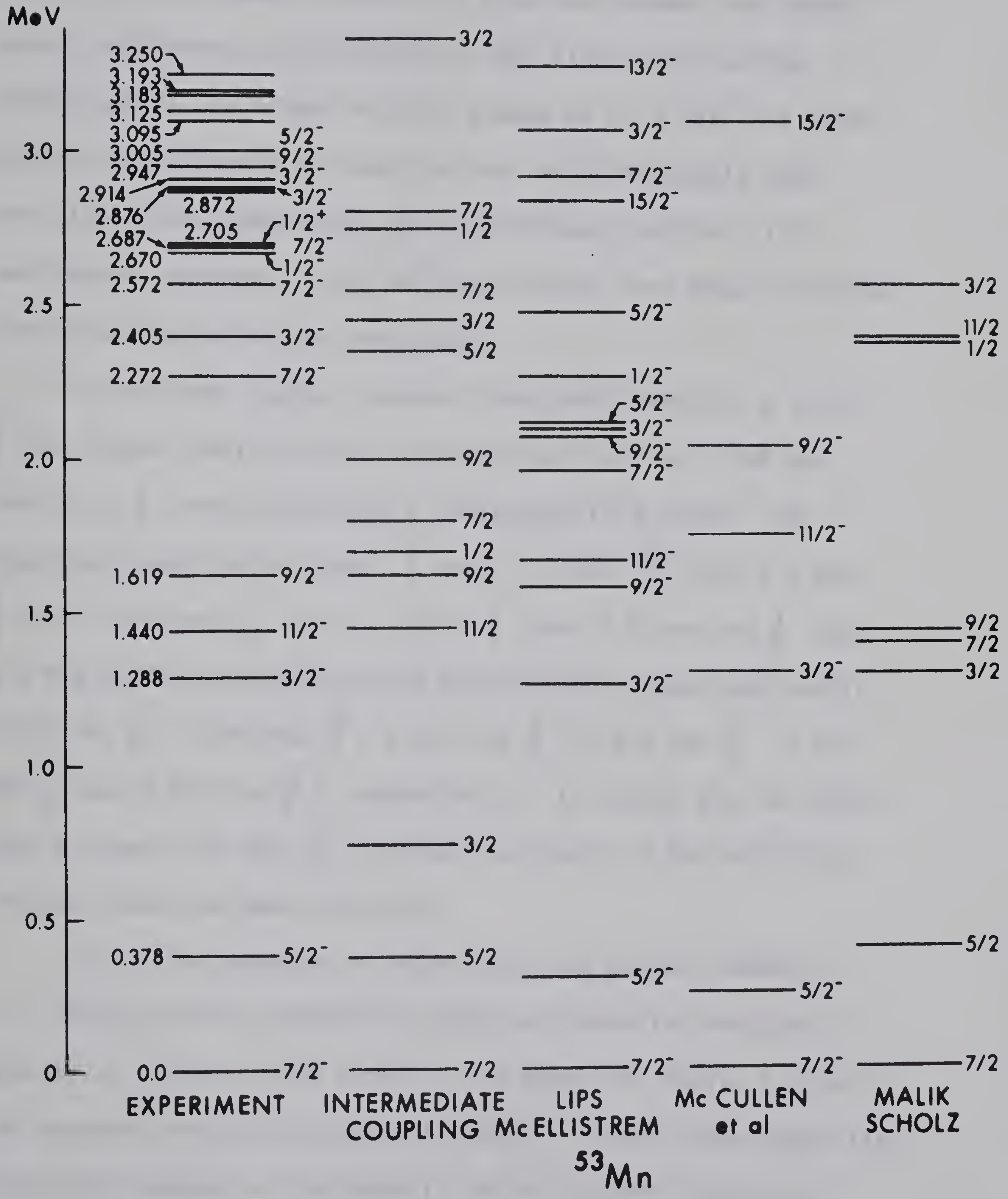
MeV
0
0.5
1.0
1.5
2.0
2.5
3.0
3.250
3.193
3.183
3.125
3.095
3.005
2.947
2.914
2.876
2.872
2.705
2.687
2.670
2.572
2.405
2.272
1.619
1.440
1.288
0.378
0.0
5/2⁻
9/2⁻
3/2⁻
3/2⁻
1/2⁺
7/2⁻
1/2⁻
7/2⁻
3/2⁻
7/2⁻
9/2⁻
11/2⁻
3/2⁻
5/2⁻
7/2⁻
EXPERIMENT
3/2
7/2
1/2
7/2
3/2
5/2
9/2
7/2
1/2
9/2
11/2
3/2
5/2
7/2
INTERMEDIATE COUPLING
13/2⁻
3/2⁻
7/2⁻
15/2⁻
5/2⁻
1/2⁻
5/2⁻
3/2⁻
9/2⁻
7/2⁻
11/2⁻
9/2⁻
3/2⁻
5/2⁻
7/2⁻
LIPS McELLISTREM
15/2⁻
9/2⁻
11/2⁻
3/2⁻
5/2⁻
7/2⁻
Mc CULLEN et al
3/2
11/2
1/2
9/2
7/2
3/2
5/2
7/2
MALIK SCHOLZ
53Mn

levels are taken from the present (p,nγ) reaction. As seen in Fig. 39, fairly good agreement is obtained between the experimental and theoretical energies in the first four excited states and in the higher excited states up to 3 MeV, the model predictions of spins and energies are also reasonably good. The figure also shows that the intermediate coupling is in much better agreement with the experimental data than any other theoretical calculations available.

In the lower region, however, the model predicts a level $\frac{3}{2}^-$ at a lower position than the observed level at 1.288 MeV with spin $\frac{3}{2}^-$, which might be a single-particle state. The predicted levels with spins, $\frac{7}{2}^-$ near 1.8 MeV, $\frac{3}{2}^-$ near 2.4 MeV, $\frac{7}{2}^-$ near 2.57 MeV, $\frac{1}{2}^-$ near 2.7 MeV, $\frac{7}{2}^-$ near 2.8 MeV and $\frac{3}{2}^-$ near 3.5 MeV would correspond to the experimentally observed levels, 2.272 MeV $\frac{7}{2}^-$, 2.405 MeV $\frac{3}{2}^-$, 2.572 MeV $\frac{7}{2}^-$, 2.670 MeV $\frac{1}{2}^-$, 2.687 MeV $\frac{7}{2}^-$,and 2.876 MeV $\frac{3}{2}^-$, respectively. It should also be noted that a level with spin $\frac{1}{2}^-$ is predicted near 1.7 MeV which has not been observed experimentally.

(ii) Electromagnetic transitions and nuclear moments

The transition probability T(σL) of gamma-ray emission is related to the multipole order L, the gamma-ray energy E_γ, and the reduced transition probability B(σL). Among these quantities, only B(σL) depends on the details of the nuclear structure. Comparisons of the calculated reduced transition probability and nuclear moment with the experimental data should, therefore,

throw further light on the validity of the model.

Calculations were performed with the free-particle g_s factor ($g_s = 5.587$) and the free-proton charge ($e_p = e$). In the present calculations, it was found that, in general, the results of the free nucleon values, as used by some investigators (Ch 67, Ca 71), were in better agreement with experiment than those of the effective values, e.g., ($g_s{}^{\text{proton}}_{\text{eff}} = 0.5\, g_s{}^{\text{proton}}$, $e_p{}^{\text{eff}} = 2e_p$). However, other authors (He 67, Ba 70, Be 71) have used the effective values for the g_s factor and nucleon charge in their intermediate coupling calculations to take into account the effects of core polarization. Values of other parameters used in the calculations are $g_\ell = 1$, $g_R = \frac{Z}{A}$, $K = 40$ MeV and $R_0 = 1.18\, A^{\frac{1}{3}}$ fm.

Reduced transition probabilities : The reduced transition probabilities, B(E2) and B(M1), were calculated using the wave functions obtained above by diagonalizing the energy matrices. These results and available experimental data are compared for ^{51}V and ^{53}Mn in tables 12 to 14.

In the case of ^{51}V, the experimental data for B(E2) were taken from various experiments by many authors as listed in table 12. The calculated B(E2) value for each of the transitions of the first and second excited states to the ground state is close to one of the corresponding experimental data listed in table 12. The B(E2) values for the third and fourth excited states are larger than the experimental values. However, for

the transition of the 1.813 MeV level to the 0.320 MeV level, the calculated B(E2) value is ten times smaller than the value measured by Horoshko _et al_. (Ho 70). The calculated B(M1) values for ^{51}V are compared with the experimental data obtained by Horoshko _et al_. (Ho 70) in table 13. The agreement with experimental results is, in most cases, not good, i.e. the theoretical values are much larger than the measured ones.

In the case of ^{53}Mn, the experimental data for B(E2) and B(M1) listed in table 14 are taken from the present (p,nγ) experiment. As seen in table 14, the calculated B(E2) values for all the transitions listed in the table are in good agreement with the experimental results within error, except for the 2.405 MeV level, which may be assumed to be a single-particle state. The predicted B(M1) values are also in good agreement with the experimental results and in particular, for the 2.687 MeV level the calculated value of 18.3 is in excellent agreement with the experimental, 17.5 (in 10^{-3} x n.m.^{2}).

Nuclear moments : The results of the present calculations and some available data, along with other predicted values, of the nuclear moments for the ground states of ^{51}V and ^{53}Mn are shown in table 15.

The magnetic dipole mements calculated by the author for both ^{51}V and ^{53}Mn are in good agreement with the experimental values. According to the recent measurements (Ch 67), however,

Table 12

Reduced transition probabilities B(E2) in ^{51}V (in $10^2 \times e^2\ fm^4$).

Transitions (MeV)	Calculated				Measured					
	Int. Coupl.	Weisskopf estimates	Talmi (Ta 67)	Lips and McEllistrem (Li 70)	Lemberg (Le 60)	Gove (Go 60)	Kendall (Ke 62)	Meriwether (Me 66)	Afonin (Af 68)	Horoshko (Ho 70)
$\frac{5}{2}$ $\frac{7}{2}$ 0.320 → 0	0.46	0.19	1.28	1.32		1.73 ± 0.35		0.67	1.23 ± 0.25	0.54 ± 0.076
$\frac{3}{2}$ $\frac{7}{2}$ 0.930 → 0	3.3	0.29	0.44	0.45	2.2	0.76 ± 0.15	1.87 ± 0.64	0.38	0.54 ± 0.11	0.76 ± 0.05
$\frac{3}{2}$ $\frac{5}{2}$ 0.930 → 0.320	0.42	0.21							< 0.47	1.07 ± 0.09 a) $0.11^{+0.093}_{-0.059}$ b)
$\frac{11}{2}$ $\frac{7}{2}$ 1.609 → 0	2.5	0.17	0.57	0.64			0.67 ± 0.32	0.33	0.60 ± 0.12	0.83 ± 0.08
$\frac{9}{2}$ $\frac{7}{2}$ 1.813 → 0	2.3	0.15	0.22	0.26			0.80 ± 0.38	0.16	0.22 ± 0.05	0.28 ± 0.05
$\frac{9}{2}$ $\frac{5}{2}$ 1.813 → 0.320	0.023	0.16								0.24 ± 0.05
$\frac{3}{2}$ $\frac{7}{2}$ 2.409 → 0	0.014	0.29								
$\frac{3}{2}$ $\frac{5}{2}$ 2.409 → 0.320	0.73	0.21								

a: with $\delta = -8.8^{+4.1}_{-\infty}$ b: with $\delta = -0.33^{+0.11}_{-0.14}$

Table 13

Reduced transition probabilities B(M1) in ^{51}V (in 10^{-3} x n.m.^{2}).

Transitions (MeV)	Calculated				Measured
	Intermediate coupling	Scholz and Malik		Weisskopf estimates	
		$\beta = -0.32$	$\beta = 0.20$		
$\frac{5}{2}$ $\frac{7}{2}$ 0.320 → 0	2880	0.036	210	3114	4.9 ± 0.4
$\frac{3}{2}$ $\frac{5}{2}$ 0.930 → 0.320	9.18	120 - 490	890	3270	a < 0.16 b 2.9 ± 0.4
$\frac{9}{2}$ $\frac{7}{2}$ 1.813 → 0	67.6	37	35	2423	0.47 ± 0.16
$\frac{3}{2}$ $\frac{5}{2}$ 2.409 → 0.320	140			3271	

a: with $\delta = -8.8^{+4.1}_{-\infty}$ b: with $\delta = -0.3^{+0.11}_{-0.14}$

Table 14

Reduced transition probabilities, B(M1) and B(E2) in ^{53}Mn.

Transitions (MeV)	B(E2) $(10^2 \times e^2\ fm^4)$			B(M1) $(10^{-3} \times n.m.^2)$		
	Int. Coupl.	Weisskopf estimates	Measured	Int. Coupl.	Weisskopf estimates	Measured
$\underset{1.288}{\frac{3}{2}} \rightarrow \underset{0}{\frac{7}{2}}$	4.6	0.31	< 6.9			
$\underset{1.440}{\frac{11}{2}} \rightarrow \underset{0}{\frac{7}{2}}$	3.5	0.18	$6.27^{+5.70}_{-3.74}$			
$\underset{1.619}{\frac{9}{2}} \rightarrow \underset{0}{\frac{7}{2}}$	3.1	0.16	$2.11^{+4.58}_{-1.58}$ a) $0.63^{+1.40}_{-0.48}$ b)	78.2	2410	$3.75^{+8.2}_{-2.8}$ a) $30.1^{+66.7}_{-23.2}$ b)
$\underset{2.405}{\frac{3}{2}} \rightarrow \underset{0}{\frac{7}{2}}$	0.0074	0.31	$0.27^{+0.19}_{-0.15}$			
$\underset{2.687}{\frac{7}{2}} \rightarrow \underset{0}{\frac{7}{2}}$	0.056	0.12	$0.072^{+0.06}_{-0.04}$	18.3	1820	$17.5^{+14.6}_{-8.4}$
$\underset{2.876}{\frac{3}{2}} \rightarrow \underset{0.378}{\frac{5}{2}}$		0.17			3250	

a: with $\delta = -3.2^{+1.5}_{-0.5}$ b: with $\delta = -0.62^{+0.1}_{-0.2}$

Table 15

Nuclear moments of ^{51}V and ^{53}Mn.

Electric quadrupole moment Q (in b)

Nucleus	Experimental	Intermediate coupling	Shell model	Strong Coriolis coupling
^{51}V	-0.04a), 0.26b), -0.52 ± 0.010c)	-0.381	-0.034 (Ho 55), -0.058 (Ta 67)	+0.04 (Ma66)
^{53}Mn		-0.457	0.0637 (Li 70)	

a) Optical hyperfine structure, ref. (Mu 66)

b) NMR, ref. (Ar 66)

c) Atomic beam magnetic resonance, ref. (Ch 67a)

Magnetic dipole moment (in n.m.)

Nucleus	Experimental	Intermediate coupling	Schmidt limit
^{51}V	+5.150 (Kn 50), +5.1450 ± 0.0002 (Sh 51)	+5.24	+5.793
^{53}Mn	+5.050 ± 0.007 (Do 56)	+5.13	+5.793

the most reliable value for the electric quadrupole moment of ^{51}V seems to be approximately -0.05. The present calculation gives a negative sign consistent with the experimental one, but too large in magnitude for the electric quadrupole moment of ^{51}V. If an adjusting procedure for the K value (different from 40 MeV) is used to get the best fit to the experimental data, the situation might be improved. Unfortunately, there is no experimental data available for the electric quadrupole moment of ^{53}Mn to compare with the theoretical calculation.

(iii) Lifetimes, branching ratios and mixing ratios

In tables 16 and 17, the calculated lifetimes, branching and mixing ratios for ^{51}V and ^{53}Mn are compared with the available experimental data. The experimental lifetime data of ^{51}V is available only for the first excited state. The value of 280 ± 50 ps for the first excited state of ^{51}V has been obtained with a pulsed-beam technique by Shipley *et al*. (Sh 69a). The experimental branching and mixing ratios in ^{51}V are taken from the recent $^{48}Ti(\alpha,p\gamma)^{51}V$ reaction by Horoshko *et al*. (Ho 70).

As seen in table 16, the model predictions in ^{51}V are, in general, in good agreement with the experimental measurements. Especially the predicted branching and mixing ratios for transitions of the 0.930 MeV level and the mixing ratio for the 2.409 → 0.320 transition are in excellent agreement with the measured values. However, the predicted lifetime, $\tau = 0.6$ ps,

Table 16

Lifetimes, branching ratios and mixing ratios in ^{51}V.

State (MeV)	τ(ps)		Transition (MeV)		Branching ratio (%)		Mixing ratio $\lvert\delta\rvert$	
	Exp.	Int. Coupl.	I_i	I_f	Exp.	Int. Coupl.	Exp.	Int. Coupl.
0.320	280 ± 50 (Sh 69)	0.60	0.320	0	100	100	$-0.32^{+0.30}_{-0.57}$	0.011
0.930		3.1	0.930	0	86	87.3		
			0.930	0.320	14	12.7	$-8.8^{+4.1}_{-\infty}$ $-0.33^{+0.11}_{-0.14}$	0.34
1.609		0.30	1.609	0	100	100		
1.813		0.079	1.813	0	75	99.8	$+3.75^{+0.76}_{-0.58}$	0.88
			1.813	0.320	25	0.20		
2.409		0.038	2.409	0	19	0.5		
			2.409	0.320	81	99.5	-0.36 ± 0.15	0.40

Table 17

Lifetimes, branching ratios and mixing ratios in ^{53}Mn.

State (MeV)	τ(ps)		Transition (MeV)		Branching ratio (%)		Mixing ratio $\lvert\delta\rvert$	
	Exp.	Int. Coupl.	I_i	I_f	Exp.	Int. Coupl.	Exp.	Int. Coupl.
1.288	> 0.19	0.45	1.288	0	57	89.8		
			1.288	0.378	43	10.2		
1.440	$0.21^{+0.31}_{-0.10}$	0.38	1.440	0	100	100		
1.619	$0.29^{+1.0}_{-0.2}$	0.10	1.619	0	90	99.8	$-3.2^{+1.5}_{-0.5}$ $-0.6^{+0.1}_{-0.2}$	0.86
			1.619	0.378	10	0.2		
2.405	$0.12^{+0.14}_{-0.05}$	0.03	2.405	0	32	0.23		
			2.405	0.378	11	85.63		
			2.405	1.288	57	14.14		
2.687	$0.072^{+0.05}_{-0.03}$	0.06	2.687	0	52	46.6	$-0.46^{+0.14}_{-0.21}$	0.39
			2.687	0.378	26	45.6		
			2.687	1.288	22	7.8		

for the first excited state turns out to be much smaller than the experimentally observed value.

Experimental data for ^{53}Mn listed in table 17 are taken from the present (p,nγ) reaction. Fairly good agreement between the predicted and measured lifetimes of ^{53}Mn is obtained, as seen in table 17. The predicted branching ratios are found to be consistent with the experimental values qualitatively, except for the 2.405 MeV state transitions. The calculated mixing ratio for the 2.687 → 0 MeV transition is shown to be in very good agreement with the measured values. It should be noted that for the transition of the 1.619 MeV state to the ground state, the predicted mixing ratio of 0.86 prefers the experimental value, $-0.62^{+0.1}_{-0.2}$.

(c) Concluding remarks

The above results indicate that the intermediate-coupling vibrational model provides a good description of the properties of low-lying states in ^{51}V and ^{53}Mn. The vibrational character of these nuclei has been suggested from the Coulomb excitation experiments (Ri 62) and the (d,n) reactions (Ok 67); this partly supports the validity of a description in terms of a single particle coupled to a vibrational even-even core, as considered in the present calculations.

The model reproduces well the energy spectra of the first four excited states and even those of higher excited states up

to 2.9 MeV in ^{53}Mn. However, the model predictions of higher levels in ^{51}V may be somewhat doubtful and the experimentally observed level with a spin of $\frac{15}{2}$ could not be predicted by the model. This may be because several other modes of excitations which might become dominant for higher excitation energies were neglected in the present calculation, as previously pointed out (Ba 70). The model reproduces the observed magnetic moments in ^{51}V and ^{53}Mn, but the predicted values for the electric quadrupole moments are too large.

To make some comments on the parameters used in the calculations, the phonon energies, $\hbar\omega$, are found to be close to the first 2^+ state energies of the corresponding cores. The coupling parameters (table 9) of ^{51}V and ^{53}Mn corresponding to the best fit of the experimental data lie in the usual intermediate-coupling region $1 \leq \xi \leq 4$.

The larger value of ξ in ^{53}Mn compared to ^{51}V, seems to exhibit a linear dependence of ξ on the mass number A in this region, as observed in the large mass region $121 \leq A \leq 149$, by Heyde and Brussaard (He 67). The coupling strength tends toward weak coupling as the mass number decreases in this mass region, since a small coupling parameter arises from a small equilibrium deformation of the nucleus (Br 70).

The validity of including states of up to only three phonons in the present calculations may be estimated by examining whether

or not the squares of the expansion coefficients corresponding to the highest phonon states should be negligible compared to unity. From tables 10 and 11, the squares are nearly negligible compared to unity, indicating the above condition to be satisfied.

As seen in tables 10 and 11, the ground and first excited states of ^{51}V and ^{53}Mn considered here are highly pure: in both nuclei, about 90% of $f_{\frac{7}{2}}$ admixtures for the ground states, about 90% of $f_{\frac{5}{2}}$ admixtures for the first excited states, and about 75% of $f_{\frac{7}{2}}$ admixtures for the second excited states.

In order to characterize the shape of the nucleus, the customary parameters β and γ are used, where β measures the quadrupole deformation and γ measures the degree of departure from the symmetry axis condition. The experimental value of the quadrupole deformation β is obtained from the observed B(E2) for excitation of the first 2^+ state using the following formula (St 60):

$$\bar{\beta}^2 = \frac{B(E2,\ 0\rightarrow 2)}{[\frac{3}{4\pi}\ Z e R_0^2\ ]^2} \ . \qquad (IV.37)$$

For rotational nuclei, this formula gives, in first approximation, the value for the equilibrium deformation, β_0, and for vibrational nuclei, it gives the root-mean-square deformation, β_{rms}, in the ground state (St 60).

In the vibrational model, the root-mean-square deformation, β_{rms}, is given by (He 67, Br 60)

$$\beta_{rms} = \left(\frac{5}{2} \hbar \right)^{\frac{1}{2}} (BC)^{-\frac{1}{4}}$$

$$= \pi^{\frac{1}{2}} \; \xi \; \frac{\hbar\omega}{K} \qquad \text{(IV.38)}$$

in terms of the intermediate-coupling parameters.

The calculated values of β_{rms}, 0.265 for ^{51}V and 0.276 for ^{53}Mn, are in the range of the experimental values (Ri 62) (typically 0.26 for ^{51}V and ^{52}Cr). This suggests that the parameters determined in the present calculations fall in the correct range.

It is concluded that the intermediate-coupling vibrational model is quite satisfactory in describing the properties of the low-lying levels in ^{51}V and ^{53}Mn. From the aspect of results of the model predictions and values of the coupling and deformation parameters obtained in the present calculations, it appears that the intermediate-coupling character becomes better established as mass number A increases in this mass region. Consequently the weak-coupling core excitation model of de-Shalit (Sh 61) seems to be more appropriate for the low-lying levels of ^{51}V, as has been suggested from the Coulomb excitation experiment by Ritter *et al*. (Ri 62).

CHAPTER V

CONCLUSIONS

From the analysis of the gamma-ray angular distributions and yield curves (Chapter II), the spins of the low-lying excited states, up to 3 MeV excitation energy in ^{53}Mn have been determined, based on the compound nuclear statistical model. The gamma-ray decay scheme, the branching and mixing ratios of the gamma-ray transitions have been also obtained. In the present experiment, the 2.84 MeV level in ^{53}Mn which was suggested in the (p,γ) work by Maripuu (Ma 70) was not found. The spins of the 2.272 and 2.687 MeV levels assigned as $\frac{7}{2}^-$ from the present work were in disagreement with the (p,γ) results (Ma 70), $J = \frac{5}{2}^-$ for both levels.

In the lifetime measurements (Chapter III), lifetimes of nine excited states in ^{53}Mn have been measured. The reduced transition probabilities, B(M1) and B(E2), were derived from the measured lifetimes, mixing and branching ratios and compared with the other available theoretical values. The present lifetime values are found to be consistent with other experiments and to be in good agreement with the intermediate-coupling predictions.

The Nilsson model calculations (Chapter IV) have been carried out for the energy levels of ^{53}Mn without taking band

mixing into consideration and the results were compared with the band mixing calculations of Malik and Scholz. It is found that the predictions in both cases, in general, are not satisfactory to describe the properties of the low-lying levels in ^{53}Mn, although a few energy levels in the low-lying states are reproduced.

The intermediate-coupling in the unified model (Chapter IV) has been applied to ^{51}V and ^{53}Mn. $^{53}_{25}\mathrm{Mn}_{28}$ would be expected to show similar behavior to that of $^{51}_{23}\mathrm{V}_{28}$, the "equivalent" nucleus, since from the point of view of the jj coupling shell model, the $(1f_{\frac{7}{2}})^{3}$ and $(1f_{\frac{7}{2}})^{-3}$ configurations should be equivalent. The model gives a reasonably good description of the low energy properties of the nuclei. From the energy spectra, lifetimes, branching and mixing ratios predicted for these nuclei, it is apparent that fairly good agreement does exist between theory and experiment. It is concluded that the intermediate-coupling character is better established for ^{53}Mn than ^{51}V, while the weak-coupling core excitation model of de-Shalit (Sh 61) seems to be more appropriate for ^{51}V.

Measurements of the electric quadrupole moment of ^{53}Mn and more detailed information on the excited states are desired to test the nuclear models properly.

REFERENCES

Ab 70 M.A. Abuzeid *et al.*, Soviet J. Nucl. Phys. 10 (1970) 4 and ibid. 270

Af 68 O.F. Afonin *et al.*, Soviet J. Nucl. Phys. 6 (1968) 160

Al 55 G. Alaga, K. Alder, A. Bohr and B.R. Mottelson, Dan. Mat. Fys. Medd. 29 (1955) N° 9

Al 70 G. Allen, *Handbook of Chemistry and Physics*, ed. by R. Weast (1970) E - 143

Ar 64 S.E. Arnell and S. Sterner, Arkiv Fysik 26 (1964) 423

Ar 65 D.D. Armstrong and A.G. Blair, Phys. Rev. 140 (1965) B 1226

Ar 66 J.O. Artman, Phys. Rev. 143 (1966) 541

Ar 67 D.D. Armstrong, A.G. Blair and H.C. Thomas, Phys. Rev. 155 (1967) 1254

Au 62 E.H. Auerbach and F.G.J. Perey, BNL 765 (T - 286), (1962) unpublished

Au 67 N. Auerbach, Phys. Lett. 24B (1967) 260

Ba 62 G. Bassani *et al.*, Nucl. Phys. 36 (1962) 471

Ba 64 G. Bassani, N.M. Hintz and C.D. Kavaloski, Phys. Rev. 136 (1964) B 1006

Ba 70 F.G. Bailey and D.C. Choudhury, Nucl. Phys. A144 (1970) 628

Be 30 H.A. Bethe, Ann. Physik 5 (1930) 325

Be 37 H.A. Bethe, Rev. Mod. Phys. 9 (1937) 69

Be 53 H.A. Bethe, *Experimental Nuclear Physics*, ed. by E. Segre Vol. 1 (1953) 166

Be 61 S.T. Belyaev, Soviet Phys. JETP 12 (1961) 968

Be 66 F. Beck, Ann. de Physique, Series 14, tome 1 (1966) 503

Be 69 M.C. Bertin, N.B. Koller and G.G. Seaman, Phys. Rev. 183 (1969) 964

Be 69a R.A.I. Bell et al., Nucl. Phys. A133 (1969) 337

Be 71 G.V. Berghe, K. Heyde and M. Waroquier, Nucl. Phys. A165 (1971) 662 and A163 (1971) 478

Bi 53 L.C. Biedenharn and M.E. Rose, Rev. Mod. Phys. 25 (1953) 729

Bi 60 G.R. Bishop, Nucl. Phys. 14 (1960) 376

Bl 33 F.Z. Bloch, Z. Physik, 81 (1933) 363, and Ann. Physik 16 (1933) 285

Bl 52 J.M. Blatt and L.C. Biedenharn, Rev. Mod. Phys. 24 (1952) 258

Bl 52a J.M. Blatt and V.F. Weisskopf, *Theoretical Nuclear Physics*, John Wiley and Sons, Inc., New York (1952)

Bl 66 A.E. Blaugrund, Nucl. Phys. 88 (1966) 501

Bo 36 N. Bohr, Nature 137 (1936) 344

Bo 37 N. Bohr and F. Kalckar, Kal. Dan. Vid. Selsk. Mat. Medd. 14 (1937) Nº 10

Bo 39 N. Bohr and J.A. Wheeler, Phys. Rev. 56 (1939) 426

Bo 48 N. Bohr, Kal. Dan. Vid. Selsk. Mat. Medd. 18 (1948) Nº 8

Bo 52 A. Bohr, Mat. Fys. Medd. Dan. Vid. Selsk. 26 (1952) Nº 14

Bo 53 A. Bohr and B.R. Mottelson, Mat. Fys. Medd. Dan. Vid. Selsk. 27 (1953) Nº 16

Bo 54 A. Bohr, Ph.D. Thesis, University of Copenhagen (1954)

Br 60 D.M. Brink, *Progress in Nuclear Physics*, Vol. 8 (1960) 99

Br 66 G. Brown, S.E. Warren and R. Middleton, Nucl. Phys. 77 (1966) 365

Br 70 A.M. Bradley and M.R. Meder, Phys. Rev. C1 (1970) 1723

Ca 70 T.P.G. Carola, Ph.D. Thesis, University of Alberta (1970)

Ca 71 T.P.G. Carola and H. Ohnuma, Nucl. Phys. A165 (1971) 259

Ch 54 D.C. Choudhury, Mat. Fys. Medd. Dan. Vid. Selsk. 28 (1954) N^{o} 4

Ch 66 D.C. Choudhury and E. Kujawski, Phys. Rev. 144 (1966) 1013

Ch 67 D.C. Choudhury and T.F. O'dwyer, Nucl. Phys. A93 (1967) 300, and T.F. O'dwyer, Ph.D. Thesis, Polytechnic Institute of Brooklyn (1967)

Ch 67a W.J. Childs and L.G. Goodman, Phys. Rev. 156 (1967) 64, and 156 (1967) 71

Ch 70 W.H. Chung, W.C. Olsen and D.M. Sheppard, BAPS 15 (1970) 784

Ch 70a W.H. Chung, University of Alberta Internal Report UAE-NPL-23 (1970) unpublished

Ch 71 D.C. Choudhury and J.N. Friedman, Phys. Rev. C3 (1971) 1619

Ch 71a W.H. Chung, D.M. Sheppard, W.C. Olsen and B.C. Robertson, BCAP, 27 (1971) 21

Ch 71b W.H. Chung, A.H. Hussein and T.C. Sharma, University of Alberta Internal Report UAE-NPL-35 (1971) unpublished

Co 61 L. Colli *et al.*, Nuovo Cim. 20 (1961) 94

Cu 68 B. Cujec, R. Dayras and I. Szöghy, BAPS 13 (1968) 723

Cu 69 B. Cujec and I.M. Szöghy, Phys. Rev. 179 (1969) 1060

Da 52 C.M. Davisson and R.D. Evans, Rev. Mod. Phys. 24 (1952) 79

Da 65 J.P. Davidson, Rev. Mod. Phys. 37 (1965) 105

Da 66 C.M. Davisson, *α, β, and γ Spectroscopy*, ed. by Siegbahn (1966) 827

De 55 S. Devons, G. Manning and D.P. Bunbury, Proc. Phys. Soc. (London) A68 (1955) 18

De 68 I. Dernedde, Z. Physik 216 (1968) 103

Do 56 W. Dobrowolski *et al.*, Phys. Rev. 104 (1956) 1378

Dr 68 I.P. Dryapachenko *et al.*, Soviet J. Nucl. Phys. 6 (1968) 321

El 48 L.G. Elliott and R.E. Bell, Phys. Rev. 74 (1948) 1869

El 66 L.R.B. Elton, *Introductory Nuclear Theory*, ed. by W.B. Saunders (1966)

Es 65 M.A. Eswaran et al., Nucl. Phys. 66 (1965) 401

Fa 63 U. Fano, Ann. Rev. Nucl. Sci. 13 (1963) 1

Fa 68 B. Fastrup, A. Borup and P. Hvelplund, Can. J. Phys. 46 (1968) 489

Fi 59 O.B. Firsov, Soviet Phys. JETP 9 (1959) 1076

Gl 60 N.K. Glendenning, Phys. Rev. 119 (1960) 213

Gl 66 R.N. Glover and A.D.W. Jones, *International Nuclear Physics Conference at Gatlinburg*, ed. by R. Becker et al. (1966) 133

Go 40 S. Goudsmit and J.L. Saunderson, Phys. Rev. 57 (1940) 24, and 58 (1940) 36

Go 56 S. Goldstein and I. Talmi, Phys. Rev. 102 (1956) 589

Go 60 H.G. Gove, Proc. 2nd Conf. 1960, Gatlinburg (1960)

Go 62 C.D. Goodman, J.B. Ball and C.B. Fulmer, Phys. Rev. 127 (1962) 574

Go 66 S. Gorodetzky et al., Nucl. Phys. 85 (1966) 576 and 85 (1966) 519

Gr 70 P. Green, University of Alberta Internal Report UAE-NPL-26 (1970) unpublished

Gu 70 P.R.H. Gutowski, M.Sc. Thesis, University of Alberta (1970)

Ha 40 D.R. Hamilton, Phys. Rev. 58 (1940) 122

Ha 49 O. Haxel, J.H.D. Jensen and H.E. Suess, Phys. Rev. 75 (1949) 1766

Ha 52 W. Hauser and H. Feshbach, Phys. Rev. 87 (1952) 366

He 67 K. Heyde and P.J. Brussaard, Nucl. Phys. A104 (1967) 81

Ho 55 H. Horie and A. Arima, Phys. Rev. 99 (1955) 778

Ho 70 R.N. Horoshko, D. Cline and P.M.S. Lesser, Nucl. Phys. A149 (1970) 562

Jo 64 C.H. Johnson, C.C. Trail and A. Galonsky, Phys. Rev. 136 (1964) B 1719

Ju 59 J.O. Juliano et al., Phys. Rev. 113 (1959) 602

Ke 56 A.K. Kerman, Dan. Mat. Fys. Medd. 30 (1956) Nº 15

Ke 62 H.W. Kendal and I. Talmi, Phys. Rev. 128 (1962) 792

Ki 60 L.S. Kisslinger and R.A. Sorensen, Mat. Fys. Medd. Dan. Vid. Selsk. 32 (1960) Nº 9

Kn 50 W.D. Knight and V.W. Cohen, Phys. Rev. 76 (1950) 1421

La 57 R.D. Lawson and J.L. Uretsky, Phys. Rev. 106 (1957) 1369

Le 50 H.W. Lewis, Phys. Rev. 78 (1950) 526

Le 60 I.K. Lemberg, *Proc. 2nd Conf. on Reactions between Complex Nuclei*, John Wiley and Sons, New York (1960)

Li 53 J. Lindhard and M. Scharff, Kgl. Dan. Vid. Selsk. Mat. Medd. 27 (1953) 15

Li 58 A.E. Litherland, H. McManus, E.B. Paul, D.A. Bromley and H.E. Gove, Can. J. Phys. 36 (1958) 378

Li 61 A.E. Litherland and A.J. Ferguson, Can. J. Phys. 39 (1961) 788

Li 61a J. Lindhard and M. Scharff, Phys. Rev. 124 (1961) 128

Li 63 A.E. Litherland, M.J.L. Yates, B.M. Hinds and D. Eccleshall, Nucl. Phys. 44 (1963) 220

Li 63a J. Lindhard, M. Scharff and H.E. Schiott, Mat. Fys. Medd. Dan. Vid. Selsk. 33 (1963) Nº 14

Li 70 K. Lips and M.T. McEllistrem, Phys. Rev. C1 (1970) 1009

Ma 49 M.G. Mayer, Phys. Rev. 75 (1949) 1969

Ma 66 F.B. Malik and W. Scholz, Phys. Rev. 150 (1966) 919

Ma 67 F.B. Malik and W. Scholz, *Nuclear Structure based on Lectures on Low-Energy Nuclear Physics*, ed. by A. Hossain et al., Dacca (1967) 34

Ma 68 J.B. Marion, Univeristy of Maryland Technical Report 656 (1968) unpublished

Ma 69 G. Mairle et al., Nucl. Phys. A134 (1969) 180

Ma 70 S. Maripuu, Nucl. Phys. A149 (1970) 593

Mc 52 C.L. McClelland, C. Goodman and P.H. Stelson, Phys. Rev. 86 (1952) 63

Mc 64 J.D. McCullen, B.F. Bayman and L. Zamik, Phys. Rev. 134 (1964) B 515

Mc 70 M.T. McEllistrem, K.W. Jones and D.M. Sheppard, Phys. Rev. C1 (1970) 1409

Me 66 J.R. Meriwether et al., Phys. Rev. 146 (1966) 804

Mo 59 B.R. Mottelson and S.G. Nilsson, Mat. Fys. Dan. Vid. Selsk. 1 (1959) Nº 8

Mo 66 S.A. Moszkowski, *α, β, and γ Spectroscopy*, ed. by Siegbahn (1966) 863

Mu 66 K. Murakawa, J. Phys. Soc. Japan 21 (1966) 1466

Ne 68 E. Newman and J.C. Hiebert, Nucl. Phys. A110 (1968) 366

Ni 55 S.G. Nilsson, Mat. Fys. Medd. Dan. Vid. Selsk. 29 (1955) Nº 16

No 63 L.C. Northcliffe, Ann. Rev. Nucl. Sci. 13 (1963) 67

Nu 70 Nuclear Data, B3-5, National Academy of Sciences (1970)

Ob 67 B.J. O'Brien et al., Nucl. Phys. A104 (1967) 609

Ok 67 V.V. Okorokov et al., Soviet J. Nucl. Phys. 4 (1967) 697

Ol 68 J.W. Olness, *Third Symposium on the Structure of Low Medium Mass Nuclei*, ed. by J.P. Davidson, University Press of Kansas (1968) 192

Pa 56 E.B. Paul, Physica 22 (1956) 1140

Pe 62 F. Perey and B. Buck, Nucl. Phys. 32 (1962) 353

Po 65 A.R. Poletti and E.K. Warburton, Phys. Rev. 137 (1965) B 595

Pr 62 M.A. Preston, *Physics of the Nucleus*, Addison-Wesley Publishing Co., Inc. (1962)

Pr 65 J.G. Pronko, Ph.D. Thesis, University of Alberta (1965)

Ra 50 J. Rainwater, Phys. Rev. 79 (1950) 432

Ra 57 G. Rakavy, Nucl. Phys. 4 (1957) 375

Ra 69 R. Raj. M.L. Rustgi and R.P. Singh, Phys. Rev. 181 (1969) 1536

Ri 62 R.C. Ritter et al., Phys. Rev. 128 (1962) 2320

Ro 57 M.E. Rose, *Elementary Theory of Angular Momentum*, Wiley, New York (1957)

Ro 67 H.J. Rose and D.M. Brink, Rev. Mod. Phys. 39 (1967) 306

Ro 69 B.C. Robertson, Ph.D. Thesis, Oxford University (1969)

Ru 59 A.R. Rutledge, Atomic Energy of Canada report CRP-851 (1959) unpublished

Sa 54 G.R. Satchler, Phys. Rev. 94 (1954) 1304

Sa 56 G.R. Satchler, Phys. Rev. 104 (1956) 1198

Sa 67 H.R. Saad et al., Z. für Physik 205 (1967) 342

Sc 66 H.E. Schiott, Mat. Fys. Medd. Dan. Vid. Selsk. 35 (1966) N^o 9

Sh 51 R.E. Sheriff and D. Williams, Phys. Rev. 82 (1951) 651

Sh 56 R.K. Sheline, Nucl. Phys. 2 (1956) 382

Sh 61 A. de Shalit, Phys. Rev. 122 (1961) 1530

Sh 63 A. de Shalit, *Selected Topics in Nuclear Theory*, ed. by F. Jonouch (1963) 209

Sh 63a E. Sheldon, Rev. Mod. Phys. 35 (1963) 795

Sh 66 E. Sheldon and D.M. van Patter, Rev. Mod. Phys. 38 (1966) 143

Sh 67 E. Sheldon and P. Gantenbein, J. Appl. Math. and Phys. 18 (1967) 397

Sh 69	E. Sheldon and R.M. Strang, Computer Phys. Comm. 1 (1969) 35
Sh 69a	E.N. Shipley, R.E. Holland and F.J. Lynch, Phys. Rev. 182 (1969) 1165
Si 67	P.P. Singh et al., Phys. Rev. 158 (1967) 1063
Sk 66	S.J. Skorka, J. Hertel and T.W. Retz-Schmidt, Nuclear Data A2 (1966) Nº 4, 347
So 69	P.C. Sood, Phys. Rev. 179 (1969) 1100
Sp 71	R.J. Sparks, Nucl. Phys. A169 (1971) 113
St 60	P.H. Stelson, *Proceedings of the International Conference on Nuclear Structure*, Kingston, Canada (1960) 787
St 52	P.H. Stelson and W.M. Preston, Phys. Rev. 86 (1952) 807
St 65	S. Sterner, L. Jonsson and A.E. Arnell, Arkiv Fysik 31 (1965) 567
Sz 70	I.M. Szöghy, B. Cujec and R. Dayras, Nucl. Phys. A153 (1970) 529
Ta 58	I. Talmi, *Proc. of the Rehovoth Conf. on Nuclear Structure,* North Holland Co. (1958) 31
Ta 62	I. Talmi, Rev. Mod. Phys. 34 (1962) 704
Ta 67	I. Talmi, Phys. Lett. 25B (1967) 313
Ta 70	S. Tanaka, P.H. Stelson, W.T. Bass and J. Lin, Phys. Rev. C2 (1970) 160
Te 66	J.W. Tepel, Nucl. Inst. and Meth. 40 (1966) 100
Ve 64	E. Veje et al., Nucl. Phys. 57 (1964) 451
Vo 68	E. Vogt, *Advances in Nuclear Physics*, Plenum Press, New York (1968) 261
Vu 66	P.H. Vuister, Nucl. Phys. 83 (1966) 593
Vu 67	P.H. Vuister, Nucl. Phys. A91 (1967) 521
Wa 63	E.K. Warburton, D.E. Alburger and D.H. Wilkinson, Phys. Rev. 129 (1963) 2180

Wa 67 E.K. Warburton, *Nuclear Research with Low Energy Accelerators*, ed. by J.B. Marion and D.M. van Patter, (1967) 43

We 37 V.F. Weisskopf, Phys. Rev. **52** (1937) 295

Wi 71 J.E. Wiest *et al.*, Phys. Rev. **C4** (1971) 2061

Wo 51 L. Wolfenstein, Phys. Rev. **82** (1951) 690

B30019